

The role of the polycystin genes, *Pkd1l1* and *Pkd2*, in the determination of left-right asymmetry

A thesis presented for the degree of Doctor of Philosophy (D.Phil)

Wolfson College, University of Oxford

Daniel T. Grimes

MRC Mammalian Geentics Unit, Harwell

Department of Physiology, Anatomy and Genetics, Oxford

Supervisors: Dr Dominic Norris (MGU, MRC Harwell)

Dr Shankar Srinivas (DPAG, Oxford)

Trinity term 2012

The role of the polycystin genes, *Pkd1l1* and *Pkd2*, in the determination of left-right asymmetry

Daniel T. Grimes

MRC Mammalian Genetics Unit, Harwell
Wolfson College, Oxford
Department of Physiology, Anatomy and Genetics, University of Oxford

A thesis presented for D.Phil., Trinity term, 2012

Abstract

Breaking bilateral symmetry is critical for vertebrate morphogenesis. In the mouse, overt left-right (L-R) asymmetries in the development of the organs is prefigured by asymmetric cascades of genes expression. The Nodal/Pitx2 pathway is active in the left lateral plate mesoderm (LPM) and remains absent from the right side of the embryo. Expression of *Nodal* in the left side is initiated downstream of a symmetry-breaking event that occurs in a midline structure called the node. Within the node, 200-300 posteriorly-tilted motile cilia rotate in the clockwise direction when viewed from the ventral aspect, and in so doing generate a unidirectional leftward flow of extra-cellular fluid across the surface of the node. This flow drives both an elevation in intracellular Ca^{2+} and changes in gene expression at the left side of the node, the first L-R asymmetrical chemical differences in the embryo. However, a major unanswered question concerns how leftward flow is sensed by the embryo, and what genes/ pathways play a role in this process.

Two mutant mouse lines were discovered as part of forward genetic screens for embryos with developmental defects. These two lines, called *rks* and *lrm4*, both exhibit severe L-R defects. Mapping of the mutants revealed *lrm4* to be a new allele of *Pkd2*, a gene known to be required for the left-sided Ca^{2+} elevation which occurs downstream of flow in the node. In contrast, *rks* was mapped to a novel gene not previously associated with L-R determination. The protein encoded by this gene, *Pkd1l1*, was a candidate for being the elusive sensor of leftward flow. This thesis describes experiments aimed at testing the hypothesis that Pkd1l1 and Pkd2 act together to sense leftward flow in the node during the determination of L-R asymmetry in the mouse.

The overt morphological and molecular L-R defects of $Pkd1l1^{rks/rks}$ and $Pkd2^{lrm4/lrm4}$ mutants are compared and found to be highly similar when assessed on the same genetic background. Both mutants exhibit a loss of the normally left-sided Nodal/Pitx2 pathway and, as a consequence, right isomerism of the lungs. *Pkd1l1* gene expression is localised to the ventral layer of the node where flow is generated and sensed, but neither *Pkd1l1* nor *Pkd2* are required for normal node morphogenesis or cilia structure/motility. Moreover, genetic experiments reveal that *Pkd1l1* and *Pkd2* both act downstream of leftward flow but upstream of early asymmetries in gene expression around the node.

In contrast to *Pkd1l1*$^{rks/rks}$ mutants, *Pkd1l1*-null embryos exhibit left lung isomerism and bilateral activation of Pitx2. This surprising observation suggests that *Pkd1l1* restricts *Nodal* to the left side during L-R determination, favouring a model in which leftward flow derepresses left-sided *Nodal* by inhibiting Pkd1l1.

Bioinformatics and structural studies support a role for an extracellular polycystic kidney disease (PKD) domain within Pkd1l1 in the sensation of flow, whilst Pkd1l1 and Pkd2 are also shown to form physical associations mediated by intracellular coiled coil domains. Finally, Pkd2 is shown to be required within the cilial compartment for L-R determination. In conclusion, the results reported in this thesis support a model in which Pkd1l1 and Pkd2 act together for the sensation of leftward flow and specifically implicate Pkd1l1's extracellular PKD domain in the sensation mechanism.

Acknowledgements

I have many people to thank. My advisor, Dominic Norris, for his guidance throughout my DPhil project and for many thought-provoking and ideas-generating discussions.

This work rests on the prior work of others: Sarah Field, who cloned *rks* and performed initial characterisation of the mutant; Andy Greenfield, Pam Siggers, and Deb Bogani, who together performed the ENU screen from which *rks* derived.

I have been fortunate in having many tutors, formal and informal, who have offered technical assistance and advice: Chris Esapa, Jeremy Sanderson, Debbie Williams, Andy Greenfield, and Deen Quawalid. I spent many an enlightening hour with Helen Hilton, perched over our most recent western blot, debating how to interpret the bands (or lack thereof). Even after attending a 'Protein Alignment and Structural Modelling' course at EMBL in Heidelberg, I remained quite inept at tackling bioinformatics problems above a sequence alignment. I was therefore lucky to have the help of Michelle Simon, who always made time (even during her own thesis writing) to answer my queries.

At Harwell, I have been part of a dynamic and talented student body, many of whom I can now count as friends. I have enjoyed our symposia and 'away days', and the nights out which followed. I wish each of you success in completing your own DPhil's.

I have had the pleasure to work closely with several people on aspects of this project. My gratitude goes to Kerry-Lyn Riley, Saloni Patel, Jennifer Keynton, and Dragos Leordean, for making our collaborations successful and enjoyable.

I will not miss the dreaded Oxford-to-Harwell daily round-trip; traffic on the A34 on a Friday afternoon is not pleasant. I will, however, remember with fondness those with whom I car-shared, twice a passenger and once a driver; Rachel Brixey, Victoria Patterson, and Saloni Patel. Thank you for making the journey to and from work an enjoyable part of the day.

I began my career at Harwell in Jenny Murdoch's lab as an undergraduate student, where I worked alongside Rachel Poole, Anju Paudyal, Christine Damrau, Ben Reeve, and Victoria Patterson. This was my first experience of working in a lab and I owe much to Jenny and the other members for teaching me not only many experimental techniques, but also for showing me that 'real science' is exciting and fun, unlike undergraduate practical classes. Without such a positive experience I would have been unlikely to remain in academia.

I have been extremely fortunate to have had a great group of friends outside the lab: Phil Dolan, Victoria Patterson, Sojin Yu, Rachel Poole and, in particular, Ben Britton.

Finally, I thank my family, most notably my parents and grandparents. It is to them that this thesis is dedicated.

Abbreviations

ADPKD	autusomal dominant polycystic kidney disease
AIE	asymmetric initiator element
A-P	anterior-posterior
ASE	asymmetric enhancer
ATP4	H^+/K^+-ATPase
Ca^{2+}	calcium ion
Cerl2	Cerberus-like 2
DFC	dorsal forerunner cells
dll1	delta-like 1
dpc	days post coitum
D-V	dorsal-ventral
Dvl	Dishevelled
ECM	extracellular matrix
FGF	fibroblast growth factor
GFP	green fluorescent protein
Gli	Glioma-associated
GRP	gastroceol roof plate
IFT	intraflagellar transport
iv	situs inversus viscerum
KV	Kupffer's vesicle
LPM	lateral plate mesoderm
L-R	left-right
Lrd	left-right dynein
LSE	left side-specific enhancer
NVP	nodal vesicular parcel
PC-2	Polycystin 2
PCD	primary ciliary dyskinesia
PCP	planar cell polarity
PDGF	platelet-derived growth factor
PFP	prospective floor plate
Pkd1	Polycystic kidney disease-1
Pkd2	Polycystic kidney disease-2
PNC	posterior notochord
Pitx2	Paired-like homeodomain transcription factor 2
RA	retinoic acid
RD	reaction diffusion
SELI	self-enhancement and lateral-inhibition
sGAG	sulphated glycosaimnoglycan
Shh	Sonic hedgehog
T	*Brachyury*
TGF	Transforming growth factor
Vangl	Van Gogh-like

Table of Contents

1. Introduction 1

1.1. Left-right asymmetry in nature 3

1.2. Asymmetric morphogenesis 4

1.3. Asymmetric patterning of the embryo 6

1.3.1. Molecular asymmetries 6

1.3.2. Nodal signalling and the patterning of the LPM 7

1.3.3. The role of the midline 13

1.4. The origin of asymmetry 15

1.4.1. The nodal flow hypothesis 15

1.4.2. Asymmetries downstream of flow: from node to LPM 20

1.4.3. The generation nodal flow 24

1.4.4. The perception of nodal flow 26

2. *Pkd1l1* is required for the establishment of left-right asymmetry in the mouse 33

2.1. INTRODUCTION 35

2.2. RESULTS 35

2.2.1. *rks*: an ENU-induced *Pkd1l1* allele 35

2.2.2. *Pkd1l1*$^{rks/rks}$ embryos exhibit severe left-right defects and arrest by 15.5 dpc 37

2.2.3. *Pkd1l1*$^{rks/rks}$ embryos strongly phenocopy *Pkd2*$^{lrm4/lrm4}$ mutants 41

2.2.4. There exists no obvious genetic interaction between *Pkd1l1*^{rks} and *Pkd2*^{lrm4} 44

2.2.5. Loss of the left-sided Nodal cascade in *Pkd1l1*$^{rks/rks}$ and *Pkd2*$^{lrm4/lrm4}$ mutant embryos 44

2.3. DISCUSSION 48

2.3.1. *rks* is a novel allele of *Pkd1l1* with severe left-right defects 48

2.3.2. *Pkd2*$^{lrm4/lrm4}$ mutants exhibit L-R defects that are distinct from *Pkd2*$^{-/-}$ mutants 48

2.3.3. *Pkd1l1*$^{rks/rks}$ and *Pkd2*$^{lrm4/lrm4}$ mutants exhibit phenotypes similar to other mutants that fail to activate LPM *Nodal* expression 49

2.3.4. Why might *Pkd1l1*$^{rks/rks}$ and *Pkd2*$^{lrm4/lrm4}$ mutants fail to initiate left LPM *Nodal* expression? 52

3. Both *Pkd1l1* and *Pkd2* act in the node to affect early asymmetries in gene expression 53

3.1. INTRODUCTION 55

3.2. RESULTS 55

3.2.1. *Pkd1l1* is expressed in the node and notochord 55

3.2.2. Node cilia of *Pkd1l1*$^{rks/rks}$ and *Pkd2*$^{lrm4/lrm4}$ mutants are structurally normal and motile 57

3.2.3. *Pkd1l1* and *Pkd2* act downstream of leftward flow 59

3.2.4. Left-sided *Cerl2* is not repressed in *Pkd1l1*$^{rks/rks}$ or *Pkd2*$^{lrm4/lrm4}$ mutants 64

3.3. DISCUSSION 66

3.3.1. Stochastic activation of the LPM Nodal cascade depends on *Pkd1l1* and *Pkd2* 67

3.3.2. Delayed activation of the LPM Nodal cascade in mutants lacking leftward flow 67

3.3.3. Repression of *Cerl2* by leftward flow requires *Pkd1l1* and *Pkd2* 68

3.3.4. A model of Pkd1l1-Pkd2 action during the establishment of left-right asymmetry 69

4. *Pkd1l1* is required to restrict *Nodal* to the left side 71

4.1. INTRODUCTION 73

4.2. RESULTS 73

4.2.1. The *Pkd1l1*$^{rks/rks}$ phenotype is slightly modified by changes in genetic background 73

4.2.2. *Pkd1l1*$^{-/-}$ mutants exhibit left-right abnormalities that are distinct from *Pkd1l1*$^{rks/rks}$ mutants 75

4.2.3. Node cilia are present and motile in *Pkd1l1*$^{-/-}$ mutants 80

4.2.4. *Pitx2* expression bilaterally expressed in *Pkd1l1*$^{-/-}$ embryos 81

4.2.5. The *Pkd1l1*^{rks} mutation disrupts an extracellular PKD domain 82

4.2.6. Preliminary experiments to assess the mechanical strength of Pkd1l1 PKD domains 85

4.3. DISCUSSION 88

4.3.1. *Pkd1l1*$^{-/-}$ and *Pkd1l1*$^{rks/rks}$ have distinct left-right defects 89

4.3.2. The *Pkd1l1*$^{-/-}$ mouse phenotype is similar to the *Pkd1l1*^{abc} medaka fish mutant phenotype 89

4.3.3. A mechanosensitive PKD domain is likely disrupted by the *Pkd1l1*^{rks} mutation 90

5. Pkd1l1 and Pkd2 physically interact and the *Pkd2*^{lrm4} mutation disrupts Pkd2's localisation to node cilia 91

5.1. INTRODUCTION 93

5.2. RESULTS 93

5.2.1. Pkd1l1 contains an intracellular coiled coil domain 93

5.2.2. Generation and expression of Pkd1l1 and Pkd2 epitope-tagged constructs 93

5.2.3. Pkd1l1 and Pkd2 interact via Pkd1l1's coiled coil domain 95

5.2.4. Pkd2 localises to primary cilia, including cilia within the node 98

5.2.5. The *Pkd2*^{lrm4} mutation disrupts Pkd2's ciliary localisation 100

5.3. DISCUSSION 102

5.3.1. Complexes of sensory polycystin proteins 102

5.3.2. Pkd2's ciliary localisation is required for L-R determination 103

6. Coda: On the concordance of organ situs in left-right mutants 105

7. Discussion 111

7.1. Summary of findings 113
7.2. *Pkd1l1* and *Pkd2* mutants 114
7.2.1. Loss of *Pkd1l1* in mouse and medaka fish 114
7.2.2. *Pkd1l1*$^{rks/rks}$ mutants 115
7.2.3. Loss of *Pkd2* in mouse and fish 115
7.2.4. *Pkd2*$^{lrm4/lrm4}$ mutants 116
7.3. Interactions between genes controlling the generation and sensation of nodal flow 117
7.3.1. Might there be a second flow-sensing molecule? 117
7.3.2. Flow relieves Pkd1l1-mediated inhibition of the left-sided Nodal cascade: a genetic model 118
7.4. How might Pkd1l1 sense leftward flow? 120
7.4.1. Polycystin proteins as sensors: the PKD domain points to mechanosensation 121
7.4.2. Two populations of cilia in the node 122
7.4.3. Two cilia are enough to break L-R symmetry 123
7.4.4. Is flow sensing alone sufficient to distinguish left from right? 124
7.4.5. Can a morphogen be biased by the flow? 124
7.5. Future directions 125
8. Experimental procedures 127
8.1. Mice 129
8.1.1. Situs inversus viscerum (*iv*) 129
8.1.2. Pkd2^{lrm4} 129
8.1.3. Pkd1l1^{rks} 130
8.1.4. Riboprobe synthesis mRNA whole mount in situ hybridisation (WISH) 130
8.1.5. X-gal staining of embryos 132

8.1.6. High-speed video microscopy 132
8.1.7. Scanning electron microscopy 132
8.2. Molecular biology 133
8.2.1. Gel electrophoresis 133
8.2.2. Purification of PCR products 133
8.2.3. DNA sequencing 133
8.2.4. Transformation of plasmid DNA 133
8.2.5. DNA preparation from colonies 133
8.2.6. Restriction enzyme digestion 134
8.2.7. Dephosphorylation of vector DNA 134
8.2.8. Ligation of vector and insert 134
8.3. Protein biochemistry 135
8.3.1. Protein extraction and quantitation 135
8.3.2. Immunoprecipiation 135
8.3.3. Western blotting 135
8.4. Tissue culture 136
8.4.1. Waking cells 136
8.4.2. Splitting cells 136
8.4.3. Freezing cells 136
8.4.4. Counting cells 137
8.4.5. Transfection of constructs 137
8.4.6. Immunocytofluorescence 137
9. References 139

CHAPTER ONE

Introduction

1.1. Left-right asymmetry in nature

The great majority of animal species have a body plan based on bilateral symmetry. They are, therefore, united in a group called the Bilateria. All deuterostomes are bilaterally symmetric, with the exception of some echinoderms such as starfish[1]. Protostomes too are bilaterally symmetrical and therefore constitute the vast majority of the Bilateria. Animals which are not bilaterally symmetrical have been grouped in the Radiata. These include cnidarians (sea anenomes, corals, jellyfish) and ctenophores (comb jellies) who are among our most distant cousins in the animal kingdom. Acoel flatworms, which lack a coelom, are bilaterally symmetrical and are considered by some to be a modern approximation of the common ancestor of all surviving bilaterians (termed Urbilateria), though this is fervently debated (Hejnol and Martindale, 2008a; Hejnol and Martindale, 2008b; Philippe et al., 2011). Indeed, the origin and nature of Urbilateria remains mysterious (De Robertis and Sasai, 1996; Kimmel, 1996; Miller and Ball, 2009).

Many animals develop conspicuous asymmetries between left and right. For example, the flatfish lie on one side of their body on the sea floor, while both of their eyes are positioned on the other side. During flatfish development, one eye begins in the 'normal' place, but then migrates around the skull to meet the other eye on the opposite side (Friedman, 2008). Snails exhibit both sinistrally and dextrally coiling shells, often within the same species (Grande and Patel, 2009a; Grande and Patel, 2009b; Wandelt and Nagy, 2004). Male fiddler crabs have one large claw used for behavioural signalling and, less often, for fighting. The narwhal tusk is a modified upper *left* incisor (Held, 2009).

In contrast, the majority of vertebrates, appear largely bilaterally symmetrical when viewed externally. However, inside the body the distribution of the visceral organs follows a very particular pattern that is not symmetrical in relation to the midline. For example, the liver and vena cava are located on the right, while the spleen and the aortic arch are positioned on the left. Paired organs, like the lungs and kidneys, are arranged more or less bilaterally but do nevertheless display differences between left and right. For example, in humans the right lung is composed of three distinct lobes while the left lung consists of two lobes. Besides

[1] Starfish and their kin are radially symmetrical in the adult phase, but their larvae are bilaterally symmetrical. They are thought to have acquired radial symmetry secondarily and they are not closely related to true radially symmetrical animals such as the jellies.

positioning, most organs also display asymmetric patterning, with morphological asymmetries between the left and right halves of the organ itself. The asymmetries in organ arrangement are highly conserved not only within any one species but across different vertebrate species.

In vertebrates, determination of left-right (L-R) asymmetry occurs with respect to the pre-existing anterior-posterior (A-P) and dorsal-ventral (D-V) axes and involves a complicated hierarchy of events that begins with the initial breaking of L-R symmetry at the midline, and concludes when the asymmetric morphogenesis of the organs has completed. This process can be considered to occur in three stages, with each stage being determined by the preceding one: (1) the initial breaking of L-R symmetry; (2) the establishment of asymmetrical pathways throughout the embryo; and (3) the asymmetric morphogenesis of the organs. In this Introduction, we will consider each in turn (in reverse order), eventually arriving at the origin of L-R asymmetry in the embryo.

1.2. Asymmetric morphogenesis

During embryonic development, the earliest manifestation of morphological asymmetry is the looping of the heart that occurs on embryonic day 23 in humans, equivalent to 8.5 days post coitum (dpc) in mouse. The heart develops from two bilaterally symmetric primordia that gradually converge and fuse at the ventral midline, forming a linear tube (Icardo and Ojeda, 1984). The tube then bends towards the right to form the cardiac loop, a process that is highly conserved in vertebrates. Shortly thereafter the embryo undergoes axial rotation (also called embryonic turning). In rodents, the early embryo is a cup shape with the endoderm on the outside and the ectoderm lining the internal cavity. Such an 'inversion of the germ layers' is corrected by an 180° twisting of the embryo along its A-P axis, the process called turning (Beddington and Robertson, 1999), which converts the embryo from a lordotic position into the foetal position. After turning, the tip of the tail is positioned to the right side of the head while the vitelline vessels become located on the left side. The mechanisms controlling the process and direction of embryonic turning are poorly understood. It is worth noting that turning is a characteristic of rodent embryos and is not shared by other mammals; early rabbit and human embryos exhibit a flat shape (disk) more similar to the chick.

The early primordia of most organs begin in an L-R symmetrical position. Asymmetries are then imparted on these primordia in three main ways: (1) asymmetrical regression/persistence; (2) differential growth/migration; (3) asymmetrical bending or rotational movements. In the majority of cases, final organ asymmetries are achieved through a combination of these processes.

A good example of asymmetrical regression/persistence is the spleen. Splenic precursor cells, marked by *Nkx2-5*, are initially are found bilaterally in *Xenopus* and mouse embryos. However, *Nkx2-5* expression is subsequently lost in right-sided precursor cells; these cells thereby lose their ability to react to local spleen-inducing signals and instead presumably regress or adopt a different developmental fate (Burn et al., 2008; Burn and Hill, 2009; Patterson et al., 2000).

Differential growth occurs in the lung bud to give rise to L-R asymmetrical patterns of lobation. The bud arises as an outgrowth from the ventral wall of the foregut. As it grows caudally, it divides into two branches forming the bronchial buds. It is from this stage that L-R asymmetry is evident, with the right bronchi showing enhanced branching compared to left to give rise to the characteristic differential numbers of lobes seen on the right and left sides (Chinoy, 2003).

Bending and rotational movements mostly effects tubular organs such as the gut and the heart. For example, the midgut – which forms the small intestine – bends into a hairpin and undergoes several rotations that properly position the small intestine anlagen with respect to the future large intestine. The dorsal mesentery, a 'neck' of mesoderm, connects the midgut tube to the body wall so that the tube is suspended in the coelom by the dorsal mesentery. It has recently been discovered that the mesenchymal cells of the dorsal mesentery are more condensed on the left side than the right side, while the overlying epithelial cells on the left exhibit a columnar morphology as opposed to the cuboidal morphology on the right (Davis et al., 2008). These asymmetrical cell characteristics, as well as alterations to cell:cell adhesion and the extracellular matrix (Kurpios et al., 2008), result in the tilting of the dorsal mesentery towards the left side, causing the midgut to bend. This remains one of the few examples in which the cellular mechanisms of asymmetrical development have been characterised.

However, it remains a major challenge in the field to determine how asymmetric morphogenesis occurs at the cellular and molecular levels. In the next

section, we consider the asymmetrical signals which are active in the embryo and which prefigure and instruct asymmetric morphogenesis of the organs.

1.3. Asymmetric patterning of the embryo

1.3.1. Molecular asymmetries

The first major breakthrough in our understanding of the molecular mechanisms which govern the establishment of L-R asymmetry came in 1995, when the first asymmetrically expressed genes were discovered. These asymmetries, initially reported in the chick embryo, included the asymmetric expression of Sonic hedgehog (*Shh*) on the left side where it induced expression of *Nodal*, first in a small domain adjacent to Hensen's node then more broadly in the left lateral plate mesoderm (LPM)(Levin et al., 1995). This provided the first molecular markers of L-R asymmetry, allowing asymmetric development to be monitored before the appearance of overt morphological asymmetries. It also identified a principle which was to hold true broadly in other organisms: that the establishment of L-R asymmetry involves the appearance of subtle asymmetries in small regions near the midline followed by the emergence of robust asymmetries in the LPM. Crucially, Nodal was identified as a key left-sided signal.

Since this initial discovery, many genes have been added to this general framework (Raya and Izpisua Belmonte, 2008). Some of these have proved specific to certain classes of vertebrate; for example, asymmetric expression of *Shh* is apparent in chick but not in mammals or fish. Nevertheless, two genes expressed downstream of Nodal have proved to be highly conserved: these are *Lefty* (encoded by *Lefty1* and *Lefty2*) and the transcription factor-encoding gene Paired-like homeodomain transcription factor-2, *Pitx2* (**Figure 1.1A**) (Davidson et al., 1999; Logan et al., 1998; Meno et al., 1996; Meno et al., 1998; Meno et al., 2001; Piedra et al., 1998; Ryan et al., 1998). Both *Lefty2* and *Pitx2* are expressed in the left LPM, while *Lefty1* is induced by Nodal in left side of the midline (Meno et al., 1998; Yamamoto et al., 2003), in the floor plate of the neural tube (**Figure 1.1A**). The left-sided expression of *Nodal* and *Pitx2* is conserved in all vertebrates studied to date (Burdine and Schier, 2000; Nakamura and Hamada, 2012). Thus, the activation of unilateral Nodal is essential for the distinction between left and right.

1.3.2. Nodal signalling and the patterning of the LPM

The Nodal signalling pathway is crucial for many aspects of pattern formation and differentiation during development (Schier, 2009; Shen, 2007). Nodal is essential for formation of mesoderm and endoderm and for correct determination of the L-R axis. In this section, I review the core components and molecular properties of the Nodal pathway then go on to address the role of Nodal during L-R axis specification.

1.3.2.1. The Nodal signalling pathway

Nodal ligands are a subfamily of transforming growth factor (TGF-β) signals that are present in deuterostomes and some protostomes (e.g. snails), though are notably absent from Ecdysozoa such as *Drosophila* and *C. elegans*. A single *Nodal* gene is found in mouse (Zhou et al., 1993), but there are three in zebrafish (*cyclops*, *squint*, and *southpaw*), and at least five in *Xenopus* (*Xnr1, 2, 4, 5,* and *6*). Nodal signals through Alk4 (a type I serine-threonine kinase receptor) and ActRII (a type II receptor), requiring the action of extracellular EGF-CFC co-receptors (Cripto and Cryptic in mammals) (**Figure 1.1B**). Binding of ligand to receptor results in phosphorylation of the type I receptor by the type II receptor, initiating intracellular pathway activation (Schier, 2009). Extracellular antagonists, including Lefty and Cerberus, antagonise the pathway (Cheng et al., 2004; Piccolo et al., 1999; Sakuma et al., 2002). Cerberus and Cerberus-like proteins bind directly to Nodal thereby inhibiting its binding to receptors. Lefty proteins block Nodal signalling by directly binding to Nodal and to EGF-CFC coreceptors (**Figure 1.1B**) (Cheng et al., 2004). Other ligands may also act through the core Nodal pathway. For example, mouse Gdf1 and Gdf3 (and the related Vg1 in zebrafish and *Xenopus*) can activate the pathway (Andersson et al., 2006; Cheng et al., 2003; Rankin et al., 2000). Indeed, Gdf1 and Nodal are both required for L-R axis specification, suggesting synergistic roles (Rankin et al., 2000); Gdf1 can heterodimerise with Nodal to generate a ligand more highly activate than either homodimer (**Figure 1.1B**).

Downstream of activated receptor complexes, pathway activity is transduced by the receptor-activated Smad (R-Smad) proteins Smad2 and Smad3 in combination with the mediator Smad (co-Smad) Smad4 (Massague et al., 2005). Smad2/3 C-terminal phosphorylation by activated receptors leads to interaction with Smad4, nuclear import, and transcriptional activity. Transcription induced by the Nodal pathway requires the activities of the forkhead box transcription factor Foxh1 and

homeodomain proteins of the Mixer subclass (Massague et al., 2005). Foxh1 and Mixer proteins contain Smad2/3 interaction domains, and together they form transcriptional complexes that activate Nodal target genes (**Figure 1.1B**) (Germain et al., 2000; Randall et al., 2004).

1.3.2.2. Expression of left-sided *Nodal*, *Lefty* and *Pitx2*

In the mouse, asymmetric *Nodal* expression in the left LPM begins at around the 2-3 somite stage in a region adjacent to the node then spreads along the A-P axis, before disappearing from the left LPM at around the 6-7 somite stage (Collignon et al., 1996; Lowe et al., 1996). A positive feedback mechanism involving signalling by Foxh1 amplifies *Nodal* expression in the left LPM (Norris et al., 2002; Saijoh et al., 2000). Foxh1 binds to two conserved sites within an asymmetric enhancer (ASE) located in intron 1 of *Nodal* that regulates *Nodal* expression (**Figure 1.1C**) (Adachi et al., 1999; Norris and Robertson, 1999; Saijoh et al., 2000). Removal of the ASE in $Nodal^{\Delta 600/\Delta 600}$ mutants results in a low level left LPM *Nodal* expression that causes both a delay in the timing of *Pitx2* induction and a posterior restriction in the extent of *Pitx2* expression (Norris et al., 2002). A second asymmetric enhancer (called AIE or LSE) lies 5' to the *Nodal* locus, though it is not clear whether this element can respond to Nodal signals (**Figure 1.1C**) (Adachi et al., 1999; Norris and Robertson, 1999; Saijoh et al., 2005; Vincent et al., 2004). Mutants lacking the AIE/LSE exhibit no obvious L-R defects or abnormal LPM *Nodal* expression (Saijoh et al., 2005; Vincent et al., 2004). It might be informative to engineer mutants lacking both ASE and AIE/LSE elements to determine whether the remaining *Nodal* expression in $Nodal^{\Delta 600/\Delta 600}$ mutants is due to a low-level compensation by AIE/LSE.

Lefty2 and *Pitx2* also contain ASE elements that are activated by Nodal signalling in a Foxh1-dependent manner (**Figure 1.1C**) (Adachi et al., 1999; Saijoh et al., 2000; Shiratori et al., 2001; Shiratori et al., 2006). While LPM *Pitx2* expression initiates concomitantly with that of *Nodal*, *Pitx2* expression persists after *Nodal* expression disappears. Thus, *Pitx2* expression remains in the LPM-derived mesenchyme of various visceral organs. Maintenance of *Pitx2* expression is conferred by the transcription factor Nkx2, which binds *Pitx2* in a 5' regulatory element, the ASE (**Figure 1.1C-D**) (Shiratori et al., 2001; Shiratori et al., 2006). Thus, after induction in the left LPM, Nodal signalling autoactivates *Nodal* expression and upregulates *Lefty2* and *Pitx2* via Foxh1 binding to ASE elements

(Adachi et al., 1999; Norris et al., 2002; Norris and Robertson, 1999; Saijoh et al., 2000; Shiratori et al., 2001; Shiratori et al., 2006).

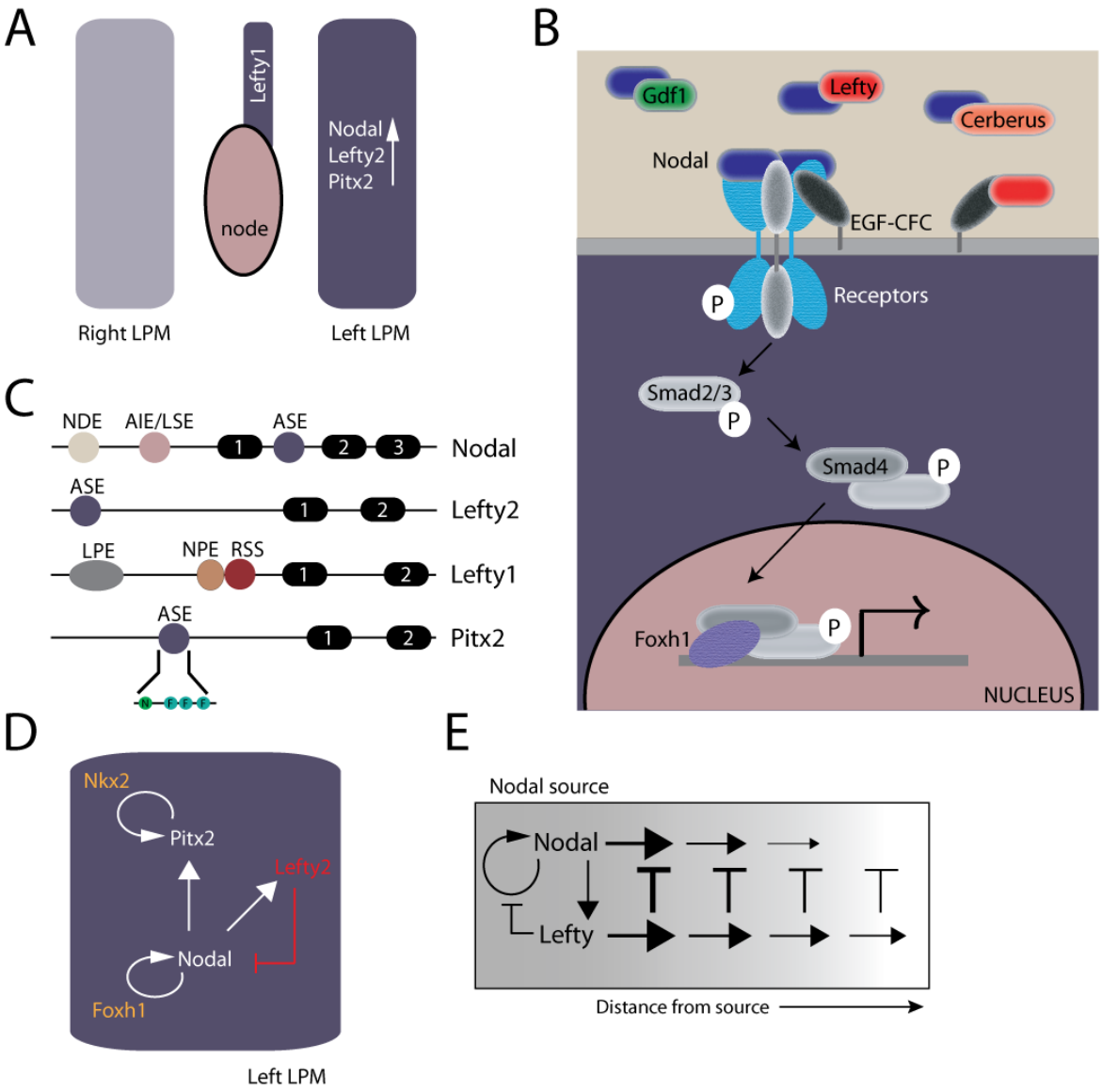

Figure 1.1 The Nodal pathway and patterning of the lateral plate mesoderm

A Schematic of the 8.5 dpc mouse embryo showing the node and expression of the *Nodal/Lefty2/Pitx2* cascade in the left LPM. *Lefty1* is expressed in the left PFP at this stage. **B** Simplified schematic of the Nodal signalling pathway. Nodal ligand signals through Alk4 and ActRII receptors, requiring EGF-CFC coreceptors. Downstream, the Smad2/3 transcription factors are phoshorylated, complex with Smad4, then enter the nucleus where they affect transcription in combination with other factors such as Foxh1. Extracellular antagonists of Nodal signalling include Lefty and Cerberus-like proteins. **C** Diagram of the elements controlling the transcriptional activation of *Nodal*, *Lefty2*, *Lefty1*, and *Pitx2* (see text for details). **D** Signalling network present in the left lateral plate mesoderm where Nodal autoactivates via Foxh1 and also activates its antagonist Lefty2. Finally, Nodal activates Pitx2, the expression of which is then maintained by positive feedback involving Nkx2. **E** Nodal ligands diffuse less effectively from the source than Lefty, resulting in reaction-diffusion like behaviours between the activator-inhibitor pair.

1.3.2.3. Nodal morphogens and L-R asymmetry

Nodal ligands have the properties of a morphogen: a signal that acts at a distance and elicits direct dose-dependent responses in receiving cells (Ashe and Briscoe, 2006; Schier, 2009). For the purposes of our discussion of Nodal signalling during the patterning of the left LPM, we need to turn our attention to two properties of the Nodal morphogen: (1) action at a distance; and (2) reaction-diffusion.

(1) Action at a distance

The best evidence that Nodal proteins can act at a distance came from the study of the zebrafish signals Cyclops and Squint (Chen and Schier, 2001). Misexpression of *squint* induced long-range activation of the Nodal pathway, though *cyclops* only had short-range activity. Crucially, Squint traversed a field of non-responsive cells to activate Nodal targets in distant wild-type cells. This shows that Squint action is direct and not mediated by a cell-cell relay-like mechanism. Other evidence that Nodal ligands act as morphogens has been provided by a study in *Xenopus* (Williams et al., 2004). Local expression of Xnr2-GFP results in the extracellular movement of the fluorescent protein from the source into non-expressing tissue. Taken together, these studies show that Nodal ligands can have direct effects at a distance from their source.

(2) Reaction-diffusion

In 1952, Alan Turing proposed the reaction-diffusion (RD) model, in which two diffusing and interacting molecules can generate complex patterns (Turing, 1952). This was extended by the postulation that pattern formation in RD models requires an activator which acts over a short range to enhance both its own production and that of a long-rang inhibitor (Gierer and Meinhardt, 1972). The real-world relevance of the model has been long-debated, but recently biological examples of its use have removed much of the scepticism (Kondo and Miura, 2010). One of these examples is the formulation of an RD model for the Nodal-Lefty LPM system during L-R patterning (Nakamura et al., 2006). Nodal and Lefty constitute an activator/inhibitor-based system in the LPM (**Figure 1.1D**). Studies in zebrafish have shown that during mesoderm induction, the two Nodal signals Cyclops and Squint and the two inhibitors Lefty1 and Lefty2 have different activity ranges: while Cyclops is a short-range activator of mesendodermal gene expression, Squint acts at a medium range, and Lefty1 and Lefty2 are long-range inhibitors (Chen and Schier,

2001; Chen and Schier, 2002; Le Good et al., 2005). It has recently been demonstrated that differential diffusivity of these signals underlies their different activity ranges (Muller et al., 2012). Thus, the central tenets of the RD system hold true for the Nodal-Lefty pair: (1) Nodals are short- to mid-range activators that enhance their own expression; and (2) Leftys are long-range inhibitors that are activated by Nodals (**Figure 1.1E**).

Incorporating these features of Nodal-Lefty interactions, a self-enhancement and lateral inhibition (SELI) model has been proposed to account for the patterning of the LPM during the establishment of L-R asymmetry (Nakamura et al., 2006). In this model, the self-enhancing component of the activator in the RD system explains the maintenance and spread of Nodal throughout the left LPM. The transient nature of *Nodal* expression in the left LPM can be theoretically explained by the subsequent diffusion of the inhibitor, Lefty2, throughout the tissue (Nakamura et al., 2006). Furthermore, the longer range diffusion of Lefty2 from the left LPM to the right side may explain the block in contralateral activation of downstream left-sided targets such as *Pitx2*. Since Lefty diffuses further that Nodal, pathway inhibition and not activation is favoured on the right side.

In the developmental context, however, the Nodal-Lefty system is not a pure RD system as it is influenced by additional constraints (Muller et al., 2012; Nakamura et al., 2006; Tabin, 2006). For example, the system is influenced by mediolateral differences in the responsiveness of different tissues to Nodal signalling. The intermediate mesoderm does not respond to Nodal, creating a gap between the high levels of left LPM Nodal and Lefty2 and the responsive LPM on the right side. Moreover, Lefty1 is induced in the midline by Nodal signalling, but Nodal itself is not expressed in this tissue (**Figure 1.1A**). The localised induction of the inhibitor but not the activator, is a departure from a pure RD system. Nevertheless, the existence of a source of inhibitor between the activator and the contralateral side creates a ‘midline barrier’, enhancing the fidelity of the system. Furthermore, when *Lefty2* is lost, *Nodal* is still turned off in the LPM, albeit with a delay (Meno et al., 2001). This suggests that factors other than feedback inhibition from Lefty2 contribute to turning off *Nodal* expression. It is reasonable to speculate that some necessary component of the Nodal pathway, perhaps Foxh1 or Cyptic, could be inactivated or downregulated bilaterally in the LPM around the 6-7 somite stage when *Nodal* expression diminishes.

1.3.3. The role of the midline

The autoactivation of Nodal throughout the left LPM poses a mechanistic issue: how does the embryo maintain asymmetric Nodal signalling in the left when the right LPM is also competent to respond to Nodal ligand? Asymmetric initiation of *Nodal*, per se, is not sufficient to maintain left-restriction. In principle, right-sided *Nodal* expression could be induced by Nodal signals from the left LPM and/or signals from the node. This necessitates the existence of a 'barrier' to prevent contralateral activation from the left and a 'repressor' to negatively regulate right-sided activating signals emanating from the node. It appears that the embryonic midline is critical for both of these functions.

The midline runs along the entire length of the A-P axis; after gastrulation it is formed by the notochord, which provides the embryo with a structural core, and the overlying neural tube. Several mutants in which midline structure and/or gene expression is perturbed exhibit L-R defects. For example, *Shh* null mice exhibit left pulmonary isomerism and bilateral expression of left LPM markers due to multiple defects including notochord degeneration, the absence of floor plate and severe neural tube defects (Chiang et al., 1996; Izraeli et al., 2001; Izraeli et al., 1999; Meyers and Martin, 1999; Zhang et al., 2001). Other midline mutants, by contrast, exhibit absence of left-sided markers: for example, in *T* mutants no asymmetric gene expression cascades are initiated due to a severe and early defect of node formation (King et al., 1998). When node disruption is less severe, asymmetric genes can be initiated, but subsequently are expressed bilaterally due to midline deficiencies. Ablation of midline structures in *Xenopus* (Danos and Yost, 1995; Danos and Yost, 1996) leads to bilateral expression of left-sided genes. Together, these findings were articulated into a 'midline barrier' model, in which the midline is thought to prevent asymmetric signalling on one side from affecting that on the contralteral side, thereby acting as a barrier to keep the left- and right-sided pathways separate.

The concept of the midline barrier was given a molecular foothold by experiments in which *Lefty1* was genetically disrupted (Meno et al., 1998). *Lefty1* is expressed in the left side of the presumptive floor plate (PFP) between the 2-6 somite stages (Meno et al., 1996), shortly after *Nodal* is induced in the left LPM (**Figure 1.1A**); indeed, genetic studies indicate that LPM Nodal activates midline

Lefty1 expression (Yamamoto et al., 2003). In the absence of *Lefty1*, the genes *Lefty2* and *Pitx2* are both expressed throughout the left LPM but also in the anterior right LPM, though the notochord and floor plate develop normally in these mutants (Meno et al., 1998; Meno et al., 2001). These results were interpreted as Lefty1 protein acting as a molecular barrier, thereby preventing Nodal from diffusing across the midline to activate right-sided *Nodal* expression (Meno et al., 1998; Yamamoto et al., 2003).

A more recent report by Hamada and colleagues demands an extension of the role of *Lefty1* in the generation of L-R asymmetry (Nakamura et al., 2006). In this study, it was demonstrated that both left and right LPM tissue receive Nodal-inducing signals from the node and that *Nodal* is induced in the right LPM, albeit at a much lower level than that in the left. Subsequently, right-sided *Nodal* expression is terminated as a result of long-range inhibition by *Lefty2* from the left LPM and *Lefty1* from the left PFP. Thus, in the absence of *Lefty1*, not only might contaminating Nodal leak from the left side, but intrinsic right-sided *Nodal* expression is not inhibited, thereby manifesting as bilateral activation (Nakamura et al., 2006; Tabin, 2006). These interpretations form a central part of the SELI model (**§1.3.2.3**; Nakamura et al., 2006). Thus, the midline plays both a molecular (expression of *Lefty1* but not *Nodal*) and physical (Lefty2 cannot reach the right side if the midline is morphologically disrupted (Danos and Yost, 1996)) roles in the suppression of right-sided *Nodal*.

Whether we consider the midline a ‘barrier’ or a ‘repressor’ depends on the source of right-sided ectopic Nodal. If left-sided Nodal truly does diffuse across the embryo to activate *Nodal* in the right LPM in the absence of *Lefty1*, as is likely given that right-sided *Nodal* is anteriorly-restricted in the *Lefty1* mutant, then the term ‘barrier’ is applicable. However, right-sided *Nodal* can also be induced from the node (and actively is at a low level, in wild-type embryos), supporting the notion that the right LPM needs to be actively repressed, not just from contamination from the left but also from induction of endogenous right-sided *Nodal*. Midline *Lefty1* and left LPM *Lefty2* both play a role in this repression.

Lefty1 is only expressed in the anterior part of the embryo. What prevents the Nodal signal from leaking around the posterior side of the node to activate right-sided *Nodal*? *Smad5* null mouse mutants exhibit such a phenotype, with *Nodal*

being expressed around the posterior side of the node and into the right LPM (Chang et al., 2000). Recent work in zebrafish has added mechanism to this observation: bone morphogenic protein (BMP) signalling appears to act as a 'posterior barrier' preventing the spread of Nodal from left to right around the posterior mesodermal tissue (Lenhart et al., 2011).

1.4. The origin of asymmetry

The mechanism of symmetry breaking must make use of pre-existing A-P and D-V information. Brown and Wolpert proposed the existence of a putative molecule, called the F molecule, that aligns with the A-P and D-V axes but also has intrinsic chirality, allowing it to differentiate between left and right along the L-R plane (Brown et al., 1990; Brown and Wolpert, 1990), and thereby distinguishing the left side from the right side.

1.4.1. The nodal flow hypothesis

The ventral surface of the mouse node is decorated with around 200-300 primary cilia (**Figure 1.2A**) (Bellomo et al., 1996; Sulik et al., 1994). Most of these node cilia have a 9+0 arrangement of axonemal microtubules, typical of immotile cilia (**Figure 1.2C**) (Satir and Christensen, 2007). However, studies focusing on the molecular motors involved in ciliogenesis revealed that not only were node cilia required for correct situs specification, but that many of these cilia are truly motile (Nonaka et al., 1998). Using high-speed video microscopy, Hirokawa and colleagues demonstrated that node cilia rotate in a circular fashion, around 10 times per second, in the clockwise direction when viewed from the ventral side (Nonaka et al., 1998). Furthermore, the rotary motion of node cilia was shown to generate a robust unidirectional flow of extracellular fluid in the node from right to left (**Figure 1.2A**) (Nonaka et al., 1998). These data were synthesised into an elegant model named the 'nodal flow hypothesis'. This posits that leftward flow in the node is the primary event breaking L-R symmetry of the mouse embryo.

It is a clear prediction of the nodal flow hypothesis that a loss of robust leftward fluid flow in the node would lead to organ laterality defects. Accordingly, the situs inversus viscerum (*iv*) mouse mutant, which possesses immotile node cilia due to a missense mutation in the axonemal dynein heavy chain gene *Dnahc11*, exhibits

randomised situs (Okada et al., 1999; Supp et al., 1997). *Kif3a* and *Kif3b* null mouse mutant embryos lack node cilia completely and exhibit severe laterality defects as a consequence (Marszalek et al., 1999; Nonaka et al., 1998; Takeda et al., 1999). However, the abnormal phenotyopes of mouse mutants that have lost leftward flow do not demonstrate that it is flow, per se, which breaks symmetry. Instead, seminal experiments where the direction of asymmetric flow was artificially reversed in cultured embryos demonstrated that flow direction alone can indeed determine situs (Nonaka et al., 2002). Using a *Pitx2-LacZ* transgene as well as heart looping and turning direction to score embryonic laterality, Nonaka and colleagues found that artificial rightward flow could overcome endogenous leftward flow if the rightward flow was sufficiently fast; rightward flow of 110 μm per second was fast enough to direct reversal of normal asymmetry but a slower flow, around 6 μm per second, was not enough to overcome endogenous leftward flow (Nonaka et al., 2002). In embryos that had lost leftward flow (*iv/iv* mutants), both fast and slow flows were able to direct asymmetries in the direction of the flow (Nonaka et al., 2002). Thus, it is flow which drives asymmetries in gene expression and subsequent asymmetric morphogenesis.

The nodal flow hypothesis also provides an explanation for the long-known but previously unexplained association between cilia motility and L-R asymmetry. Kartagener's syndrome (OMIM 2444000) is caused by dysfunctional cilial motility, most often as a result of the loss of outer dynein arms (Ul Hassan et al., 2009; Zariwala et al., 2011). Patients exhibit bronchiectasis and sinusitis due to abnormal respiratory tract cilia motility, while situs inversus of the internal organs is also observed (Afzelius, 1976). Moreover, other human syndromes that result from defective cilia motility, collectively termed primary ciliary dyskinesia (PCD) (Sutherland and Ware, 2009), usually have an L-R component. These observations are now explained by dysfunctional motility of L-R cilia in the embryonic node leading to aberrant leftward flow. Thus, the link between cilia and L-R development is firmly established.

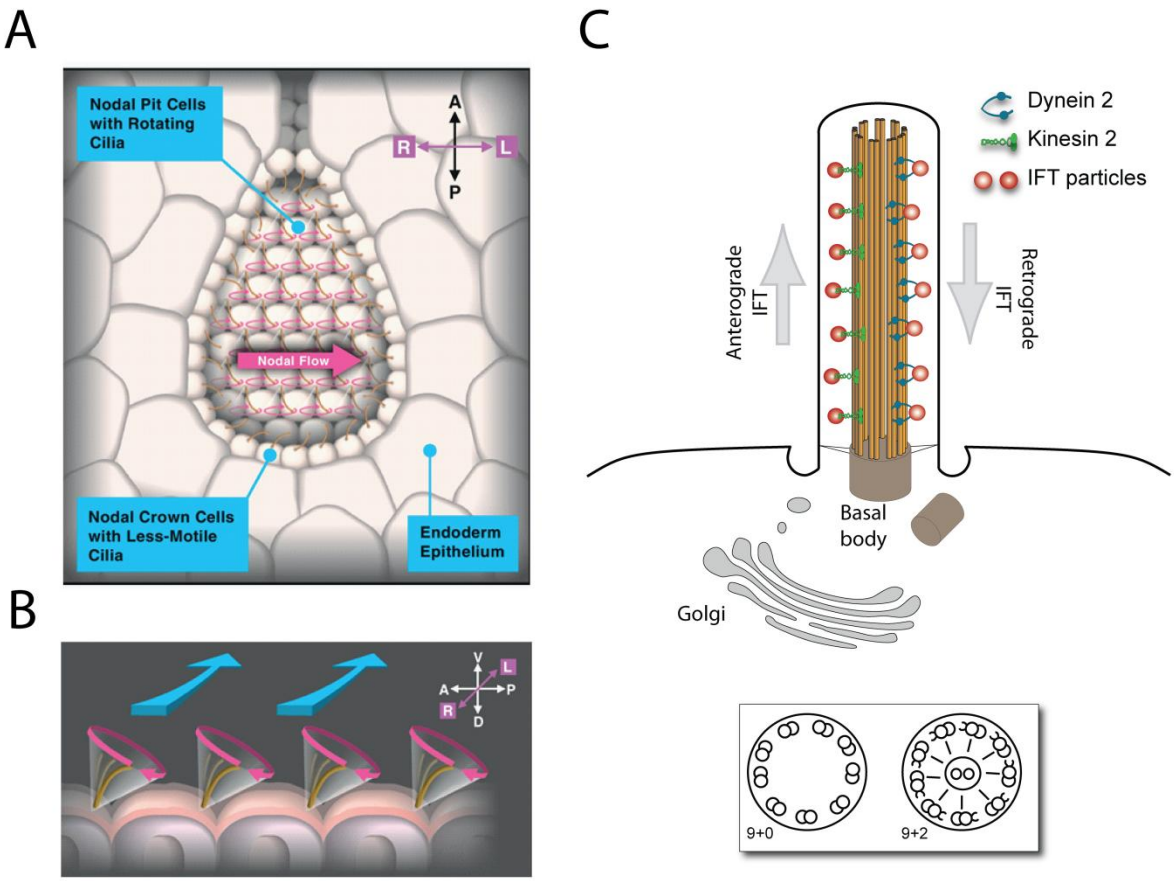

Figure 1.2. Cilia generate leftward flow in the node cavity

A Ventral view of the node showing pit cells with motile cilia and peripheral crown cells, where the majority of immotile cilia are located. The node is surrounded by endodermal cells. Leftward flow (pink arrow) is generated in the node by the action of rotating cilia (Taken from Hirokawa et al., 2012). **B** Cilia tilt towards the posterior and, by rotating clockwise when viewed ventrally, generate a leftward flow of fluid because the rightward stroke is less effective at moving fluid than the leftward stroke; this is because the rigthward stroke is closer to the cell surface, which retards fluid motion (Taken from Hirokawa et al., 2012). **C** Schematic of a primary cilium, showing anterograde and retrograde IFT particles with associated motors (see text). The box shows a cross section through a 9+0 and a 9+2 cilium, with a central pair of microtubules being present in the latter (Adapted from Norris and Grimes, 2012).

1.4.1.1. Conservation of flow

Since the discovery of nodal flow in mouse, it has become apparent that other organisms also use a flow-based mechanism to break L-R symmetry during embryogenesis. Unidirectional flow has now been described in the rabbit, the teleosteans zebrafish and medaka fish, and the frog *Xenopus laevis* (Essner et al., 2005; Kramer-Zucker et al., 2005; Okada et al., 2005; Schweickert et al., 2007).

Disruption to asymmetric flow, by mutation or experimental alteration, in all of these cases leads to laterality defects, while asymmetric expression of *Nodal* (or its homologues) is found around the structure in which flow occurs.

In all of these organisms, leftward flow occurs in a transient structure at the posterior end of the notochord. In rabbit embryos no cilia are found on Hensen's node but motile cilia similar to those found in the mouse 'node' do exist along the notochordal plate, including at the wider posterior end, called the posterior notochord (PNC) (Blum et al., 2007). Partly based on these observations it has been argued that the distal indentation of the egg cylinder in mouse is actually homologous to the rabbit PNC, being distinct from the node (the homologue of Spemann's organiser) (Blum et al., 2007; Blum et al., 2009). Based on the realisation that the organiser did not correspond directly to the ciliated field of cells responsible for breaking L-R symmetry, Blum and colleagues reanalysed *Xenopus* embryos and found motile cilia in the gastroceol roof plate (GRP), a transient structure in the dorsal endoderm of the archenteron (Schweickert et al., 2007). Whilst others had previously speculated about the role of these cilia in L-R asymmetry (Shook et al., 2004), Schweickert and colleagues demonstrated by embryological manipulations and gene knock-down techniques that the cilia in the GRP generate a leftward flow that is required to drive asymmetries in gene expression (Schweickert et al., 2010; Schweickert et al., 2007). Similar GRP structures in which cilia produce a leftward flow have also been found in *X. tropicalis* and *Ambystoma mexicanum*, the axolotl (Blum et al., 2009).

In the teleost fish zebrafish and medaka fish the ciliated structure responsible for breaking L-R symmetry is the Kupffer's vesicle (KV) (Essner et al., 2005; Kramer-Zucker et al., 2005; Okada et al., 2005). First forming after gastrulation, the KV is another transient structure that appears in the tail bud to the posterior of the notochord. In zebrafish, the KV is spherical with motile cilia being found throughout the inside. The flow dynamics in the zebrafish KV are not fully understood, but asymmetries might be generated by differential rates of cilia rotation or by the distribution of ciliated cells within the KV becoming asymmetric (Okabe et al., 2008; Wang et al., 2011; Wang et al., 2012). In contrast, the medaka KV is dome-shaped with motile cilia being found on only one surface (Okada et al., 2005). Whilst zebrafish and medaka are excellent model organisms, they belong to two highly derived groups of teleosteans. By closely scrutinising scanning electron

micrographs from white sturgeon embryos (Bolker, 1993), a member of the most basal group of ray-finned fishes, Blum and colleagues found a ciliated GRP-like structure (Blum et al., 2009). They argue therefore that the KV has evolved from the GRP of a common ancestor of ray-finned fishes[2].

In contrast to mammals, fish, and amphibians, the chick embryo appears to break L-R asymmetry via a different mechanism that does not utilise leftward flow (Cui et al., 2009; Gros et al., 2009). Scanning electron microscopy experiments have failed to detect any candidate ciliated cells at the time when flow would be required to break symmetry (Manner, 2001). *Nodal* asymmetry, a sign of leftward flow in other organisms, is apparent around Hensen's node (Levin et al., 1995) but Hensen's node itself is not ciliated. Indeed, the *Talpid3* chick mutant lacks cilia and exhibits neural tube and limb patterning defects but not L-R defects (Yin et al., 2009); in contrast, mice and zebrafish with functional inactivation of *Talpid3* do exhibit L-R defects (Bangs et al., 2011; Ben et al., 2011). Instead of a flow-based mechanism, Hensen's node becomes morphologically asymmetrical resulting in gene expression asymmetries at the node, notochord, and floor plate (Boettger et al., 1999; Levin, 1998; Levin et al., 1995). Though it is known that Hensen's node undergoes rotational movements which biases gene expression to one side or the other (Cui et al., 2009; Gros et al., 2009), the molecular mechanisms driving these asymmetrical cell movements are not understood. Thus, it seems likely that flow has been lost during bird evolution. However, Blum and colleagues note that the chick is an ambiguous case as chick embryos lack superficial mesoderm (Blum et al., 2009; Shook et al., 2004). They argue that a study of more primitive birds like ostriches or even basal taxa such as crocodiles and turtles will be necessary to ascertain when flow was lost during bird evolution (Blum et al., 2009).

Whilst the lack of flow in chick embryos remains a curiosity, the presence of the GRP in amphibians and basal fish, the KV in teleosteans and the PNC in mammals, argues strongly that flow was present at the base of the vertebrates, and therefore the flow-based mechanism should be considered as the ancestral method used to break L-R symmetry throughout the vertebrate lineage.

---

[2] The nomenclature 'L-R coordinator' has been suggested to refer to the mammalian PNC, teleost KV, or amphibian GRP (Blum et al., 2009). This term is occasionally used in this thesis when referring broadly to the structure in which asymmetrical flow occurs.

1.4.1.2. The ion flux model

A second model explaining the origin of L-R symmetry, which opposes the nodal flow hypothesis, argues that asymmetries upstream of left-sided *Nodal* require a maternally-derived L-R signal present in the very early embryo. It is argued that asymmetric activity of the H^+/K^+-ATPase pump (ATP4) at the four cell stage sets up an asymmetric voltage gradient (Levin, 2003; Levin et al., 2002), which results in the asymmetric distribution of a molecule (thought to be serotonin (Fukumoto et al., 2005)) through gap junctions (Esser et al., 2006) in blastomeres at the 34 cell stage in *Xenopus*. In support of this model, serotonin and ATP4 are both found to be asymmetrically localised in *Xenopus* embryos (Fukumoto et al., 2005; Levin et al., 2002), while inhibition of gap junctional communication is known to effect laterality in vertebrates (Levin and Mercola, 1998a; Levin and Mercola, 1998b). However, recently this theory has been discredited by several studies. Firstly, serotonin is now known to be required for the Wnt-dependent specification of the GRP in frog embryos, and so impacts asymmetric flow (Beyer et al., 2012a). Secondly, ATP4 is required for *Foxj1* expression in the GRP, which in turn controls the development of the full length motile cilia that drive asymmetrical flow (Walentek et al., 2012). Finally, several connexin proteins have been implicated in the transfer of laterality information from the node/GRP to the LPM, implicating gap junctions in the nodal flow model (Beyer et al., 2012b; Saund et al., 2012; Viotti et al., 2012). Thus, all of the major molecules implicated in the early 'ion flux' model have now also been incorporated into the nodal flow hypothesis. Much of the experimental support in favour of the ion flux model is based on chemical treatments which could have lasting effects and thereby impact asymmetric flow. Therefore, at the present time, the nodal flow hypothesis seems the most likely explanation of how L-R asymmetry originates during embryogenesis.

1.4.2. Asymmetries downstream of flow: from node to LPM

1.4.2.1. Perinodal chemical asymmetries

Several genes are expressed asymmetrically in or around the node before the appearance of the left-sided LPM Nodal cascade. Cerberus-like genes, for example, are expressed asymmetrically around the L-R coordinator in a variety of organisms. Mouse Cerberus-like 2 (*Cerl2;* MGI – *Dand5*) displays a unique asymmetric pattern

of expression, being more highly expressed on the right side of the node than the left throughout early somite stages (Pearce et al., 1999). In this way, *Cerl2* assumes a complementary pattern to the one of *Nodal* at this stage (Collignon et al., 1996; Lowe et al., 1996). Cerl2 is a potent antagonist of Nodal signalling (**§1.3.2.1**) (Marques et al., 2004), leading to the notion that asymmetries in *Cerl2* expression repress the autoactivation of *Nodal* on the right side of the node. In support of this, *Cerl2*$^{-/-}$ mutant embryos exhibit a high incidence of bilateral expression of the normally left LPM-restricted genes *Nodal*, *Lefty2* and *Pitx2* (Marques et al., 2004). These results were articulated into a model in which the role of Cerl2 is to restrict Nodal activity to the left side of the node, preventing activation of the Nodal cascade in the right LPM (Marques et al., 2004; Schweickert et al., 2010).

In the zebrafish embryo, the cerberus molecule *charon* is expressed in a horse-shoe pattern in the KV at the 10 somite stage (14 hours post fertilisation) (Hashimoto et al., 2004). Whilst *charon* was initially reported to be expressed symmetrically around the KV in zebrafish (Hashimoto et al., 2004), it has subsequently been established that *charon*, as for mouse *Cerl2*, is expressed with a right-sided (Hojo et al., 2007). Charon is a functional inhibitor of all three zebrafish Nodal signals (Rebagliati et al., 1998; Sampath et al., 1998), while *charon* knock-down by morpholino oligonucleotides leads to bilateral LPM activation of the Nodal cascade (Hashimoto et al., 2004).

More recently, the *Xenopus* Cerberus gene *Coco* has been implicated in the establishment of L-R asymmetry (Schweickert et al., 2010; Vonica and Brivanlou, 2007). *Coco* is co-expressed with the *Xenopus* Nodal gene *Xnr-1* in cells surrounding the GRP (Schweickert et al., 2010), while *Coco* expression is upregulated on the right at the 19-20 somite stage (Schweickert et al., 2010; Vonica and Brivanlou, 2007). Finally, while left-side specific *Coco* knock-down had no effect on L-R asymmetry, knock-down exclusively on the right side of the GRP resulted in the bilateral activation of the LPM Nodal cascade (Schweickert et al., 2010; Vonica and Brivanlou, 2007). Furthermore, elegant experiments in *Xenopus* have shown that *Coco* is a critical target of leftward flow (Schweickert et al., 2010), thereby linking leftward flow to upregulated *Nodal* in left sided cells around the node.

Together, these results from multiple organisms support a model in which a Cerberus molecule is required on the right side of the L-R coordinator to inhibit

activation of the Nodal cascade in the right LPM. In contrast, on the left side, Cerberus is downregulated by flow, resulting in the derepression of *Nodal* and, subsequently, left sided LPM *Nodal* induction. Two other genes, *Ablim1* and *Lplunc1*, are also known to have L-R asymmetric expression patterns at the node (Hou et al., 2004; Stevens et al., 2010). However, the function of these genes in the determination of L-R asymmetry is not understood.

As well as perinodal asymmetries in gene expression, asymmetric Ca^{2+} elevations are observed around the L-R coordinators of several species (Kreiling et al., 2008; McGrath et al., 2003; Raya et al., 2004; Schneider et al., 2008; Tanaka et al., 2005). In the mouse embryo, elevated intracellular Ca^{2+} is observed at the left edge of the node, spreading laterally in the endoderm (McGrath et al., 2003). This spike depends on the polycystin cation channel protein Polycystin-2 (PC-2 or Pkd2) (McGrath et al., 2003), and is known to depend on robust leftward flow in the node (Song et al., 2010). In zebrafish, Ca^{2+} signalling appears to be required for several steps in L-R patterning, including proper migration of the dorsal forerunner cells (DFCs) that go on to form the KV (Kreiling et al., 2008; Schneider et al., 2008), and for correct cilial beating within the KV itself (Sarmah et al., 2005; Sarmah et al., 2007; Shu et al., 2007).

By contrast, in chick, elevated *extracellular* Ca^{2+} levels have been detected on the left side of Hensen's node (Raya et al., 2004). It is argued that this signal potentiates Notch signalling, resulting in increased expression of the Notch ligand delta-like 1 (*dll1*) on the left side. Since overexpression of a dominant negative form of *dll1* in the chick perinodal region led to a loss of left-sided *Nodal* expression, it was argued that elevated left-sided extracellular Ca^{2+} around Hensen's node drives the upregulation of left-sided *Nodal* via the Notch pathway (Raya et al., 2004). It will be interesting in the future to ascertain whether there is a relationship between the asymmetric extracellular Ca^{2+} response in chick and the asymmetric intracellular Ca^{2+} signals in the mouse and zebrafish. Notch signalling is also required for proper L-R determination in mouse and fish (Gourronc et al., 2007; Krebs et al., 2003; Raya et al., 2003), but it has not yet been linked to Ca^{2+} signalling in those organisms.

1.4.2.2. Transfer of a laterality signal from node to LPM

How these initial asymmetries result in Nodal induction in the left LPM is poorly understood. An obvious model is that some signal emanating from the node transits the paraxial mesoderm to induce *Nodal* in the left LPM. Since *Nodal* is more highly expressed and phosphorylated Smad2 more active at the left side of the node than the right (Collignon et al., 1996; Kawasumi et al., 2011; Lowe et al., 1996), and Nodal is able to induce its own expression (Norris et al., 2002), it has been argued that Nodal itself travels from node to LPM to induce left-sided expression. In support of this model, *Nodal* expression at the node is required for LPM *Nodal* induction (Brennan et al., 2002; Saijoh et al., 2003). While Nodal ligand could potentially travel through the extracellular matrix of the paraxial mesoderm (internal route) or between the endoderm and the overlying Reichert's membrane (external route), several experiments favour the former hypothesis (Oki et al., 2007).

The left biased intracellular Ca^{2+} elevation might also play a role in transferring asymmetric signals from node to LPM. Asymmetric Ca^{2+} signals have been observed not only at the left edge of the node but also more laterally, spreading between the node and the LPM in endodermal tissue (McGrath et al., 2003). By analysing *Sox17*$^{-/-}$ mouse embryos, two studies have recently added to our understanding of signal transfer through the endoderm. *Sox17* is required for formation of the definitive endoderm (Kanai-Azuma et al., 2002); significantly, embryos lacking *Sox17* did not activate Nodal in either the left or right LPM, whilst perinodal gene asymmetries were maintained (Saund et al., 2012; Viotti et al., 2012). Furthermore, *Sox17*$^{-/-}$ embryos did not express the gap junction protein Connexin43, normally found in the definitive endoderm (Saund et al., 2012; Viotti et al., 2012). Dye injections into the definitive endoderm showed that small dye molecules could move freely through the endoderm in wild-type but not *Sox17*$^{-/-}$ embryos (Viotti et al., 2012). Importantly, dye particles never crossed the midline, even in wild-type embryos (Viotti et al., 2012), demonstrating that the two sides of the embryo are not coupled by gap junctions. Not only, therefore, does the midline act as a source of Lefty1 to inhibit right-sided *Nodal*, but it also seems to be required to prevent side-specific signals from contaminating the contralateral side by moving through gap junctions. Thus, the spread of Ca^{2+} through the endoderm between the node and the LPM is likely mediated by gap junctional communication, a finding that can explain the heterotaxia found in humans with *CONNEXIN43* mutations (Britz-

Cunningham et al., 1995). This is also supported by the recent observation that gap junctional communication, acting through Connexin26, is required for situs specification in *Xenopus* (Beyer et al., 2012b).

These two models of node-to-LPM signal transfer, one being Nodal transiting through paraxial mesoderm and the second being Ca^{2+} moving through gap junctions in the overlying endoderm, might be acting together to achieve robust left sided *Nodal* activation. The following series of events are therefore a strong possibility. Sensing of leftward flow results in a downregulation of left-side *Cerl2* in crown cells and a subsequent derepression of *Nodal*, resulting in more highly activated Nodal ligand emanating from the left side of the node compared to the right side. Concomitantly, flow results in elevated intracellular Ca^{2+} levels at the left side of the node, which can then spread laterally through gap junctions in the endoderm. Furthermore, in chondrocytes purigenic Ca^{2+} signalling requiring primary cilia is known to be accompanied by increased secretion of sulphated glycosaminioglycans (sGAGs) (Wann et al., 2012). Inhibition of sGAG synthesis prevents signal transfer from node/GRP to LPM in mouse and *Xenopus*, respectively (Marjoram and Wright, 2011; Oki et al., 2007), and sGAGs are known to be part of the extracellular matrix (ECM) in basement membrane structures between the endoderm and the paraxial mesoderm (Oki et al., 2007). Thus, it is conceivable that spreading Ca^{2+} signals in the left-sided endoderm result in increase sGAG secretion which in turn aids in the transfer of Nodal signals from the left side of the node to the left LPM, where Nodal autoactivates.

1.4.3. The generation nodal flow

The nodal flow hypothesis provides a satisfactory explanation for the origin of L-R asymmetry during embryogenesis. However, it raises a number of mechanistic issues such as how nodal cilia generate a unidirectional fluid flow and how responding cells detect and interpret flow.

1.4.3.1. Tilted cilia generate asymmetric flow

It was not immediately obvious how rotating node cilia could generate a unidirectional leftward fluid flow in the node. Wouldn't rotary motion simply create a vortex in the node cavity? It was suggested that the shape of the node might aid the generation of unidirectional flow (Nonaka et al., 1998). However, theoretical studies

and analyses of organisms with different shaped L-R coordinators homologous to the mouse node – KV in fish and the GRP in *Xenopus* - have shown that this is not the case (Cartwright et al., 2004; Okada et al., 2005). Instead, in a beautiful example of the application of physical theory and computational modelling, Cartwright and colleagues predicted that in order to generate unidirectional flow, node cilia must tilt in the plane of the A-P axis; a leftward flow necessitates a posterior tile (Cartwright et al., 2008; Cartwright et al., 2004; Okada et al., 2005). Subsequently, close examinations of cilia in the mouse node have shown that cilia do indeed tilt towards the posterior side at an angle of around 30° (Chen and Schier, 2001; Nonaka et al., 2005; Okada et al., 2005). This posterior tilt is imparted by the posterior positioning of node cilia together with the concave architecture of the ventral surface of node pit cells (**Figure 1.2B**). Posteriorly tilted cilia can produce a leftward flow instead of a vortex because the leftward swish is far from the cell surface and is therefore efficient at moving fluid. On the contrary, the swish in the rightward direction is close to the cell surface and is inefficient at dragging fluid (**Figure 1.2B**); this is because fluid contacting a solid surface does not move and therefore impedes the overlying fluid from being dragged by moving cilia (Brokaw, 2005; Cartwright et al., 2004). This effect, called the no-slip boundary condition, is greatest nearer the cell surface and so has a larger effect on the rightward stroke. The combination of efficient leftward and inefficient rightward strokes results in a net leftward flow of fluid in the node.

1.4.3.2. Planar cell polarity governs the posterior tilt of node cilia

In the mouse, though most node cilia become posteriorly positioned by the 1 somite stage, they initially emerge from basal bodies located centrally on node pit cells. Over the course of several hours, node cilia shift from a central position towards the posterior (Hashimoto and Hamada, 2010; Hashimoto et al., 2010). Even in wild-type embryos, a minority of cilia are positioned to the anterior of node pit cells; these cilia tilt anteriorly, suggesting that no mechanism exists to impart a posterior tilt upon node cilia regardless of basal body positioning. The posterior tilt of node cilia was impaired in *Bicaudal C* mutants that exhibit disrupted basal body positioning (Maisonneuve et al., 2009); this was the first demonstration of mutants that exhibit L-R abnormalities due to mis-aligned node cilia, confirming the crucial requirement

that node cilia tilt posteriorly to correctly establish asymmetric flow and subsequently situs.

The mechanism that positions the basal bodies of node cilia appears to involve the non-canonical Wnt (planar cell polarity (PCP)) pathway (Antic et al., 2010; Hashimoto et al., 2010; Song et al., 2010). Compound mouse mutants of the core PCP genes *Dishevelled* (*Dvl*) 1, 2 and 3 and *Van Gogh-like* (*Vangl*) 1 and 2 exhibit situs defects due to mis-aligned node cilia (Hashimoto et al., 2010; Song et al., 2010). Vangl2 is also required for the posterior tilting of cilia within zebrafish KV and pronephric duct (Borovina et al., 2010), while morpholino-mediated disruption of *Vangl2* prevents the posterior localisation of cilia with the GRP of *Xenopus* (Antic et al., 2010; Borovina et al., 2010). These data confirm the conserved role of PCP for positioning of node cilia across the vertebrates that utilise asymmetric flow.

1.4.4. The perception of nodal flow

Asymmetrical fluid flow in the mouse node is a biophysical phenomenon. Downstream of flow, asymmetrical gene expression cascades are initiated which eventually determine situs. Therefore, a mechanism must exist to convert asymmetric fluid flow into chemical asymmetries. This is the problem of 'flow perception' which, to date, has proved challenging to understand. It is an emerging notion that cilia are not only required for flow generation, but also for flow sensation. Two major models have been proposed to explain this sensation: (1) the chemical sensation model and (2) the mechanical sensation model. In this section, the cilium is described as a sensory organelle in the node, then the two models are discussed.

1.4.4.1. Flow perception by sensory cilia: the 'two cilia model'

For many decades it was thought that the primary cilium was a purely vestigial organelle without function (Bloodgood, 2009). However, over the past decade many roles for cilia in development and physiology have emerged. The numerous requirements for cilia are reflected in the broad spectrum of phenotypes associated with ciliopathies, a collective term for an apparently disparate group of human diseases that all result from defects in the formation and/or function of cilia (Badano et al., 2006; Baker and Beales, 2009; Fliegauf et al., 2007; Norris and Grimes, 2012; Oh and Katsanis, 2012). The role of cilia in cell-cell signalling is becoming increasingly understood. The hedgehog pathway, for example is tightly associated

with cilia in vertebrates; pathway components are shuttled into and out of the cilium in response to ligand, resulting in changes in the ratio of processed to unprocessed Gli protein, a transcriptional effector of the hedgehog pathway (Eggenschwiler and Anderson, 2007; Goetz and Anderson, 2010; Murdoch and Copp, 2010). Cilia have also recently been implicated in fibroblast growth factor (FGF), platelet-derived growth factor (PDGF), Notch, and canonical and non-canonical Wnt signalling (Ezratty et al., 2011; Schneider et al., 2005; Tanaka et al., 2005; Wallingford and Mitchell, 2011). Furthermore, primary cilia play various sensory roles, including mechanosensation, osmosensation, thermosensation, and photoreception (Berbari et al., 2009). Thus, the cilium is now considered as the cells 'antenae', being a major sensory organelle required for the transduction of a plethora of extracellular signals, both chemical and mechanical (Reiter, 2008; Singla and Reiter, 2006).

Primary cilia themselves are small microtubule-based outgrowths of the plasma membrane that extend from a modified centriole, called the basal body, which serves as a microtubule organising centre (**Figure 1.2C**). The axoneme of primary cilia consists of nine peripheral microtubule doublets (9+0); motile cilia usually contain an extra pair of microtubule doublets in the centre (9+2). The building and maintenance of the cilium requires intraflagellar transport (IFT), a mechanism by which cargo is transported along the ciliary axoneme by molecular motors. Anterograde IFT (base to tip) is mediated by IFT-B particles and the kinesin 2 motor (composed of Kif3a, Kif3b and Kap) (Ishikawa and Marshall, 2011; Taschner et al., 2012), whilst retrograde IFT (tip to base) requires IFT-A complexes and the cytoplasmic dynein 2 motor. In mammals, the cytoplasmic dynein 2 motor is poorly understood, but it is known to contain the dynein proteins Dync2h1 and Dync2li (Blacque et al., 2008; Verhey et al., 2011) as well as the intermediate chain Wdr34 and the light chain Dynll1 (Dominic Norris, unpublished data). Proteins are typically trafficked to the base of the cilium before being loaded into IFT particles. Trafficking of proteins from the Golgi to the cilium is not understood well, but is known to require the action of small GTPases of the Rab family and some members of the IFT-B complex (IFT54 and IFT20) (Follit et al., 2006; Follit et al., 2009; Lim et al., 2011).

Cilia in the node appear to be a special case of 9+0 motile primary cilia (Nonaka et al., 1998). Some controversy about whether all cilia in the node are 9+0 was raised by a study that used rapid fixation techniques that revealed a central pair

of microtubules in a proportion of cilia (Caspary et al., 2007). Interestingly, tracheal cilia (9+2) normally beat in a single plane but have been found to rotate in a node cilia-like fashion in individuals with central pair defects (Chilvers et al., 2003). Intriguingly, other microtubule doublet arrangements, including 9+4 cilia at the rabbit PNC, have been described (Feistel and Blum, 2006). However, directly linking motility to cilial ultrastructure in the node is beyond current experimental approaches.

Not all cilia in the node are motile. By performing localisation studies on Dnahc11 (also called left-right dynein (LRD)), an axonemal dynein heavy chain required for cilia motility (Okada et al., 1999; Supp et al., 1999; Supp et al., 1997), McGrath and colleagues showed that two populations of cilia exist in the mouse node; a central motile subset, and a more peripheral immotile population on the surface of crown cells around the node circumference (McGrath et al., 2003). These observations were synthesised into the 'two cilia' hypothesis in which the central motile cilia generate the leftward flow which is subsequently sensed by the peripheral immotile cilia (McGrath et al., 2003; Tabin and Vogan, 2003)[3]. Because the peripheral cilia are mainly immotile, it was assumed that these cilia are of the more classical sensory type than the more central rotating cilia.

Recently, the absolute requirement of the peripherally localised crown cell cilia for flow sensing has been demonstrated (Yoshiba et al., 2012). Yoshiba and colleagues utilised *Kif3a*$^{-/-}$ mutants, which lack all cilia (Marszalek et al., 1999; Takeda et al., 1999), but then rescued *Kif3a* expression specifically in node crown cells. In these embryos, the peripheral cilia were able to sense artificially applied unidirectional flow, demonstrating that crown cell cilia alone are sufficient for flow sensation (Yoshiba et al., 2012), and so strongly supporting the two cilia hypothesis.

Thus, cilia in the node, and in particular the lateral-most crown cell cilia, are crucial for the sensation of leftward flow. However, it remains unknown how flow elicits a sensory response. Two major models have been suggested in which cilia sense (1) a chemical determinant molecule (chemosensation) or (2) the force of fluid flow itself (mechanosensation). These two possibilities are now discussed.

---

[3] It should be noted that the 'two cilia' hypothesis originally stated that the immotile cilia sense the mechanical force of fluid flow (McGrath et al., 2003; Tabin and Vogan, 2003). However, I am taking 'two cilia' to mean that there are both motile and immotile cilia in the node, with the immotile subset sensing *either* mechanical force or a chemical determinant.

1.4.4.2. Chemical sensation

The chemical sensation model proposes that a morphogen is secreted into the node from the pit cells (Nonaka et al., 1998). This putative morphogen is then biased to the left edge of the node, due to leftward flow, where it binds to cell surface receptors and activates intracellular signalling cascades causing the initiation of asymmetric gene expression. The identity of this potential morphogen is unknown, though theoretical work suggests that it is likely to fall within the 40-50 kDa mass range (Okada et al., 2005). This model was extended by the discovery of large membrane-sheathed structures, called nodal vesicular parcels (NVPs), that bud from the node surface in a process controlled by FGF signalling, and move leftwards in the flow (Tanaka et al., 2005). NVPs are proposed to carry the morphogens Sonic hedgehog (Shh) and retinoic acid (RA). This cargo of morphogens is delivered to the left side of the node where NVPs open at the left edge, thereby invoking an asymmetrical signal (Tanaka et al., 2005). Theoretical considerations suggest that the forces in the node would be insufficient to break open NVPs physically (Cartwright et al., 2007), so instead there must exist an active opening mechanism.

1.4.4.3. Mechanical sensation

The second major model of flow perception is the mechanical sensation model, originally known as the 'two cilia' hypothesis (McGrath et al., 2003; Tabin and Vogan, 2003). This idea proclaims that flow itself is directly perceived cells within the node. Two types of cilia are found at the node of mouse embryos: (1) a centrally located motile cohort in which Dnahc11 (also called lrd) localises; and (2) a peripheral subset on the surface of node crown cells that do not express Dnahc11 (McGrath et al., 2003). This led to the idea that the motile cilia drive leftward fluid flow while the immotile cilia sense the flow. In support of this notion, it has recently been shown that cilia on the surface of crown cells are sufficient for the sensation of artificial flow when all other cilia are lost (Yoshiba et al., 2012). Importantly, the stress imparted on left-sided sensory cilia is thought to be greater than that at the right-hand side, thereby eliciting an asymmetrical response to force (Chen et al., 2011).

1.4.4.4. Ca^{2+} and polycystins: lessons from kidney

In the mouse node (McGrath et al., 2003) and zebrafish KV (Sarmah et al., 2005), the intracellular Ca^{2+} elevation observed on the left side is considered to be a readout of flow. The Ca^{2+} spike appears to occur in cells at the left edge of the node, but the signal then spreads more laterally in the endoderm between node and LPM (McGrath et al., 2003; Tabin and Vogan, 2003). How this Ca^{2+} signal relates to asymmetric gene expression at the node is unknown. One possibility is that the Ca^{2+} elevation could facilitate signalling through transcriptional regulation or morphogen movement, but at the moment these are speculative.

The left-sided Ca^{2+} elevation depends on the polycystin transmembrane cation channel Pkd2. Pkd2 localises to all node cilia, and loss of *Pkd2* causes severe L-R defects with loss of the left-sided Ca^{2+} spike (McGrath et al., 2003; Pennekamp et al., 2002; Tuson et al., 2011). Expression of *Pkd2* in the crown cells only of an otherwise *Pkd2* null transgenic embryo rescues L-R development, while loss of Pkd2 localisation to node cilia prevents its function (Yoshiba et al., 2012). These data argue that Pkd2 is required in crown cell cilia to sense flow and drive the asymmetric Ca^{2+} response, thereby cohering most simply with the mechanosensation hypothesis.

In humans *PKD2* mutations cause autosomal dominant polycystic kidney disease (ADPKD; OMIM 173900). ADPKD is characterised by the development of fluid filled cysts in the kidney, but can also affect other organs, including the liver and pancreas (Harris and Torres, 2009). As well as *PKD2*, a major gene implicated in ADPKD is *PKD1* which encodes another large transmembrane polycystin protein called Pkd1. Both *Pkd1*- and *Pkd2*- null mice die between 14.5 dpc and birth, exhibiting severe kidney cysts and vascular defects (Boulter et al., 2001; Wu et al., 2000). A model explaining the roles of Pkd1 and Pkd2 in kidney posits that the two proteins form a flow-sensing channel complex localised to cilia in the kidney lumen. The ectodomain of Pkd1 is thought to sense membrane stress caused by fluid flow (Nauli et al., 2003; Nauli and Zhou, 2004; Praetorius et al., 2003; Praetorius and Spring, 2003), while Pkd1 and Pkd2 are known to physically interact (Hanaoka et al., 2000; Qian et al., 1997). Stress sensing by Pkd1 is thought to induce the opening of Pkd2 channels, which elicit a Ca^{2+} response that have anti-growth, and thereby anti-cystic effects (Harris and Torres, 2009). Given that *Pkd2* mutants also

exhibit L-R defects and lose the asymmetric Ca^{2+} response around the node (McGrath et al., 2003; Pennekamp et al., 2002), it seems sensible to argue that a similar mechanism is acting in the node. However, Pkd2 is not known to have any mechanosensory properties, while Pkd1 is not to be involved in L-R determination (Karcher et al., 2005). Thus, at the outset of this thesis it was unknown what molecule was actually sensing the leftward flow in the node.

CHAPTER TWO

Pkd1l1 is required for the establishment of left-right asymmetry in the mouse

2.1. INTRODUCTION

Two ENU-based forward genetic screens were carried out to identify novel genes involved in embryonic development (Bogani et al., 2009; Ermakov et al., 2009; Field et al., 2011; Patterson et al., 2009). Phenotypic analysis of two lines derived from the screens – called *rks* and *lrm4* – revealed consistent defects in the establishment of left-right (L-R) asymmetry. The *lrm4* mutant disrupts *Pkd2*, a known component of the L-R pathway (Bisgrove et al., 2005; Ermakov et al., 2009; Pennekamp et al., 2002; Schottenfeld et al., 2007). The *rks* line, in contrast, was mapped to a novel locus not previously associated with the establishment of L-R asymmetry: *Pkd1l1*. In this thesis, I describe my work characterising these two mutant lines and assessing the cellular function of the two genes, *Pkd1l1* and *Pkd2*. In this chapter, the gross morphological abnormalities in establishing L-R asymmetry in *rks* and *lrm4* mutant embryos are described.

2.2. RESULTS

2.2.1. *rks*: an ENU-induced *Pkd1l1* allele

During a forward genetics ENU mutagenesis screen (**Figure 2.1A**) (Bogani et al., 2009; Patterson et al., 2009), a mouse mutant exhibiting whole-body oedema and situs defects was discovered[4]. The mutant line was named rikishi (*rks*). To characterise the genetic lesion causing the *rks* phenotype, positional cloning was carried out by Sarah Field (Field, 2009). These experiments revealed a minimal region of 0.2 Mb on Chromosome 11 in which the *rks* mutation resides; this region contains only the gene *Pkd1l1* and two pseudogenes, RP23-39H1.3-001 and RP23-39H1.2-001 (**Figure 2.1B**). Sequencing of the annotated coding elements of *Pkd1l1* (53 exons) and the two pseudogenes revealed a single difference between wild-type and mutant DNA sequence: an A-to-G transition at position 1232 (A1232G) within *Pkd1l1* (**Figure 2.1B**) (Field, 2009). This mutation was therefore a strong candidate as the phenotype-causing genetic lesion in *rks* mutants.

There exist three common methods for designating ENU mutants as alleles of particular genes (Kile and Hilton, 2005). First, the minimal region is narrowed until

[4] Andy Greenfield and colleagues performed the ENU screen which led to the discovery of the *rks* line.

it contains only a single gene; second, the putative allele fails to complement a second allele of the same gene; and third, the mutant phenotype can be rescued by addition of a functional copy of the candidate gene e.g. by bacterial artificial chromosome (BAC)-mediated expression. Having already narrowed the minimal region to contain only one coding gene, we also implemented the second method to assess whether the A1232G mutation in *Pkd1l1* is responsible for the *rks* phenotype by performing a complementation test. To this end, we intercrossed *rks* with an engineered *Pkd1l1* null mutant (to be described in detail in **§4.2.2**). At 13.5 days *post coitum* (dpc), mouse embryos exhibit several overt morphological indications of L-R asymmetric development. For example, both the heart and stomach lie towards the left side of the body cavity, while the right and left lungs have different numbers of lobes, four and one respectively (R:L=4:1). Wild-type embryos and single heterozygotes exhibited this normal situs of the lungs, stomach, and heart. On the contrary, all six *trans*-heterozygotes were phenotypic, exhibiting gross situs defects including reversed heart positioning (n=2/6), reversed stomach positioning (n=2/6) and right pulmonary isomerism, with four lung lobes on both the left and right sides (R:L=4:4; n=4/6) (**Figure 2.1C-D**). Thus, the *Pkd1l1* null and *rks* alleles belong to the same complementation group. Together, these results designate *rks* as a bona fide allele of *Pkd1l1*, henceforth named *Pkd1l1*^{rks}.

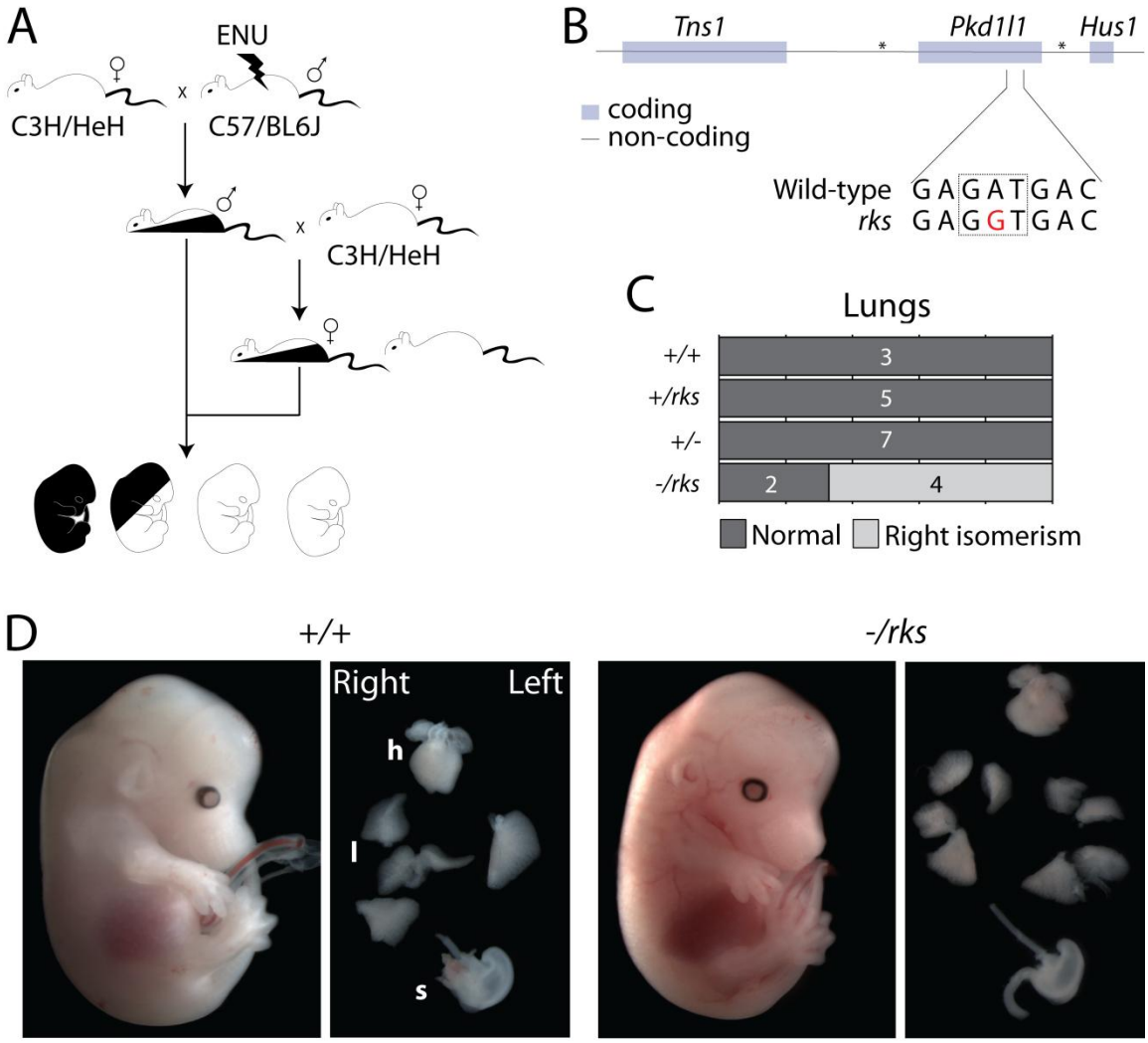

Figure 2.1. The ENU-induced mutation *rks* resides within the *Pkd1l1* gene

A Schematic of the three-generation ENU-mutagenesis screen from which the rks line arose. ENU-mutagenised C57/Bl6J males were bred with wild-type C3H/HeH females to produce F1 mice. F1 males were then crossed to C3H/HeH females, producing F2 females that were back-crossed to their fathers, yielding G3 embryos that were examined at 13.5 dpc for morphological abnormalities. **B** The *rks* minimal region was mapped to the *Pkd1l1* locus (between the asterisks). Sequencing of this region revealed a single A-to-G transition in the 8th exon of *Pkd1l1*. **C, D** Complementation test between *rks* and a *Pkd1l1* null mutant generated trans-heterozygous mutants with situs defects. Right pulmonary isomerism was evident in 4/6 embryos (C,D) whilst inverted heart and/or stomach positioning, were also observed. h - heart; l - lungs; s - stomach.

2.2.2. *Pkd1l1*$^{rks/rks}$ embryos exhibit severe left-right defects and arrest by 15.5 dpc

The *Pkd1l1*^{rks} mutation arose on the B6J background. The line was then maintained on a C3H/HeH background; continued backcrossing to C3H provided a uniform

genetic background for analyses and also segregated away other possible, though undiscovered, ENU-mutations that could have impacted upon the phenotype. The remainder of this thesis describes analyses performed using congenic C3.B6-*Pkd1l1*^{rks} mice, unless otherwise stated.

During the ENU screen, *rks* embryos exhibited gross situs and heart defects at 13.5 dpc (Andy Greenfield, personal communication). We therefore supposed that embryos arrest *in utero*. To assess age-of-death, we performed dissections and genotyping of embryos aged 13.5-15.5 dpc from *Pkd1l1*$^{+/rks}$ intercrosses. At both 13.5 and 14.5 dpc, normal Mendelian genotype frequencies were evident (**Figure 2.2A**). By 15.5 dpc, however, only two living *Pkd1l1*$^{rks/rks}$ homozygotes were identified from 23 total embryos (4 litters) (**Figure 2.2A**). Moreover, both these mutant embryos were developmentally delayed and appeared close to death. This indicates that *Pkd1l1*$^{rks/rks}$ mutants usually fail to survive in significant numbers beyond 14.5 dpc.

The dextral looping of the embryonic heart is the earliest known signature of morphological asymmetry in mouse. Normally the heart tube loops from left to right, describing a C-shape when viewed from the ventral aspect. Subsequently, the embryo rotates into a foetal position, with the tail becoming positioned to the embryos right side. Given that gross situs defects were observed in the *rks* line during the ENU screen, we generated *Pkd1l1*$^{rks/rks}$ embryos at 9.5 dpc and scored the direction of axial rotation and the direction of heart tube looping. Genetically wild-type and *Pkd1l1*$^{+/rks}$ embryos exhibited normal axial rotation (**Figure 2.2B**). Contrarily, *Pkd1l1*$^{rks/rks}$ mutants exhibited either normal (n=4/16) or reversed (n=9/16) directions of rotation (**Figure 2.2B; Table 2-1**); the remaining three embryos turned in no particular direction (n=3/16), with the tail becoming positioned centrally (**Table 2-1**). The process of turning itself occurred in all *Pkd1l1*$^{rks/rks}$ embryos. Heart tube looping was normal in wild-type and *Pkd1l1*$^{+/rks}$ heterozygotes. In *Pkd1l1*$^{rks/rks}$ mutants, however, the heart tube occasionally looped in the reverse direction (n=4/29), though the majority of the 29 mutants analysed exhibited normal heart tube looping (n=19/29) (**Table 2-1**). Moreover, a proportion of *Pkd1l1*$^{rks/rks}$ retained a linear heart tube (n=6/29), with neither leftward nor rightward looping occurring at 9.5 dpc (**Table 2-1**).

When scored at 13.5 dpc, *Pkd1l1*$^{rks/rks}$ mutants displayed other morphological abnormalities characteristic of deranged L-R development. Wild-type and *Pkd1l1*$^{+/rks}$ heterozygotes exhibited normal lung situs, with four right sided lobes and a single left lobe (4:1) (**Figure 2.2E**). However, all 46 mutant embryos examined demonstrated right pulmonary isomerism, with the right and left lungs being largely symmetrical, having four lobes on each side (4:4) (**Figure 2.2H**; **Table 2-1**). This result is indicative of a lack of specification of the left-side. Normal asymmetric morphogenesis of the heart and stomach results in these structures being positioned to the left side in the body cavity (**Figure 2.2D**). By contrast, the hearts and stomachs of *Pkd1l1*$^{rks/rks}$ mutants were often mispositioned (**Table 2-1**). While 32/46 *Pkd1l1*$^{rks/rks}$ exhibited a normal left-sided heart (laevocardia) (**Figure 2.2G; Table 2-1**), 13/46 mutants demonstrated reversal of heart positioning (dextrocardia) (**Figure 2.2G'; Table 2-1**); a single *Pkd1l1*$^{rks/rks}$ embryo had a centrally positioned heart apex (mesocardia) (**Table 2-1**). Similarly, stomach situs was often normal (n=14/23) but also frequently reversed (n=8/23) or central (n=1/23) in *Pkd1l1*$^{rks/rks}$ mutants (**Figure 2.2G; Table 2-1**).

As well as gross mispositioning of the heart, *Pkd1l1*$^{rks/rks}$ mutants exhibited defects of heart patterning. Cardiac malformations including double outlet right ventricle, transposition of the great arteries, and ventral septal defects were observed in mutants at 13.5-14.5 dpc (Field, 2009). Heart defects such as these are often caused by aberrant L-R patterning (Ramsdell, 2005). Oedema around the heart, and sometimes whole-body oedema was also observed in mutants; we reasoned that cardiac defects caused this phenotype, as well as the embryonic death by 15.5 dpc.

Thus, *Pkd1l1*$^{rks/rks}$ mutants exhibit abnormalities in the direction of axial rotation and heart tube looping, as well as right pulmonary isomerism, gross mispositioning of the heart and stomach, and heart patterning defects. Taken together, these data therefore demonstrate that *Pkd1l1*$^{rks/rks}$ mutants exhibit severe morphological L-R abnormalities.

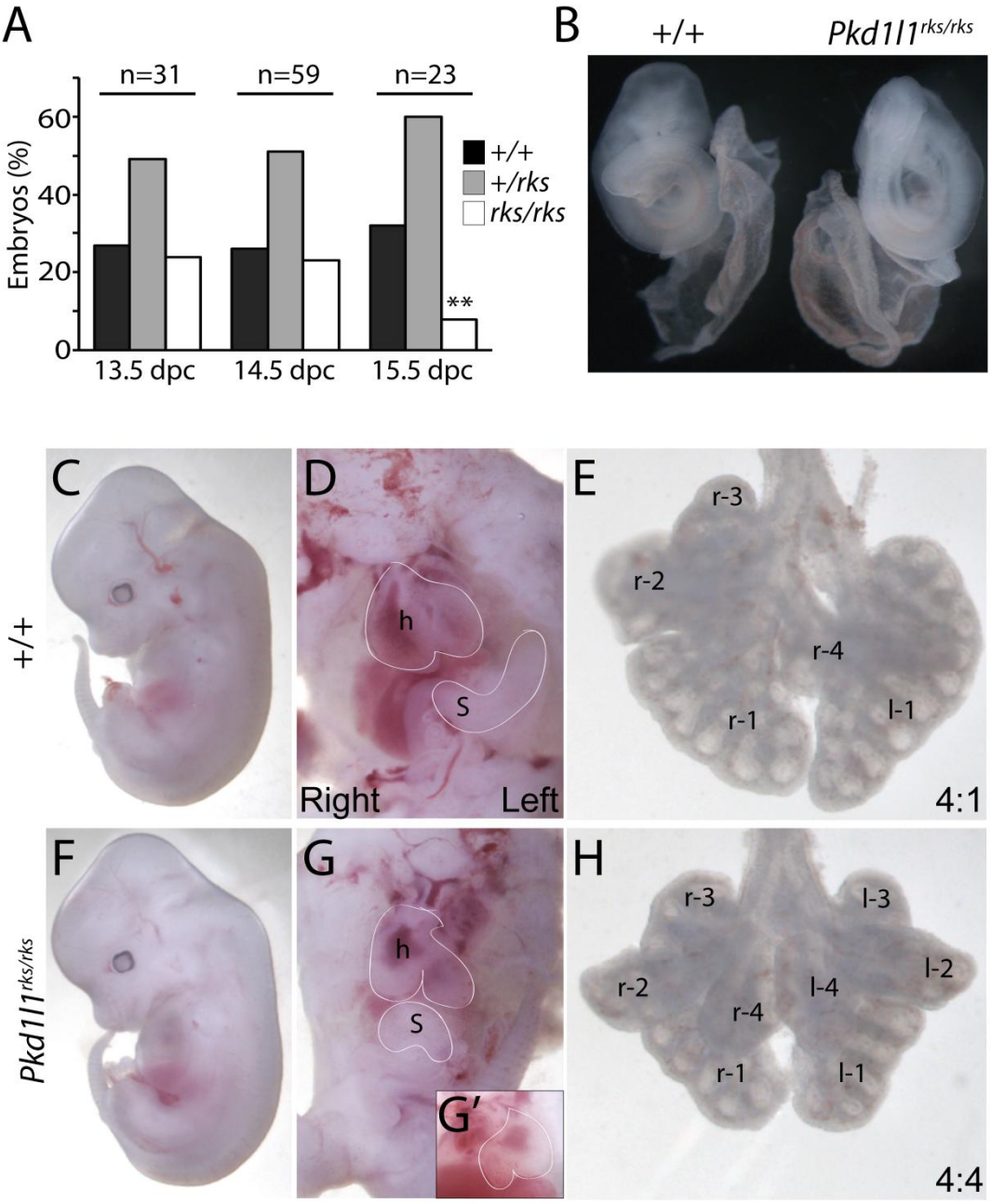

Figure 2.2. *Pkd1l1*$^{rks/rks}$ mutants exhibit gross situs defects and arrest by 15.5 dpc

A Number of living embryos of indicated genotypes at 13.5, 14.5, and 15.5 dpc. At 15.5 dpc, the number of homozygous embryos significantly departs from that expected ($p>0.01$, **). **B** Wild-type and *Pkd1l1*$^{rks/rks}$ mutant embryos at 9.5 dpc showing reversed embryonic turning in the mutant. **C** Wild-type whole embryo at 13.5 dpc showing **D** leftward heart apex and stomach positioning and **E** normal lung situs (4:1). **F** *Pkd1l1*$^{rks/rks}$ mutant embryo with **G** normal heart apex positioning but a centrally localised stomach and **H** right pulmonary isomerism (4:4). **G'** A second *Pkd1l1*$^{rks/rks}$ mutant embryo exhibiting a reversed heart apex position. h - heart, s - stomach, l - left lung lobe, r - right lung lobe.

Table 2-1 Gross phenotype of *Pkd1l1*$^{rks/rks}$ and *Pkd2*$^{lrm4/lrm4}$ embryos

	Normal	Inverted	Midline	RI	n
***Pkd1l1*$^{rks/rks}$**					
Axial rotation	4 (25.0)	9 (56.3)	3 (18.8)	-	16
Heart looping	19 (65.5)	4 (13.8)	6 (20.7)	-	29
Lung situs			-	46 (100)	46
Heart apex	32 (70.0)	13 (28.0)	1 (2.0)	-	46
Stomach situs	14 (60.9)	8 (34.8)	1 (4.3)	-	23
***Pkd2*$^{lrm4/lrm4}$**					
Axial rotation	3 (27.2)	7 (63.6)	1 (9.1)	-	11
Heart looping	6 (33.3)	12 (66.7)		-	18
Lung situs	1 (2.0)		-	48 (98.0)	49
Heart apex	21 (52.5)	17 (42.5)	2 (5.0)	-	40
Stomach situs	20 (52.6)	12 (31.7)	6 (15.8)	-	38

Axial rotation and heart looping were scored at 9.5 dpc. Lung situs, heart apex and stomach situs were scored at 13.5 dpc. Shown is the number of embryos exhibiting the defect among the total number examined (n), with percentages in brackets. RI – right isomerism

2.2.3. *Pkd1l1*$^{rks/rks}$ embryos strongly phenocopy *Pkd2*$^{lrm4/lrm4}$ mutants

The *Pkd1l1*$^{rks/rks}$ phenotype struck us as being similar to that of *Pkd2* null mutant mice that also exhibit highly penetrant right pulmonary isomerism (Pennekamp et al., 2002). Left-right mutant 4 (*lrm4*) is an ENU-induced point mutation in *Pkd2* (Ermakov et al., 2009) that encodes a glutamic acid-to-glycine amino acid point substitution at position 442 in the protein (to be discussed in **Chapter five**). Analyses performed during the ENU screen, when embryos were on a mixed genetic background and likely harboured additional ENU mutations, showed that *Pkd2*$^{lrm4/lrm4}$ mutants exhibited a high penetrance of right pulmonary isomerism (around 70%) (Ermakov et al., 2009). To compare the *Pkd2*^{lrm4} phenotype with *Pkd1l1*^{rks}, we generated a C3H congenic *Pkd2*^{lrm4} line and analysed gross situs as for *Pkd1l1*^{rks}. The remainder of this thesis describes work performed using congenic C3.C-*Pkd2*^{lrm4} mutants, unless otherwise stated.

Like *Pkd1l1*$^{rks/rks}$ mutants, *Pkd2*$^{lrm4/lrm4}$ embryos exhibited a very high incidence of right pulmonary isomerism at 13.5 dpc (4:4; n=48/49) (**Figure 2.3H; Table 2-1**), notably higher than was observed on a mixed genetic background (Ermakov et al., 2009). Whole-body oedema was also obvious in *Pkd2*$^{lrm4/lrm4}$ mutants, likely owing to heart patterning defects (Ermakov et al., 2009). The stomach and heart apex position were often either reversed or central in mutants, rather than leftwards (**Figure 2.3G; Table 2-1**). At 9.5 dpc, *Pkd2*$^{lrm4/lrm4}$ mutants exhibited incidences of abnormal direction of embryonic turning and heart tube looping (**Figure 2.3B**; **Table 2-1**). Thus, *Pkd2*$^{lrm4/lrm4}$ mutants also exhibit severe L-R defects that appear highly similar to those of *Pkd1l1*$^{rks/rks}$ mutants.

Statistical testing was employed to assess the similarities/differences in phenotypes between *Pkd1l1*$^{rks/rks}$ and *Pkd2*$^{lrm4/lrm4}$ mutants. There were no statistically significant differences in axial rotation, stomach positioning, heart apex positioning or lung situs between the two mutants (**Table 2-2**). However, the direction of heart tube looping at 9.5 dpc, being normal in 65.5% of *Pkd1l1*$^{rks/rks}$ (n=19/29) but reversed in 66.7% of *Pkd2*$^{lrm4/lrm4}$ (n=12/18), represented a statistically significant difference between the two mutants.

Like *Pkd1l1*$^{rks/rks}$ embryos, *Pkd2*$^{lrm4/lrm4}$ mutants also arrested at approximately 14.5 dpc (**Figure 2.3A**). Together, these data argue that the *Pkd1l1*^{rks} and *Pkd2*^{lrm4} mutant phenotypes are highly similar when assessed on an identical genetic background, arguing that Pkd1l1 and Pkd2 act in the same or closely overlapping biochemical pathways during the establishment of L-R asymmetry.

Table 2-2 Statistical comparison *Pkd1l1*$^{rks/rks}$ and *Pkd2*$^{lrm4/lrm4}$ phenotypes

	P value	Significant (CI=95%)	Significant (CI=99%)	Test
Axial rotation	0.7854	No	No	Chi-square
Heart looping	0.0006	Yes	Yes	Chi-sqaure
Lung situs	1.0000	No	No	Fisher's exact
Heart apex	0.2535	No	No	Chi-sqaure
Stomach situs	0.3958	No	No	Chi-sqaure

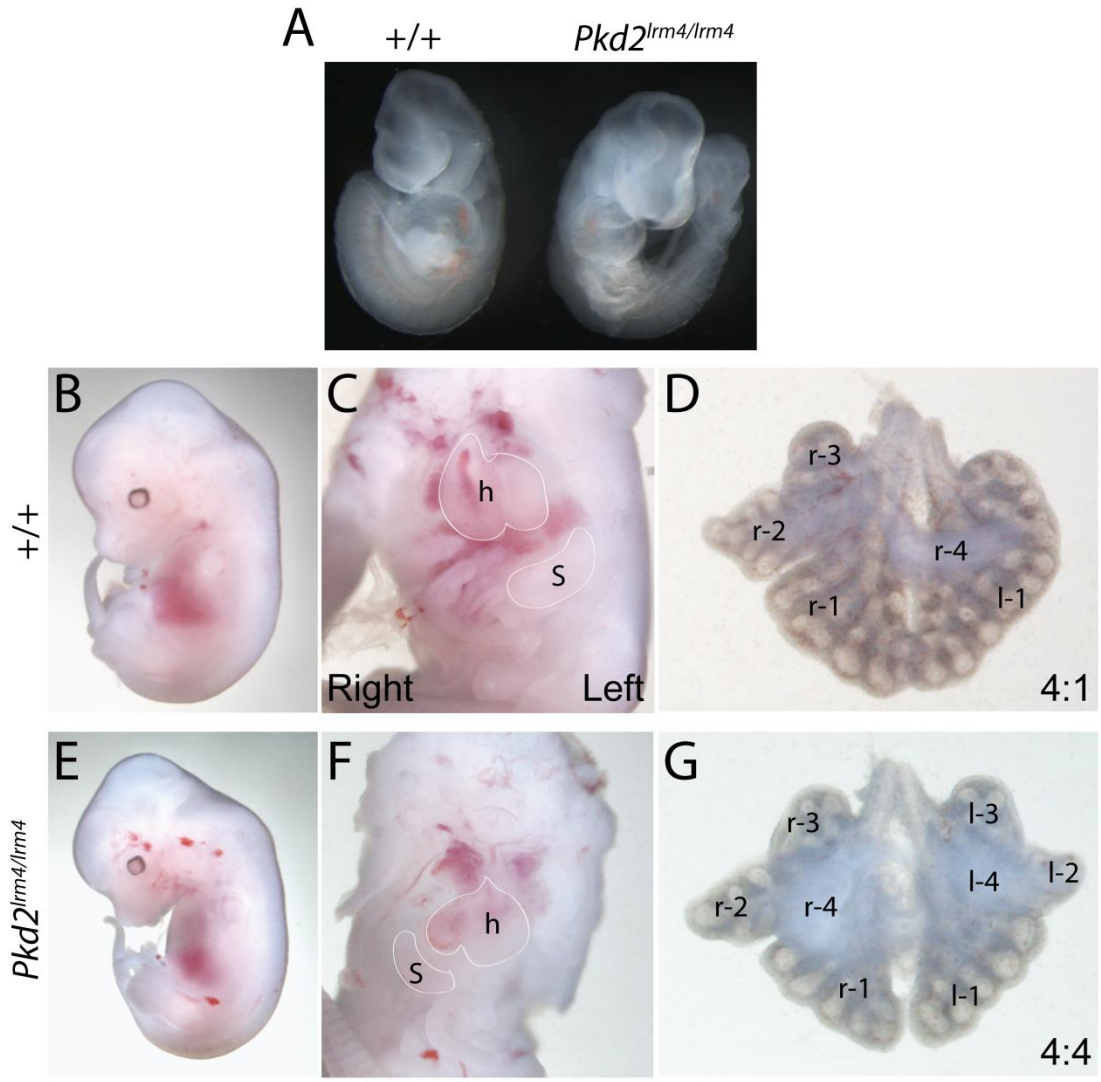

Figure 2.3. *Pkd2*$^{lrm4/lrm4}$ mutants exhibit gross situs defects

A Wild-type and *Pkd2*$^{lrm4/lrm4}$ mutant embryos at 9.5 dpc showing reversed embryonic turning in the mutant. **B** Wild-type whole embryo at 13.5 dpc showing **C** leftward heart apex and stomach positioning and **D** normal lung situs (4:1). **E** *Pkd2*$^{lrm4/lrm4}$ mutant embryo with **F** reversed heart apex and stomach positioning and **G** right pulmonary isomerism (4:4). h - heart, s - stomach, l - left lung lobe, r - right lung lobe.

2.2.4. There exists no obvious genetic interaction between *Pkd1l1*^{rks} and *Pkd2*^{lrm4}

No situs defects were evident in adult *Pkd1l1*$^{+/rks}$ or *Pkd2*$^{+/lrm4}$ mice, indicating that these alleles are genetically recessive. To test for a genetic interaction between the two, which can reveal functional relationships between genes and pathways (Mani et al., 2008), we crossed *Pkd1l1*$^{+/rks}$ and *Pkd2*$^{+/lrm4}$, generating 178 mice. Analysed at weaning, neither single nor double heterozygotes demonstrated situs defects: heart, stomach, spleen and lung situs were assessed. Furthermore, all genotypes were represented at Mendelian frequencies, with no loss of either single or double heterozyotes (**Figure 2.4**). Thus, no obvious genetic interaction exists between *Pkd1l1*^{rks} and *Pkd2*^{lrm4} alleles.

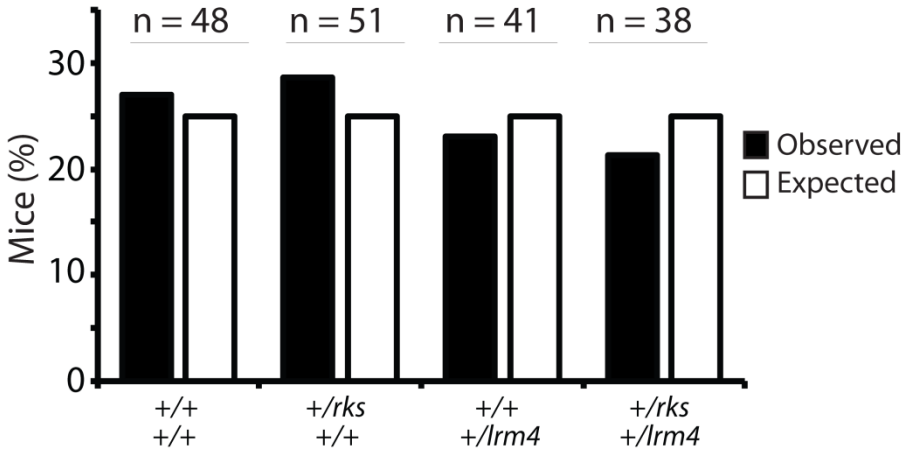

Figure 2.4. There exists no obvious genetic interaction between *Pkd1l1*^{rks} and *Pkd2*^{lrm4}

Intercrosses between *Pkd1l1*$^{+/rks}$ and *Pkd2*$^{+/lrm4}$ mice resulted in the expected ratio of genotypes (p=0.857; Chi square test).

2.2.5. Loss of the left-sided Nodal cascade in *Pkd1l1*$^{rks/rks}$ and *Pkd2*$^{lrm4/lrm4}$ mutant embryos

During the establishment of L-R asymmetry, *Nodal* is expressed asymmetrically in the left lateral plate mesoderm LPM, but remains absent from the right side of the embryo (Collignon et al., 1996; Lowe et al., 1996). In the left LPM, Nodal activates the expression of *Lefty2* and *Pitx2* (Burdine and Schier, 2000; Collignon et al., 1996; Levin et al., 1995; Logan et al., 1998; Lowe et al., 1996; Meno et al., 1996; Ryan et al., 1998). This left sided Nodal cascade is highly conserved and is crucial for

generating L-R asymmetric differences during embryogenesis. Therefore, in order to understand the origin of the L-R defects exhibited by *Pkd1l1*$^{rks/rks}$ and *Pkd2*$^{lrm4/lrm4}$ embryos, we assessed Nodal activity in the LPM of mutants by performing a whole mount in situ hybridisation (WISH) expression study of *Nodal* and its targets *Lefty1*, *Lefty2*, and *Pitx2*. Intercrosses between heterozygotes (*Pkd1l1*$^{+/rks}$ x *Pkd1l1*$^{+/rks}$ and *Pkd2*$^{+/lrm4}$ x *Pkd2*$^{+/lrm4}$) were set up; embryos were dissected at 8.5 dpc (usually staged between 2-7 somites), then processed for WISH (see **Experimental Procedures**). Genotyping was performed post-WISH and after gene expression pattern had been scored to eliminate bias.

All wild-type and heterozyous littermates (*Pkd1l1*$^{+/rks}$ and *Pkd2*$^{+/lrm4}$) exhibited the normal pattern of *Nodal*, with expression observed in the left LPM between the 3-6 somite stages (**Figure 2.5A**), consistent with published data (Collignon et al., 1996; Lowe et al., 1996). *Nodal* is also expressed perinodally at this stage (**Figure 2.5A**; see Discussion in **Chapter 3**). In contrast to the exclusively left sided expression in control embryos, *Nodal* was not expressed in LPM tissue in either *Pkd1l1*$^{rks/rks}$ (n=17/17) or *Pkd2*$^{lrm4/lrm4}$ (n=16/16), though expression was maintained around the node (**Figure 2.5A; Table 2-3**).

In the left LPM, Nodal signalling activates the expression of *Lefty2* and *Pitx2*, while Nodal ligand diffusing to the midline activates *Lefty1* expression in the left prospective floor plate (Yamamoto et al., 2003). We observed these expression patterns in wild-type, *Pkd1l1*$^{+/rks}$ and *Pkd2*$^{+/lrm4}$ embryos (**Figure 2.5B-C**). However, *Pkd1l1*$^{rks/rks}$ and *Pkd2*$^{lrm4/lrm4}$ mutants demonstrated absence of expression of both *Lefty* genes as well as *Pitx2* (**Figure 2.5B-C; Table 2-3**).

Table 2-3 Molecular phenotype of *Pkd1l1*$^{rks/rks}$ and *Pkd2*$^{lrm4/lrm4}$ embryos

	Left	Absent	Bilateral	n
***Pkd1l1*$^{rks/rks}$**				
LPM *Nodal*	0	17	0	17
LPM/midline *Lefty*	0	9	0	9
LPM *Pitx2*	0	43	1	44
***Pkd2*$^{lrm4/lrm4}$**				
LPM *Nodal*	0	16	0	16
LPM/midline *Lefty*	0	19	0	19
LPM *Pitx2*	0	17	0	17

Expression of *Nodal*, *Lefty1/2* and *Pitx2* were examined by whole mount in situ hybridisation (WISH) of 8.5 dpc embryos. Shown is the number of embryos exhibiting the indicated expression pattern among the total examined (n). LPM – lateral plate mesoderm.

The loss of activity of the Nodal cascade in the LPM of mutant embryos could be due to a loss in the integrity of the LPM structure. However, we observed normal expression of *Twist*, a marker of the LPM, in *Pkd1l1*$^{rks/rks}$ and *Pkd2*$^{lrm4/lrm4}$ mutants (data not shown), suggesting that LPM is specified normally in mutants. Similarly, *Shh* and *Foxa2* were expressed normally in the midline of *Pkd1l1*$^{rks/rks}$ and *Pkd2*$^{lrm4/lrm4}$ embryos (data not shown), showing that this important tissue is present and correctly specified in mutants. Furthermore, the fact that both *Pkd1l1*$^{rks/rks}$ and *Pkd2*$^{lrm4/lrm4}$ mutants develop normally, notwithstanding L-R and associated cardiac defects, until 14.5 dpc argues strongly that the LPM and midline are correctly specified in mutants.

In conclusion, *Pkd1l1*$^{rks/rks}$ and *Pkd2*$^{lrm4/lrm4}$ mutants entirely lack LPM Nodal induction, a phenotype which explains the organ situs defects apparent in older embryos. Based on these data alone, we cannot ascertain whether the mutations affect the competence of the LPM to perform Nodal signalling, or whether mechanisms upstream of left LPM *Nodal* induction have been disrupted.

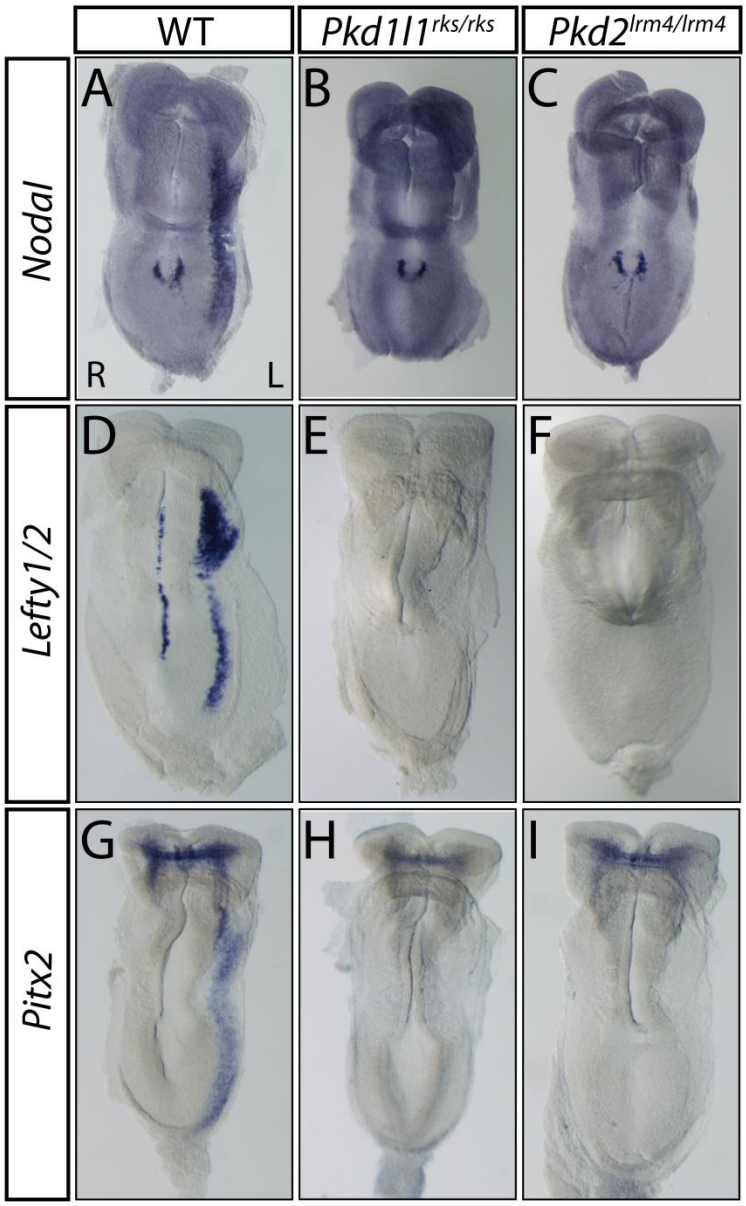

Figure 2.5. Loss of left sided loci in *Pkd1l1*$^{rks/rks}$ and *Pkd2*$^{lrm4/lrm4}$ mutants

A-I Whole mount in situ hybridisation for *Nodal, Lefty1/2*, and *Pitx2* in *Pkd1l1*$^{rks/rks}$ and *Pkd2*$^{lrm4/lrm4}$ mmutants and wild-type (WT) control embryos. **A-C** *Nodal* expression is present around the node but is lost in the left LPM in mutant embryos. As a result, *Lefty1/2* (D-F) and *Pitx2* (G-H) left-sided expression is also lost.

2.3. DISCUSSION

In this chapter, a new L-R mutant, harbouring a mutation at the *Pkd1l1* locus, has been characterised and compared directly to *Pkd2*^{lrm4} mutants. *Pkd1l1*$^{rks/rks}$ and *Pkd2*$^{lrm4/lrm4}$ have almost identical L-R phenotypes; strikingly, both mutations prevent initiation of the crucial left-sided Nodal cascade. This work, therefore, has uncovered an important new molecule required for L-R patterning in mouse. Although, we found no evidence of a genetic interaction between *Pkd1l1*^{rks} and *Pkd2*^{lrm4} in doubly heterozygous mice, the fact that *Pkd1l1* and *Pkd2* mutants have very similar phenotypes suggests that the two genes act in the same or closely related pathways to control L-R asymmetry.

2.3.1. *rks* is a novel allele of *Pkd1l1* with severe left-right defects

The *rks* mutation was derived from a three generation ENU mutagenesis screen (Bogani et al., 2009; Patterson et al., 2009). Sequencing of candidate causative genes revealed an A1232G transition within *Pkd1l1* (Field, 2009). A complementation test with a known *Pkd1l1* null allele (Vogel et al., 2010) demonstrated that the phenotype in *rks* mutants was caused by disruption of *Pkd1l1*. Severe L-R defects are apparent in *Pkd1l1*$^{rks/rks}$ mutants including right lung isomerism and randomisation of heart and stomach situs. These defects are consistent with lack of establishment of asymmetric gene expression, and indeed we find a loss of the normally left-restricted LPM Nodal cascade in mutants. Recently, it has been found that *Pkd1l1* is also required for L-R patterning in the medaka fish (Kamura et al., 2011). Together with our data, this reveals the requirement for *Pkd1l1* during the establishment of L-R asymmetry to be conserved.

2.3.2. *Pkd2*$^{lrm4/lrm4}$ mutants exhibit L-R defects that are distinct from *Pkd2*$^{-/-}$ mutants

Homozygous *Pkd2*$^{lrm4/lrm4}$ mutants exhibited almost identical L-R phenotypes to *Pkd1l1*$^{rks/rks}$ mutants, with right pulmonary isomerism and loss of the left LPM Nodal cascade. Previously, the L-R defects of a *Pkd2* null allele (MGI - *Pkd2*^{tm1Dwo}) have been assessed (Pennekamp et al., 2002). Intriguingly, Pennekamp and colleagues reported a *Pkd2*$^{-/-}$ phenotype that is similar to *Pkd2*$^{lrm4/lrm4}$, but with some notable differences as well. For example, while right pulmonary isomerism was reported in

90% of mutants, *Pitx2* was expressed bilaterally in the LPM in 67% of *Pkd2*$^{-/-}$ embryos (Pennekamp et al., 2002). Moreover, *Nodal* and *Lefty2* were not expressed in the LPM in 87% and 100% of *Pkd2*$^{-/-}$ embryos, respectively. The authors argue that the right isomerism in *Pkd2*$^{-/-}$ mutants results from *Pitx2* expression, though bilateral, being restricted to the posterior LPM (Pennekamp et al., 2002). Nevertheless, it is difficult to reconcile the very low level *Nodal* activation in mutants with the fact that two thirds express *Pitx2* bilaterally. The authors suggest that *Nodal* might be induced bilaterally at levels too low to be detected by WISH (Pennekamp et al., 2002). Recently, another analysis of *Pkd2*$^{-/-}$ embryos has been reported (Yoshiba et al., 2012), with results highly similar to the Pennekamp report. Yoshiba and colleagues found that 100% of *Pkd2*$^{-/-}$ mutants lacked LPM *Nodal*, while 45% lacked *Pitx2*; of the others, *Pitx2* expression was left (10%), right (15%) or bilateral (30%) (Yoshiba et al., 2012).

There are two likely explanations for the phenotypic discrepancy between *Pkd2*$^{lrm4/lrm4}$ and *Pkd2*$^{-/-}$ mutants: (1) *Pkd2*^{lrm4} is not a null, but rather a more complicated allele (discussed further in **Chapter 5**); or (2) The phenotypic differences are due to differences in genetic background; *Pkd2*^{lrm4} mutants were assessed here on the C3H background, while *Pkd2*$^{-/-}$ were on a mixed 129;B6 background (Pennekamp et al., 2002), and the background used by Yoshiba and colleagues was not reported (Yoshiba et al., 2012). Indeed, more outcrossed *Pkd2*$^{lrm4/lrm4}$ mutants assessed during the initial screen only showed 70% right pulmonary isomerism (Ermakov et al., 2009), arguing that genetic background affects the penetrance of abnormalities in *Pkd2*$^{lrm4/lrm4}$ mutants. It seems feasible to suggest that a combination of these two explanations results in the phenotypic differences observed.

2.3.3. *Pkd1l1*$^{rks/rks}$ and *Pkd2*$^{lrm4/lrm4}$ mutants exhibit phenotypes similar to other mutants that fail to activate LPM *Nodal* expression

Pkd1l1$^{rks/rks}$ and *Pkd2*$^{lrm4/lrm4}$ mutants both exhibit loss of left-sided *Nodal* and *Pitx2* expression at 8.5 dpc. This is manifest in the phenotypes that the mutants exhibit later in development, with both demonstrating abnormalities of heart looping and embryonic turning as well as heart apex position, stomach sidedness, and lung lobation (**Table 2-1**). These phenotypes are highly similar to those of other mutants

that have lost left-sided *Nodal* expression. Mice lacking *Cryptic*, a mouse EGF-CFC gene, for example, exhibit normal node *Nodal* expression but fail to initiate the left LPM Nodal cascade, resulting in absence of asymmetric LPM *Nodal*, *Lefty2*, and *Pitx2* (Gaio et al., 1999; Yan et al., 1999). The loss of *Nodal* and *Pitx2* in the LPM of *Cryptic* mutants results in right pulmonary isomerism in 100% of animals, together with randomised stomach and heart apex positioning (Gaio et al., 1999; Yan et al., 1999), identical to *Pkd1l1*$^{rks/rks}$ and *Pkd2*$^{lrm4/lrm4}$ mutants. Other mutants that affect the core Nodal pathway present with similar defects (**Table 2-4**) including *Nodal*$^{\Delta node/-}$ (Brennan et al., 2001), *ActRIIB*$^{-/-}$ (Oh and Li, 1997) and *Gdf1*$^{-/-}$ (Rankin et al., 2000). Thus, in the absence of left LPM *Nodal* induction, positioning of the heart and stomach is usually randomised, while the lungs develop right isomerism.

One mechanism by which Nodal signalling is thought to act in situs-specific organogenesis is by inducing the homeobox gene *Pitx2* in the left LPM. After *Nodal* is switched off in the LPM, *Pitx2* expression is maintained during organogenesis by a feed-forward loop involving Nkx2 (Shiratori et al., 2001). Loss of left LPM *Pitx2* expression in mouse, by deletion of the ASE enhancer required for activation by Nodal-FoxH1 signalling, causes occasional reversal of heart apex position (n=5/18) and fully penetrant right pulmonary isomerism (n=18/18) (Shiratori et al., 2006). However, heart looping, embryonic turning, and stomach positioning were not affected by loss of *Pitx2* (**Table 2-4**) (Shiratori et al., 2006), suggesting that other factors downstream of Nodal activity are required for these aspects of side-specific organogenesis. This implies that at least two pathways operate downstream of left-sided Nodal to affect asymmetric morphogenesis; one requiring both Nodal and Pitx2 and a second being dependent on Nodal but not on Pitx2. In *Pkd1l1*$^{rks/rks}$ and *Pkd2*$^{lrm4/lrm4}$ mutants, both *Nodal* and *Pitx2* are lost in the LPM and so asymmetric morphogenesis that is dependent on *Pitx2* is affected but so too are any features that require *Nodal* for asymmetric development.

Table 2-4 Phenotypic comparison of various L-R mutants

	Axial rotation	Heart looping	Heart apex	Stomach position	Lung situs
Pkd1l1$^{rks/rks}$	Random*	Most normal, some reversed	Random	Random	Right isomerism
Pkd2$^{lrm4/lrm4}$	Random	Random	Random	Random	Right isomerism
Pitx2$^{\Delta ASE/\Delta ASE}$	Normal	Normal	Random	Normal	Right isomerism
Cryptic$^{-/-}$	ND	ND	Random	Random	Right isomerism
Nodal$^{\Delta node/-}$	ND	Random	Random	Random	Right isomerism
Gdf1$^{-/-}$	ND	ND	Random	Random	Right isomerism
ActRIIB$^{-/-}$	ND	ND	Random	Normal	Right isomerism
Lefty1$^{-/-}$	ND	ND	Normal	ND	Left isomerism
Lefty2$^{\Delta ASE/\Delta ASE}$	ND	ND	Normal	ND	Left isomerism

*Phenotypes are defined as 'random' if they are not significantly different to a 50/50 randomised phenotype (Chi-square analysis applied). ND – not determined

In contrast to mutants that fail to establish the left-sided Nodal cascade, *Lefty1*$^{-/-}$ mutants activate the cascade bilaterally, though ectopic right-sided activation is restricted to the anterior half of the LPM (Meno et al., 1998). In *Lefty2*$^{-/-}$ mutants, *Nodal* and *Pitx2* are expressed in both the left and right LPM, while *Nodal* expression is maintained for a few hours after it would normally be swithed off at the 6 somite stage (Meno et al., 2001). In both *Lefty1*$^{-/-}$ and *Lefty2*$^{\Delta ASE/\Delta ASE}$ mutants, pulmonary left isomerism is fully penetrant, though mutants nearly always exhibit a normal leftward pointing heart apex (Meno et al., 1998; Meno et al., 2001).

In summary, *Pkd1l1*$^{rks/rks}$ and *Pkd2*$^{lrm4/lrm4}$ mutants fail to initiate the left-sided Nodal cascade, and exhibit defects in situs development similar to other mutants that have lost left LPM *Nodal*. Strikingly, these defects include right pulmonary isomerism, the complete opposite phenotype to what is found in *Lefty1*$^{-/-}$ and *Lefty2*$^{\Delta ASE/\Delta ASE}$ mutants that express *Nodal* bilaterally.

2.3.4. Why might *Pkd1l1*$^{rks/rks}$ and *Pkd2*$^{lrm4/lrm4}$ mutants fail to initiate left LPM *Nodal* expression?

There are several possibilities as to why *Pkd1l1*$^{rks/rks}$ and *Pkd2*$^{lrm4/lrm4}$ mutants fail to initiate the left-sided Nodal cascade. It might be that the LPM, though clearly normally specified, is not competent to perform Nodal signalling in mutants. A second possibility is that events upstream of left LPM *Nodal* induction are disrupted in *Pkd1l1*$^{rks/rks}$ and *Pkd2*$^{lrm4/lrm4}$ mutants: this hypothesis is addressed in the next chapter.

Chapter Three

Both *Pkd1l1* and *Pkd2* act in the node to affect early asymmetries in gene expression

3.1. INTRODUCTION

Both *Pkd1l1*$^{rks/rks}$ and *Pkd2*$^{lrm4/lrm4}$ mutants fail to initiate the normally left-sided LPM Nodal cascade. This suggests that *Pkd1l1* and *Pkd2* act upstream of asymmetric *Nodal* induction, perhaps within the node. Though *Pkd2* is expressed ubiquitously in the 7.5-8.5 dpc mouse embryo (Pennekamp et al., 2002), the expression pattern of *Pkd1l1* was unknown. Thus, we set out to characterise *Pkd1l1* expression in the mouse embryo during the time when L-R asymmetry is established. Next, we investigated the hypothesis that *Pkd1l1*$^{rks/rks}$ and *Pkd2*$^{lrm4/lrm4}$ mutants harbour a defect upstream of left LPM *Nodal*, in the node itself.

3.2. RESULTS

3.2.1. *Pkd1l1* is expressed in the node and notochord

To determine the spatiotemporal expression pattern of *Pkd1l1* during embryogenesis we performed whole mount in situ hybridisation (WISH) on C3H wild-type embryos using sense and antisense riboprobes to portions of exons 10 and 11 of *Pkd1l1*. As expected, the sense probe did not produce a coloured precipitate demonstrating a lack of non-specific hybridisation (data not shown). The antisense probe revealed *Pkd1l1* transcript to be strikingly localised to the node during the critical 7.5-8.5 dpc time window when L-R asymmetry is established (**Figure 3.1**). Histological sectioning showed weak expression throughout the endodermal layer surrounding the node in 7.5 dpc embryos, though this was less obvious in early somite stage embryos (**Figure 3.1C',F'**). At 8.5 dpc, *Pkd1l1* was also expressed throughout the notochord (**Figure 3.1D**). To further characterise *Pkd1l1* expression, we made use of a *Pkd1l1-LacZ* transgene in which a β-geo cassette replaces exons 10-12 of *Pkd1l1* (Vogel et al., 2010). X-gal staining of *Pkd1l1*$^{+/LacZ}$ embryos revealed expression patterns that were consistent with the WISH data (**Figure 3.2**). At 7.5 dpc, stain was present in the node, extending in to the anteriorly migrating cells of the definitive endoderm (**Figure 3.2A-B**). By 8.5 dpc, *Pkd1l1*-LacZ was strongly expressed in the node as well as the entire notochord (**Figure 3.2C-E**). This notochordal staining was maintained in 9.5 dpc embryos where it spanned the entire rostro-caudal extent of the embryo (**Figure 3.2F-G**). At 9.5 dpc we also found LacZ staining in the gut endoderm (**Figure 3.2F-G**).

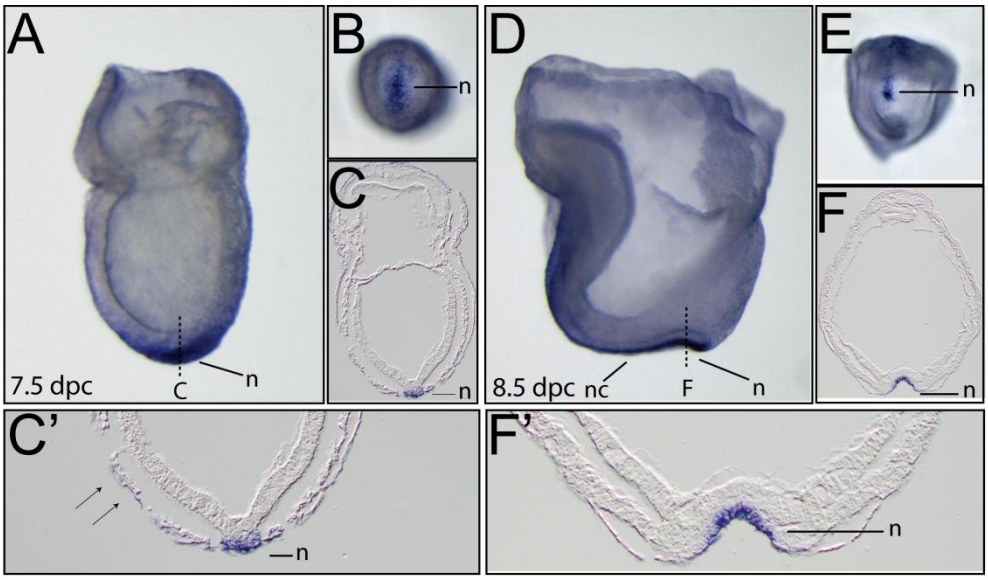

Figure 3.1. *Pkd1l1* is strongly enriched in the embryonic node

A-F *Pkd1l1* mRNA expression visualised by WISH in 7.5 dpc (A-C) and 8.5 dpc (D-F) wild-type mouse embryos. Highly enriched expression evident in the forming node (A,B) is clearly localised to the ventral node when viewed in section (C,C'). Higher magnification views reveal low level expression in the visceral endoderm (C', arrows). Enriched expression in the node and midline (D,E) is particularly obvious in sections (F,F'), revealing node expression solely in the ventral layer. n - node; nc - notochord. Planes of section are indicated by dashed lines.

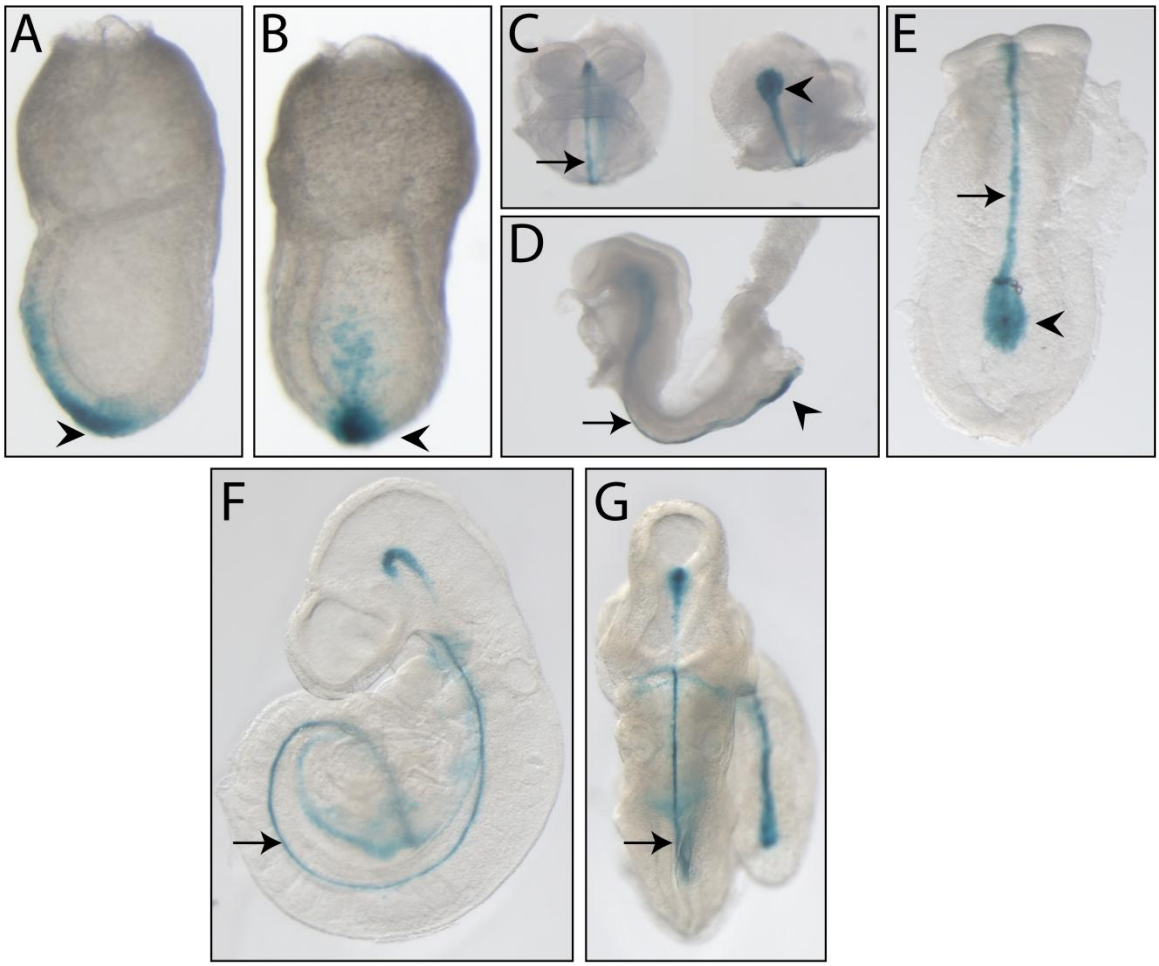

Figure 3.2. *Pkd1l1* expression by X-gal staining

A-G *Pkd1l1* expression visualised by X-gal staining of *Pkd1l1-LacZ* embryos. Expression is evident in the node at 7.5-8.5 dpc (A-E, arrow heads), but it is also strikingly expressed throughout the midline notochord tissue (C-G, arrows).

3.2.2. Node cilia of *Pkd1l1*$^{rks/rks}$ and *Pkd2*$^{lrm4/lrm4}$ mutants are structurally normal and motile

During the establishment of L-R asymmetry, asymmetric gene expression is biased by the action of motile cilia in the node that generate a unidirectional leftward flow. Since both gross phenotypic and expression-based data pointed to a defect upstream of asymmetric *Nodal* initiation in *Pkd1l1*$^{rks/rks}$ and *Pkd2*$^{lrm4/lrm4}$ mutant embryos, we analysed node cilia morphology and motility. To this end, 2-4 somite stage *Pkd1l1*$^{rks/rks}$ and *Pkd2*$^{lrm4/lrm4}$ embryos, together with littermate controls, were collected, genotyped, and prepared for scanning electron microscopy (SEM). SEM of embryonic nodes revealed an approximately tear drop-shaped depression in the embryo; higher magnification revealed several hundred cilia within the node (**Figure**

3.3A-B). We observed no differences between wild-type embryos (n=7) and *Pkd1l1*$^{rks/rks}$ (n=4) or *Pkd2*$^{lrm4/lrm4}$ (n=2) mutants in the gross morphology of the node or node cilia (**Figure 3.3C-F**). Lengths were quantified for 30 cilia per embryo, with no significant differences between wild-type controls and mutant embryos being found (**Figure 3.3G**).

In wild-type embryos, cilia-driven leftward flow in the node breaks bilateral symmetry (Nonaka et al., 1998). We therefore sought to visualise the rotation of node cilia in *Pkd1l1*$^{rks/rks}$ and *Pkd2*$^{lrm4/lrm4}$ mutants. Embryos were dissected at 8.5 dpc and mounted with the node facing up; high-speed videos of nodes were taken with differential interference contrast (DIC) microscopy (by Kerry-Lyn Riley). Both wild-type and mutant (*Pkd1l1*$^{rks/rks}$ and *Pkd2*$^{lrm4/lrm4}$) embryos exhibited motile cilia which rotated approximately 10 times per second (**Figure 3.3H**), consistent with published data (Nonaka et al., 1998). For quantitation, at least 20 cilia per embryo for at least 3 embryos of each genotype were scored. These data demonstrate that the L-R defects exhibited by *Pkd1l1*$^{rks/rks}$ and *Pkd2*$^{lrm4/lrm4}$ embryos are not a consequence of perturbed cilia structure or function.

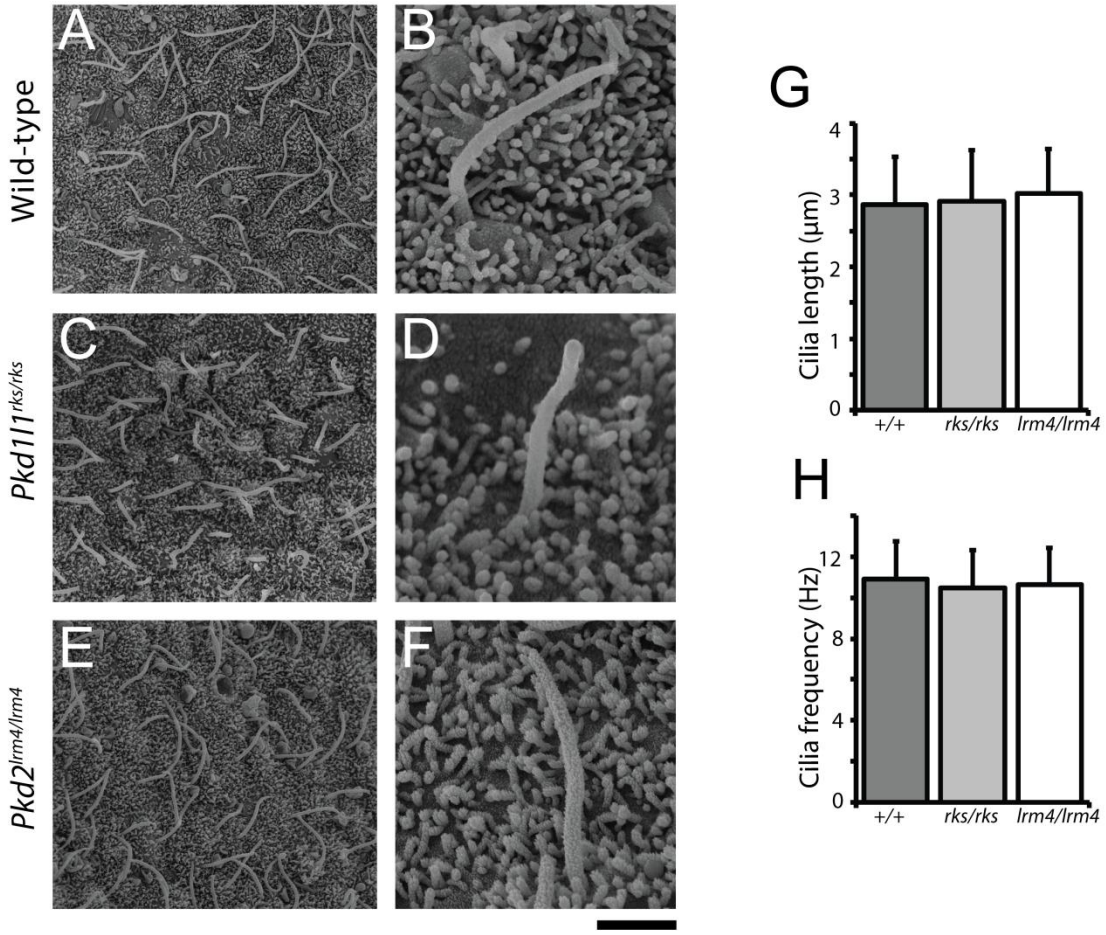

Figure 3.3. Node morphology and cilia motility are normal in *Pkd1l1*$^{rks/rks}$ and *Pkd2*$^{lrm4/lrm4}$ mutants

A-F Scanning electron micrographs of wild-type (A,B), *Pkd1l1*$^{rks/rks}$ (C,D), and *Pkd2*$^{lrm4/lrm4}$ (E,F) 8.25 dpc mouse embryos. Scale bar: 5 µm for A,C,E; 1 µm for B,D,F. **G** Average cilia lengths do not vary between wild-type and mutant embryos. **H** Rotational speed of cilia is equivalent in wild-type and mutant embryos. Error bars in G and H indicate standard deviation.

3.2.3. *Pkd1l1* and *Pkd2* act downstream of leftward flow

Since *Pkd1l1*$^{rks/rks}$ and *Pkd2*$^{lrm4/lrm4}$ mutants have structurally normal and motile node cilia, it seems plausible that Pkd1l1 and Pkd2 act downstream of nodal flow to affect left-sided *Nodal* expression. To understand the relationship between flow and the function of *Pkd1l1* and *Pkd2*, we analysed the overt and molecular L-R defects of *iv/iv* mutants that have lost leftward flow (Okada et al., 1999). We then generated *iv/iv;Pkd1l1*$^{rks/rks}$ and *iv/iv;Pkd2*$^{lrm4/lrm4}$ double mutants to assess the epistatic interaction between these genes.

3.2.3.1. Randomisation of L-R asymmetry in *iv/iv* mutants

The situs inversus viscerum (*iv*) mouse mutant harbours an amino acid point mutation within the axonemal dynein heavy chain Dnahc11 (**Figure 3.4A**; (Supp et al., 1997)). The cilia on the ventral surface of the node are immotile in *iv/iv* homozygotes (data not shown;(Okada et al., 1999)), resulting in a loss of leftward flow and randomisation of LPM Nodal signalling (Collignon et al., 1996; Okada et al., 1999; Supp et al., 1997). We generated a congenic C3H-*iv* line, so that the genetic background was the same as for the *Pkd1l1*^{rks} and *Pkd2*^{lrm4} lines, then assessed organ situs in 13.5 dpc embryos from *+/iv* intercrosses as well as *+/iv* x *iv/iv* crosses. In wild-type and *+/iv* embryos, the normal pattern of lung lobation was observed, with four right-sided lobes and a single left-sided lobe (4:1) (**Figure 3.4B; Table 3-1**). By contrast, in *iv/iv* mutants incidences of wild-type lung situs were observed (n=24/70), though mutants also exhibited a high proportion of situs inversus (1:4; n=25/70) (**Figure 3.4B; Table 3-1**). The remaining *iv/iv* mutants demonstrated left pulmonary isomerism (1:1, n=10/70) or partial isomerism (e.g. 2:1 or 4:3), but never right isomerism (4:4) (**Figure 3.4B; Table 3-1**). In wild-type embryos, the apex of the heart and stomach are positioned leftward of the midline. By contrast, a significant number of *iv/iv* mutants exhibited reversal of heart positioning (n=42/78) or stomach sidedness (n=44/74) (**Table 2-1**), consistent with randomised L-R determination. This suggests that *iv/iv* belongs to a different class of L-R mutant than *Pkd1l1*$^{rks/rks}$ and *Pkd2*$^{lrm4/lrm4}$; not surprising since the *iv* mutation affects cilia motility, while cilia are motile in all *Pkd1l1*$^{rks/rks}$ and *Pkd2*$^{lrm4/lrm4}$ embryos.

Table 3-1 Overt morphological defects of left-right asymmetry in *iv/iv* mutants

	Normal	Inverted	LI	PI	n
iv/iv					
Lung situs	24 (34)	25 (36)	10 (14)	11 (16)	70
Heart apex	36 (46)	42 (54)	-	-	78
Stomach situs	30 (41)	44 (59)	-	-	74

Lung situs, heart apex and stomach situs were scored at 13.5 dpc. Shown is the number of embryos exhibiting the defect among the total number examined (n), with percentages in brackets. LI – left isomerism; PI – partial isomerism.

To understand the molecular basis of the L-R defects in *iv/iv* embryos, we assessed *Pitx2* expression in mutant embryos at 8.5 dpc. In wild-type embryos, *Pitx2*

expression is activated in the left LPM at the 3 somite stage and maintained into organogenesis (**Figure 3.5A-B**) (Ryan et al., 1998). By contrast, *iv/iv* mutants displayed a mixture of left (n=11/60), right (n=12/60), bilateral (n=24/60), and absent (n=13/60) LPM *Pitx2* expression between the 3-7 somite stages (**Figure 3.5A-B**). When expression was analysed by somite stage, it became apparent that of the 3-7 somite stage *iv/iv* mutants with absent *Pitx2* expression, ten out of thirteen had 3 somite pairs while the remaining three had 4 somite pairs (**Figure 3.5D**). Thus, 45/48 (94%) of *iv/iv* mutants exhibited LPM *Pitx2* expression, regardless of side, by the 4 somite stage. By the 5 somite stage and onwards, 100% of *iv/iv* mutants had LPM *Pitx2* expression. This implies that, as well as there being a randomisation of *Pitx2* expression in *iv/iv* mutants, there is also a delay of approximately 2 hours (1 somite) in the activation of LPM *Pitx2* (**Figure 3.5C**). Furthermore, by the 6-7 somite stages 62% of *iv/iv* mutants exhibited bilateral *Pitx2* expression; earlier, at the 4-5 somite stages, only 41% of mutants exhibited this phenotype. This may be indicative of contralateral activation of one side by the other as the embryo ages, though no defect in *Lefy1* expression has been reported in *iv/iv* mutants and this was not investigated further here.

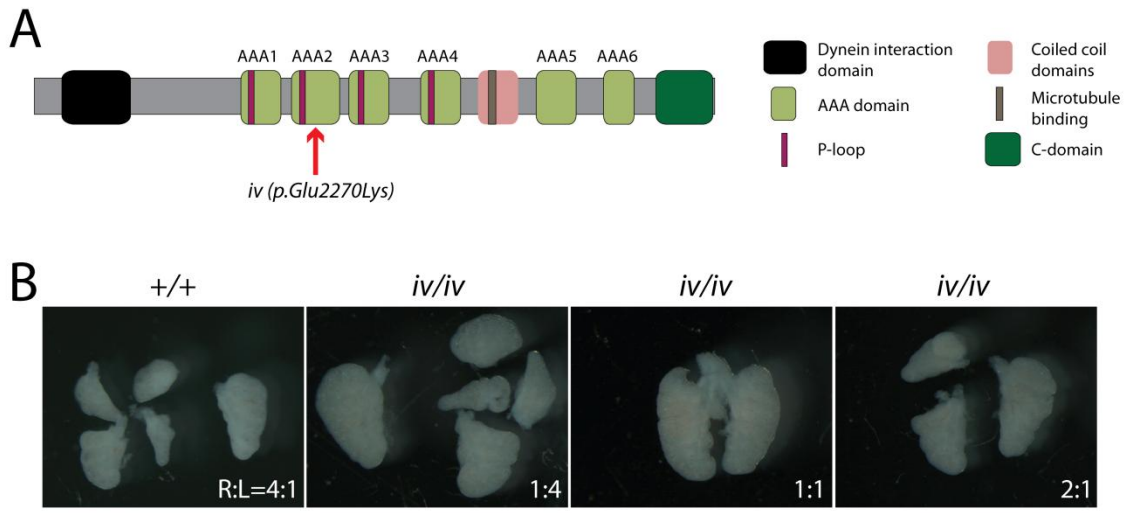

Figure 3.4. Overt morphological defects of left-right asymmetry in *iv/iv* mutants

A Schematic diagram of the domain structure of Dnahc11, showing the position of the *iv* mutation. **B** Wild-type and *iv/iv* homozygous lungs dissected at 13.5 dpc showing normal lung situs in wild-type (4:1) and a range of situs abrormalities in *iv/iv*, including reversed situs (1:4), left isomerism (1:1) and partial left isomerism (2:1).

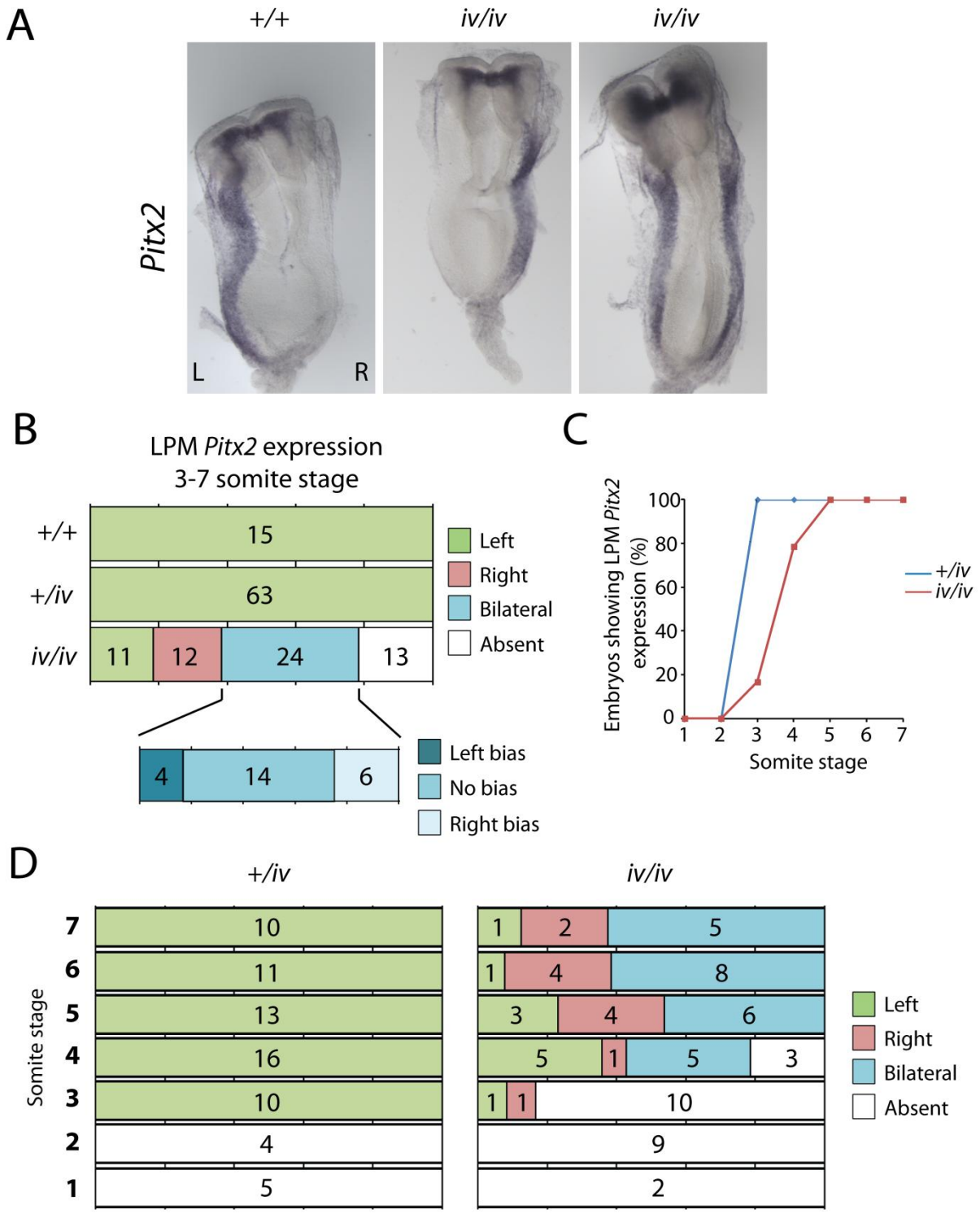

Figure 3.5. *Pitx2* expression is randomised with delay in *iv/iv* mutants

A Whole mount in situ hybridisation for *Pitx2* in *iv/iv* mmutants and wild-type control embryos. **B** *Pitx2* expression data for wild-type, *+/iv* and *iv/iv* embryos. **C** *Pitx2* expression data by somite stage where percentage embryos exhibiting LPM *Pitx2* is scored. **D** LPM *Pitx2* expression data in *iv/iv* embryos by somite stage.

3.2.3.2. *iv/iv;Pkd1l1*$^{rks/rks}$ double mutants exhibit right pulmonary isomerism

The generation and phenotyping of double mutant embryos can provide information about the order in which the underlying genes act on a genetic pathway (Mani et al., 2008). By generating *iv/iv;Pkd1l1*$^{rks/rks}$ double mutant embryos, we therefore addressed whether leftward nodal flow contributes to the L-R phenotype of *Pkd1l1*$^{rks/rks}$ embryos. At 13.5 dpc, *iv/iv;Pkd1l1*$^{+/+}$ and *iv/iv;Pkd1l1*$^{+/rks}$ embryos demonstrated either normal (4:1) or reversed (1:4) lung situs, or left pulmonary isomerism (1:1) (**Figure 3.6A-B**), similar to the results obtained for *iv/iv* single mutants (**Figure 3.4B; Table 3-1**). In contrast, double mutant embryos always exhibited right pulmonary isomerism (4:4; n=8/8) (**Figure 3.6A-B**), thereby phenocopying *Pkd1l1*$^{rks/rks}$ embryos and not *iv/iv* mutants. Intriguingly, though *Pkd1l1*$^{rks/rks}$ mutants always exhibited right pulmonary isomerism when assessed in isolation (**Table 2-1**), when in the presence of *+/iv*, we found that 1/6 embryos exhibited normal lung situs (**Figure 3.6B**). This could represent a low level genetic interaction, however, the very low numbers of embryos with this genotype assessed makes it impossible to draw any conclusions from this data. Nevertheless, the fact that all eight double mutant embryos exhibit right pulmonary isomerism, like *Pkd1l1*$^{rks/rks}$ mutants, supports a model in which Pkd1l1 acts downstream of leftward flow. Furthermore, preliminary data suggests that *iv/iv;Pkd1l1*$^{rks/rks}$ double mutants also exhibit loss of LPM *Pitx2* expression at 8.5 dpc (n=1/1), like *Pkd1l1*$^{rks/rks}$ mutants but unlike *iv/iv* mutants. These data support the idea that *Pkd1l1* is epistatic to *Dnahc11*, but more double mutant embryos need to be assessed at this age to fully assess the *Pitx2* expression phenotype.

3.2.3.3. *iv/iv;Pkd2*$^{lrm4/lrm4}$ mutants phenocopy *Pkd2*$^{lrm4/lrm4}$ embryos

We similarly generated *iv/iv;Pkd2*$^{lrm4/lrm4}$ double mutant embryos, to address whether leftward flow contributes to the L-R phenotype of *Pkd2*$^{lrm4/lrm4}$ embryos. At 13.5 dpc, *+/+;Pkd2*$^{lrm4/lrm4}$ and *+/iv;Pkd2*$^{lrm4/lrm4}$ mutants demonstrated right lung isomerism (4:4), while *iv/iv;Pkd2*$^{+/lrm4}$ and *iv/iv;Pkd2*$^{+/+}$ exhibited various patterns of lung lobation including 4:1, 1:4, 1:1, and 2:1 (**Figure 3.6C-D**), as expected. Double mutant *iv/iv;Pkd2*$^{lrm4/lrm4}$ embryos phenocopied *Pkd2*$^{lrm4/lrm4}$ mutants with right pulmonary isomerism (4:4) (**Figure 3.6C-D**); all five double mutant embryos demonstrated this phenotype. Futhermore, when the activation of LPM Nodal signalling was assessed by *Pitx2* in situ hybridisation, *iv/iv;Pkd2*$^{lrm4/lrm4}$ double

mutant embryos resembled *Pkd2*$^{lrm4/lrm4}$ mutants, exhibiting absent LPM *Pitx2* expression in all cases (n=5/5) (**Figure 3.6E-F**). These results indicate that the *Pkd2*$^{lrm4/lrm4}$ phenotype manifests independently of flow and are consistent with the notion that Pkd2 acts downstream of nodal flow on the L-R pathway.

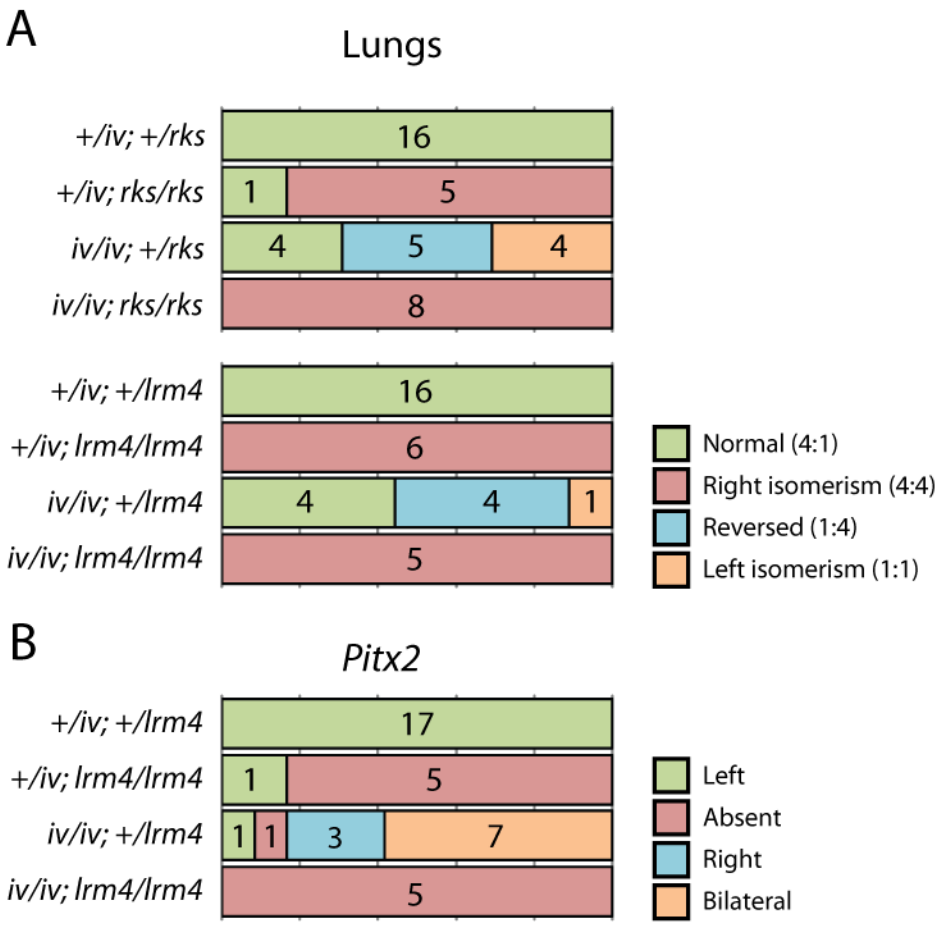

Figure 3.6. Pkd1l1 and Pkd2 act downstream of flow

A-B Lung phenotype and Pitx2 expression from double mutant and control embryos for crosses between *Pkd1l1*^{rks} or *Pkd2*^{lrm4} and *iv*. Shown is the number of embryos in each category.

3.2.4. Left-sided *Cerl2* is not repressed in *Pkd1l1*$^{rks/rks}$ or *Pkd2*$^{lrm4/lrm4}$ mutants

Cerberus-like 2 (*Cerl2*; MGI - *Dand5*) encodes a member of the Cerberus-Dan family of secreted cysteine-knot proteins that act as inhibitors of other signalling molecules including Nodal, BMP and Wnt (Bell et al., 2003; Marques et al., 2004). *Cerl2* is homologous to zebrafish *charon* and *Xenopus Coco*; loss of *Cerl2* function results in L-R defects in the mouse, frog, and fish (Hashimoto et al., 2004; Hojo et

al., 2007; Marques et al., 2004; Schweickert et al., 2010; Vonica and Brivanlou, 2007). *Cerl2* is coexpressed with *Nodal* in the crown cells at the lateral-most edge of the node pit (Marques et al., 2004; Pearce et al., 1999). At the early headfold stage (EHF), *Cerl2* expression is symmetrical, describing a horseshoe shape around the node periphery (Kawasumi et al., 2011). By the 1 somite stage, subtle asymmetries in *Cerl2* expression are observed, with the right-sided domain being more intense than that at the left side (**Figure 3.7A**). These asymmetries are maintained throughout the early somite stages (**Figure 3.7A**) until *Cerl2* expression is lost at around the 7 somite stage (data not shown; (Pearce et al., 1999)). *Cerl2* is arguably the earliest known marker of L-R asymmetry in the mouse embryo, appearing before *Nodal* asymmetry in the crown cells (Kawasumi et al., 2011). Indeed, right-sided Cerl2 is likely to inhibit Nodal, resulting in the left-sided bias in *Nodal* expression and the subsequent activation of left LPM Nodal signalling (Marques et al., 2004).

To test how Pkd1l1 and Pkd2 act in relation to Cerl2, we analysed *Cerl2* expression in *Pkd1l1*$^{rks/rks}$ and *Pkd2*$^{lrm4/lrm4}$ mutant embryos. Expression patterns were grouped into three categories: equal intensities (R=L), right bias (R>L), and left bias (R<L); embryos were scored blindly prior to genotyping. All embryos assessed were between the 2-4 somite stages, a time when *Cerl2* expression is always R>L in wild-type embryos (**Figure 3.7A,C**). However, we found that a strikingly high proportion of both *Pkd1l1*$^{rks/rks}$ and *Pkd2*$^{lrm4/lrm4}$ mutants exhibited equal expression, R=L (**Figure 3.7B-C**). Of 20 *Pkd1l1*$^{rks/rks}$ embryos, 18 were scored as R=L; the remaining two embryos were exhibited R>L expression. Similar results were obtained with *Pkd2*$^{lrm4/lrm4}$ mutants, with 9/12 embryos exhibiting the R=L expression pattern (**Figure 3.7B-C**). Furthermore, the intensity of staining on both sides in most R=L mutant embryos was similar to that observed on the right side of wild-type embryos (compare **Figure 3.7B** with **3.7A**), implying that the left-sided domain was not repressed in *Pkd1l1*$^{rks/rks}$ and *Pkd2*$^{lrm4/lrm4}$ mutant embryos. Together, these data suggest that Pkd1l1 and Pkd2 act upstream of asymmetric *Cerl2* expression in the L-R pathway (see **Figure 3.7D** for model).

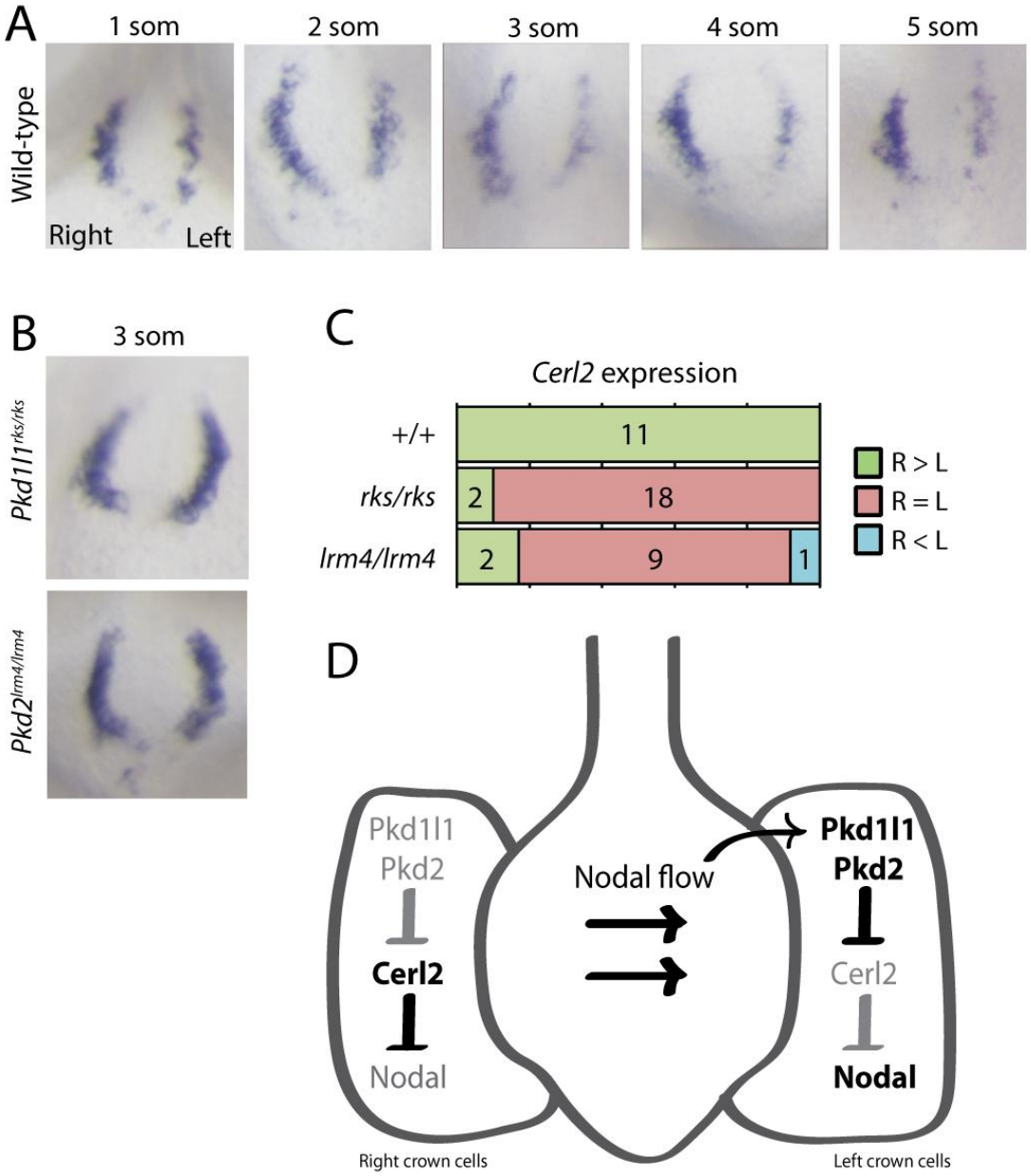

Figure 3.7. *Cerl2* expression remains symmetrical in *Pkd1l1*$^{rks/rks}$ and *Pkd2*$^{lrm4/lrm4}$ mutants

A *Cerl2* in situ hybridisation. In wild-type embryos, *Cerl2* exhibits a right-sided expression bias throughout the early somite stages. **B-C** *Cerl2* expression remains symmetrical in the crown cells in the majority of mutant embryos. **D** Model of Pkd1l1 and Pkd2 action, with these genes acting downtream of Nodal flow to affect *Cerl2*, and thereby *Nodal*, expression in the crown cells at the node periphery.

3.3. DISCUSSION

Pkd1l1 is expressed abundantly in the ventral layer of the node during the time when L-R asymmetry is established, implying a role for Pkd1l1 in the node itself. However, *Pkd1l1*$^{rks/rks}$ mutants exhibit structurally normal and motile cilia, as do *Pkd2*$^{lrm4/lrm4}$ mutants. Genetic epistasis experiments reveal that loss of nodal flow

can be suppressed by the *Pkd1l1*^{rks} and *Pkd2*^{lrm4} mutations, suggesting that *Pkd1l1* and *Pkd2* act downstream of flow. Furthermore, *Cerl2* expression, normally biased to the right side of the node, remains symmetrical in *Pkd1l1*$^{rks/rks}$ and *Pkd2*$^{lrm4/lrm4}$ mutants. Taken together, these data argue that Pkd1l1 and Pkd2 act downstream of flow to regulate *Cerl2* expression (**Figure 3.7D**).

3.3.1. Stochastic activation of the LPM Nodal cascade depends on *Pkd1l1* and *Pkd2*

Homozygous *iv/iv* mutants exhibit paralysed nodal cilia and, consequently, lose leftward flow (Okada et al., 1999). This results in randomisation of LPM Nodal activity, with left, right, and bilateral activation observed. Furthermore, the activation of the LPM cascade, assayed by the onset of LPM *Pitx2* expression, is delayed by approximately 2 hours (equivalent to the development of one somite) in *iv/iv* mutants. Similar observations were made by Okada and colleagues who used a *Lefty2-ASE-hsp-LacZ* transgene to monitor left-sided activation (Okada et al., 1999). This implies that in the absence of leftward flow, the LPM Nodal cascade becomes stochastically activated with a delay. Since stochastic activation never occurs in *Pkd1l1*$^{rks/rks}$ or *Pkd2*$^{lrm4/lrm4}$ mutants, it seems likely that both Pkd1l1 and Pkd2 are necessary components not only of normal flow-induced left-sided Nodal activity, but also of stochastic activation in the absence of flow. Since *Pkd1l1* expression is restricted to the node, it is reasonable to assume that random pathway activation in the absence of flow is dependent upon stochastic signals emanating from the node and not from autonomous LPM activity. What then is the nature of stochastic activation in the absence of flow? An explanation of this phenomenon perhaps fits most readily with the morphogen/NVP hypothesis; it could be that a chemical signal being released into the node, which is normally biased to the left by nodal flow, instead gradually diffuses to both sides where it results in randomised (but most often bilateral) induction of the Nodal cascade.

3.3.2. Delayed activation of the LPM Nodal cascade in mutants lacking leftward flow

The delayed activation of LPM Nodal activity in *iv/iv* mutants suggests that stochastic activation occurs approximately two hours after normal flow-induced

activation. Indeed, this delay is likely crucial for the system to normally restrict *Nodal* induction to the left side. In wild-type embryos, Nodal activity is biased to the left side by flow then, by inducing *Lefty1* and *Lefty2* expression in the left prospective floor plate (PFP) and left LPM, respectively, left-sided signals inhibit any possibility of right-sided *Nodal* induction; this is the essence of the SELI model (Nakamura et al., 2006). However, some time will be required for this contralateral inhibition to take effect: the left-sided signal must reach sufficient levels to induce *Lefty1* and *Lefty2*, which then must be transcribed, translated, and secreted. Finally, time will also be required for Lefty1 and Lefty2 proteins to diffuse to the right side and inhibit any Nodal activity there. Thus, it is crucial for the system to operate correctly, that left-sided activation occurs significantly before any stochastic pathway activation. This reasoning can be expressed mathematically. If T_L and T_R are the times at which the left and right sides are initially activated, respectively, and t is the time between initial activation of one side and effective lateral inhibition of the other side, then in wild-type embryos:

$$T_L - T_R > t$$

That is, the time difference between flow-induced left-sided activation and stochastic right-sided activation must be greater than the time taken for the activated left side to cross-inhibit the right side. We can also explain the observed *iv/iv* phenotypes in the following ways, with ΔT_{LR} being the difference in time between stochastic activation of the left and right sides:

$\Delta T_{LR} = 0$	Bilateral expression, symmetrical
$\Delta T_{LR} > t$	Unilateral expression, right or left
$\Delta T_{LR} < t \neq 0$	Bilateral expression, biased

As expected based on this simplified model, in 4-7 somite stage *iv/iv* embryos both left-sided, right-sided, and bilateral (symmetrical or biased) *Pitx2* expression was observed.

3.3.3. Repression of *Cerl2* by leftward flow requires *Pkd1l1* and *Pkd2*

In mouse, perinodal *Cerl2* expression becomes asymmetric with a right-sided bias after the onset of leftward flow (Pearce et al., 1999; Marques et al., 2004). Elegant studies in frog embryos have revealed the *Cerl2* (*Coco* in *Xenopus*) is a critical

target of leftward flow (Schweickert et al., 2010), while in mouse loss of *Cerl2* leads to bilateral LPM Nodal activation (Marques et al., 2004), probably owing to over activation (lack of repression) of perinodal Nodal activity.

The results presented here support the model that leftward flow represses left-sided *Cerl2* thereby resulting in increased Nodal activity and, owing to positive feedback, increased *Nodal* expression. Notably, we find that *Cerl2* R>L asymmetry is apparent at the 1 somite stage, that is earlier than the reported R<L *Nodal* expression asymmetry but still after the onset of leftward flow. In *Pkd1l1*$^{rks/rks}$ and *Pkd2*$^{lrm4/lrm4}$ mutants, however, *Cerl2* asymmetry is not established. In mutants, left-sided *Cerl2* expression is approximately as intense as right-sided wild-type expression, supporting the idea that left-sided *Cerl2* is normally repressed in contrast to the proposition that right-sided *Cerl2* is upregulated (Marques et al., 2004). This demonstrates that both *Pkd1l1* and *Pkd2* are required for (i.e. act upstream of) *Cerl2* asymmetry. Since *Pkd1l1* and *Pkd2* act downstream of leftward flow, a likely model is that leftward flow activates Pkd1l1 and Pkd2 on the left side only, resulting in inhibition of Cerl2 and thereby a derepression of left-sided Nodal activity (**Figure 3.7D**).

3.3.4. A model of Pkd1l1-Pkd2 action during the establishment of left-right asymmetry

Pkd1l1 is a member of the polycystin family of proteins, which also includes Pkd1 and Pkd2. In humans, mutations in *PKD1* or *PKD2* result in autosomal dominant polycystic kidney disease (ADPKD); the proteins encoded by these genes localise to primary cilia in the renal epithelium (Yoder et al., 2002). PKD2 is known to form a functional ion-conducting channel with some specificity for Ca^{2+}, whereas PKD1, with its large extracellular domain, is thought to sense the bending of a primary cilium induced by fluid flow in the renal tubule, thus functioning as a mechanosensor (Nauli et al., 2003; Nauli and Zhou, 2004). Pkd1l1 and Pkd1 are structurally similar: both are 11-pass transmembrane proteins with a large N-terminal region. Based on this alone, it is sensible to suggest that the two proteins might have similar functions. Thus, Pkd1l1 might be a mechanosensor of leftward flow in the node, acting to sense flow then open Pkd2 channels, permitting the Ca^{2+} spike observed at the left edge of the node which is lost in *Pkd2*$^{-/-}$ mutants (McGrath et al., 2003).

Thus, the data presented here that mutation of *Pkd1l1* or *Pkd2* both prevent activation of the left-sided Nodal cascade fit most simply with the two-cilia model in which leftward flow is directly sensed by polycystin proteins. This model is considered in greater depth in the general discussion (**Chapter seven**).

CHAPTER FOUR

Pkd1l1 is required to restrict *Nodal* to the left side

4.1. INTRODUCTION

Whilst the analysis of *Pkd1l1*$^{rks/rks}$ mutants was ongoing, the first *Pkd1l1* null allele (MGI – *Pkd1l1*^{tm1Lex}) was described (Vogel et al., 2010). In this study, Vogel and colleagues reported that around 35% of homozygous *Pkd1l1*$^{-/-}$ mutants survived to adulthood, with around one third of these animals exhibiting situs inversus of the viscera; the remainder demonstrated normal situs (Vogel et al., 2010). However, the authors did not assess situs in *Pkd1l1*$^{-/-}$ embryos; nor did they perform any molecular analyses of L-R asymmetrically expressed genes. Nevertheless, the finding that a significant proportion of *Pkd1l1*$^{-/-}$ mutants survive to adulthood is strikingly different to the 100% embryonic lethality observed in *Pkd1l1*$^{rks/rks}$ mutants. We therefore set out to investigate the reason for this phenotypic discrepancy.

4.2. RESULTS

4.2.1. The *Pkd1l1*$^{rks/rks}$ phenotype is slightly modified by changes in genetic background

In this thesis, *Pkd1l1*$^{rks/rks}$ mutants have been assessed on the C3H/HeH genetic background. In contrast, Vogel and colleagues used a mixed 129:B6J background for their analysis of *Pkd1l1*$^{-/-}$ mutants (Vogel et al., 2010). Thus, it seemed possible that genetic background differences might explain the phenotypic discrepancies between the two alleles. To test this, we outcrossed *Pkd1l1*$^{rks/rks}$ mice, crossing C3.B-*Pkd1l1*$^{+/rks}$ heterozygotes to either 129SV/Ev or C57BL6/J wild-type animals. This produced F1 progeny, which were then intercrossed to generate *Pkd1l1*$^{rks/rks}$ mutants on a mixed genetic background. The resultant embryos were assessed at 13.5 dpc for heart, lung, and stomach situs. The data is presented in **Table 4-1** alongside data from **Chapter two** for congenic C3.B-*Pkd1l1*$^{rks/rks}$ mutants for comparison.

(C3 x 129)F2-*Pkd1l1*$^{rks/rks}$ mutants, henceforth referred to as 129-*Pkd1l1*$^{rks/rks}$, exhibited severe situs defects that were similar, but not identical, to congenic C3.B-*Pkd1l1*$^{rks/rks}$ mutants. Whilst wild-type and heterozygous embryos exhibited the normal pattern of lung lobation, with four right-sided lobes and a single left lobe (4:1), 129-*Pkd1l1*$^{rks/rks}$ mutants demonstrated right pulmonary isomerism in the majority of embryos (4:4; n=13/18). However, mutants also occasionally exhibited

other patterns of lung lobation with normal (4:1; n=2/18) and reversed (1:4; n=1/18) patterns being observed. Finally, two mutants exhibited phenotypes close to right isomerism: one had four right lobes and three left lobes (4:3; n=1/18), whilst the second exhibited three right lobes and four left lobes (3:4; n=1/18), grouped together as partial isomerisms in **Table 4-1**. Heart situs was also affected in 129-*Pkd1l1*$^{rks/rks}$ mutants: of the 18 embryos scored, half had normal (n=9/18) and half had reversed (n=9/18) heart apex positioning. Similarly, stomach situs was either normal (n=10/18), reversed (n=7/18) or central (n=1/18). Both of the embryos which exhibited normal lung patterning also exhibited normal heart and stomach positioning, implying that these embryos were normal and would likely have survived to birth; whilst overt heart defects were not evident in these embryos, they were also not actively scored. The embryo that exhibited situs inversus of the lungs, in contrast, exhibited discordance between the heart and stomach and therefore demonstrated a heterotaxic phenotype. It is also worth noting that we observed low level L-R defects in 129-*Pkd1l1*$^{+/+}$ mice; of a total of 20 embryos examined, one exhibited a reversed stomach with normal heart positioning and lung situs, while a second demonstrated reversed heart and stomach positioning but normal lung situs. This is indicative of low level effects of the mixed genetic background on L-R asymmetry. We found no defects in 129-*Pkd1l1*$^{+/-}$ heterozygotes (n=26). The number of embryos observed in each genotype category was not different to the expected number ($p = 0.4302$, Chi-square analysis applied), suggesting that there was no loss of 129-*Pkd1l1*$^{rks/rks}$ embryos prior to 13.5 dpc. However, two dead embryos were recovered at 13.5 dpc, both which had recently arrested; these were genotyped as *Pkd1l1*$^{rks/rks}$ homozygotes.

As for 129-*Pkd1l1*$^{rks/rks}$ mutants, the majority of B6-*Pkd1l1*$^{rks/rks}$ mutants exhibited right pulmonary isomerism (n=17/19) (**Table 4-1**). The remaining two embryos showed normal lung situs (**Table 4-1**). We also saw incidences of reversed heart and stomach positions in mutants, as expected (**Table 4-1**). However, the B6-*Pkd1l1*$^{rks/rks}$ phenotype was not significantly different to that of C3H congenic *Pkd1l1*$^{rks/rks}$ mutants. Thus, mixing the genetic background of *Pkd1l1*^{rks} by outcrossing to 129SV/Ev or C57BL6/J does subtly alter the *Pkd1l1*$^{rks/rks}$ phenotype, but the great majority of embryos still exhibit right pulmonary isomerism.

Table 4-1 Gross phenotype of *Pkd1l1*$^{rks/rks}$ on mixed genetic background

	Normal	Inverted	Midline	RI	PI	n
129-*Pkd1l1*$^{rks/rks}$						
Lung situs	2 (11.1)	1 (5.6)	-	13 (72.2)	2 (11.1)	18
Heart apex	9 (50.0)	9 (50.0)	0	-	-	18
Stomach situs	10 (55.6)	7 (38.9)	1 (5.6)	-	-	18
B6-*Pkd1l1*$^{rks/rks}$						
Lung situs	2 (10.5)	0 (0)	-	17 (89.5)	0 (0)	19
Heart apex	11 (57.9)	8 (42.1)	0 (0)	-		19
Stomach situs	9 (47.4)	9 (47.4)	1 (5.3)	-		19
Con C3.B-*Pkd1l1*$^{rks/rks}$						
Lung situs	0 (0)	0 (0)	-	46 (100)	0 (0)	46
Heart apex	32 (70.0)	13 (28.0)	1 (2.0)	-		46
Stomach situs	14 (60.9)	8 (34.8)	1 (4.3)	-		23

Lung situs, heart apex and stomach situs were scored at 13.5 dpc. Shown is the number of embryos exhibiting the defect among the total number examined (n), with percentages in brackets. RI – right isomerism; PI – partial isomerism; con – congenic. Congenic C3.B-*Pkd1l1*$^{rks/rks}$ data, first described in Chapter 2, is given here for comparison.

4.2.2. *Pkd1l1*$^{-/-}$ mutants exhibit left-right abnormalities that are distinct from *Pkd1l1*$^{rks/rks}$ mutants

Given the apparent differences between *Pkd1l1*$^{-/-}$ and *Pkd1l1*$^{rks/rks}$ mutants, we decided to assess the embryonic phenotype of *Pkd1l1*$^{-/-}$ embryos. To this end, we imported the *Pkd1l1*^{tm1Lex} line, used by Vogel and colleagues, into the Mary Lyon Centre (MLC) quarantine facility, then rederived the line into the MLC proper by in vitro fertilisation (IVF) with embryo transfer into clean females[5]. We then backcrossed the line to C3H for at least four generations prior to analysis; this significantly reduced the genetic background differences between the *Pkd1l1*$^{-}$ and *Pkd1l1*^{rks} lines. Unless otherwise stated, the remainder of the work performed on the *Pkd1l1*$^{-}$ line described in this thesis refers to mice that have been backcrossed to C3H for at least four generations, but often more.

To assess situs in adult mice, we intercrossed *Pkd1l1*$^{+/-}$ mice and obtained all three possible genotypes at weaning; however, the ratio of genotypes was

[5] IVF was performed by the Frozen Embryo and Sperm Archive (FESA) team at MRC Harwell.

significantly different to that expected, with an obvious loss in the number of *Pkd1l1*$^{-/-}$ animals surviving to adulthood (**Table 4-2**; p=0.0016 – chi-sqaure analysis applied). Indeed, only 37% of the expected number of homozygotes were present at weaning. This is strikingly close to the 35% survivability reported by Vogel and colleagues for *Pkd1l1*$^{-/-}$ mice on a mixed genetic background (Vogel et al., 2010), suggesting that genetic background has not affected the likelihood of surviving loss of *Pkd1l1*. Of the 8 *Pkd1l1*$^{-/-}$ mutants that survived to adulthood, we noticed that two had reversed stomach situs, scored by the side of the milk spot, while the other 6 mutants all had normal stomach situs. Thus, 25% of surviving *Pkd1l1*$^{-/-}$ mice likely have reversed situs; similar data was reported by Vogel and colleagues (Vogel et al., 2010). The situs features other than stomach positioning have not yet been scored in these 8 individuals, as they are currently been used for breeding.

Table 4-2 Genetic ratios from *Pkd1l1*$^{+/-}$ intercrosses

	Expected	Observed	p value
Adult			
Pkd1l1$^{+/+}$	26.33	25	
Pkd1l1$^{+/-}$	52.67	54	0.0016
Pkd1l1$^{-/-}$	26.33	8	

Expected number of animals is based on Mendelian genotype frequencies. P value is calculated using Chi-square analysis with the assumption loss of of homozygotes (see **Experimental Procedures**).

We used a combination of *Pkd1l1*$^{+/-}$ intercrosses and *Pkd1l1*$^{+/-}$ x *Pkd1l1*$^{-/-}$ crosses to generate 13.5 dpc embryos for phenotypic analysis. At this age, embryos normally exhibit left-sided stomach and heart apex positioning, as well as a 4:1 ratio of right:left lung lobes (**Figure 4.1B-D**), all overt morphological characteristics of proper L-R asymmetry. We observed this normal situs in all wild-type (n=6/6) and *Pkd1l1*$^{+/-}$ embryos (n=54/54). However, we found a striking departure from this normal arrangement in *Pkd1l1*$^{-/-}$ mutants (**Figure 4.1E-H; Table 4-3**). Specifically, we observed a high incidence of inverted heart (n=20/29) and stomach (n=17/29) positioning in *Pkd1l1*$^{-/-}$ mutants (**Figure 4.1F**). Lung situs in *Pkd1l1*$^{-/-}$ embryos was variable. Most often, embryos exhibited left isomerism (1:1; n=14/28) (**Figure 4.1H**), where a single lung lobe is present on both the left and right sides, or reversed lung situs (1:4; n=7/28) (**Table 4-3**). A small number of mutants had normal lung situs

(4:1; n=2/28), while some exhibited partial isomerisms (n=5/28) (**Table 4-3**). Two of the five cases of partial isomerism included embryos in which the right lung had lost lobes (3:1 and 2:1), and so are partial left isomerisms. Two embryos had a 1:3 ratio, suggesting an inversion of situs with the left lung not fully acquiring 'right-sided' character. Finally, one embryo exhibited a 3:4 phenotype (**Figure 4.1G**), signifying a partial right isomerism with reversed situs.

Table 4-3 Overt morphological defects of left-right asymmetry in *Pkd1l1*$^{-/-}$ mutants

	Normal	Inverted	Central	LI	PI	n
***Pkd1l1*$^{-/-}$**						
Lung situs	2 (7.1)	7 (25.0)	-	14 (50.0)	5 (17.9)	28
Heart apex	8 (27.6)	20 (68.8)	1 (3.5)	-	-	29
Stomach situs	11 (37.9)	17 (58.6)	1 (3.5)	-	-	29

Lung situs, heart apex and stomach situs were scored at 13.5 dpc. Shown is the number of embryos exhibiting the defect among the total number examined (n), with percentages in brackets. LI – left isomerism; PI – partial isomerism.

At 13.5 dpc, several embryos from *Pkd1l1*$^{+/-}$ x *Pkd1l1*$^{+/-}$ intercrosses or *Pkd1l1*$^{+/-}$ x *Pkd1l1*$^{-/-}$ crosses were found to have died in utero. Of 16 dead embryos discovered and genotyped, 13 were *Pkd1l1*$^{-/-}$ mutants and 3 were *Pkd1l1*$^{+/-}$ heterozyogtes; no genetically wild-type embryos were found dead (**Figure 4.1A**). Given that we observed 29 living *Pkd1l1*$^{-/-}$ mutants, this implies that around 31% of total *Pkd1l1*$^{-/-}$ embryos had died prior to dissection at 13.5 dpc, thereby representing a significant reduction in the expected number of homozygotes (p=0.02 – chi-square analysis applied). This might suggest that *Pkd1l1*$^{-/-}$ embryos harbour an as yet unknown phenotype that causes them to arrest prior to 13.5 dpc.

In summary, after backcrossing to C3H for at least four generations, *Pkd1l1*$^{-/-}$ mutants exhibit severe morphological L-R defects. Intriguingly, these defects are strikingly different to those of *Pkd1l1*$^{rks/rks}$ embryos (**Table 4-4**): most obviously while right pulmonary isomerism is fully penetrant in *Pkd1l1*$^{rks/rks}$ embryos, it never occurs in *Pkd1l1*$^{-/-}$ mutants. The lung phenotype of *Pkd1l1*$^{-/-}$ is furthermore indicative that the normally left-restricted Nodal cascade, which is never activated in *Pkd1l1*$^{rks/rks}$ mutants, is present in *Pkd1l1*$^{-/-}$ embryos. Based on the phenotype at 13.5 dpc, the pathway is likely to be activated on either the left or right side or, most often, bilaterally. Though the molecular phenotype of *Pkd1l1*$^{-/-}$ embryos has not yet been

assessed, if the Nodal cascade is indeed activated in the manner that the lung phenotype suggests, this would represent another striking difference to the phenotype of *Pkd1l1*$^{rks/rks}$ mutants. Indeed, the 13.5 dpc phenotype of *Pkd1l1*$^{-/-}$ mutant is quite similar to that of *iv/iv* mutants in which the Nodal cascade is activated randomly (**Table 4-4**).

Table 4-4 Statistical comparison of laterality phenotypes

	P value	Significant (CI=95%)	Significant (CI=99%)	Test
***Pkd1l1*$^{rks/rks}$ vs *Pkd1l1*$^{-/-}$**				
Lung situs	5.998×10^{-14}	Yes	Yes	Chi-square
Heart apex	0.0131	Yes	No	Chi-sqaure
Stomach situs	0.2459	No	No	Chi-sqaure
Pkd1l1*$^{-/-}$ vs *iv/iv				
Lung situs	0.0219	Yes	No	Chi-square
Heart apex	0.0973	No	No	Chi-sqaure
Stomach situs	0.1792	No	No	Chi-sqaure

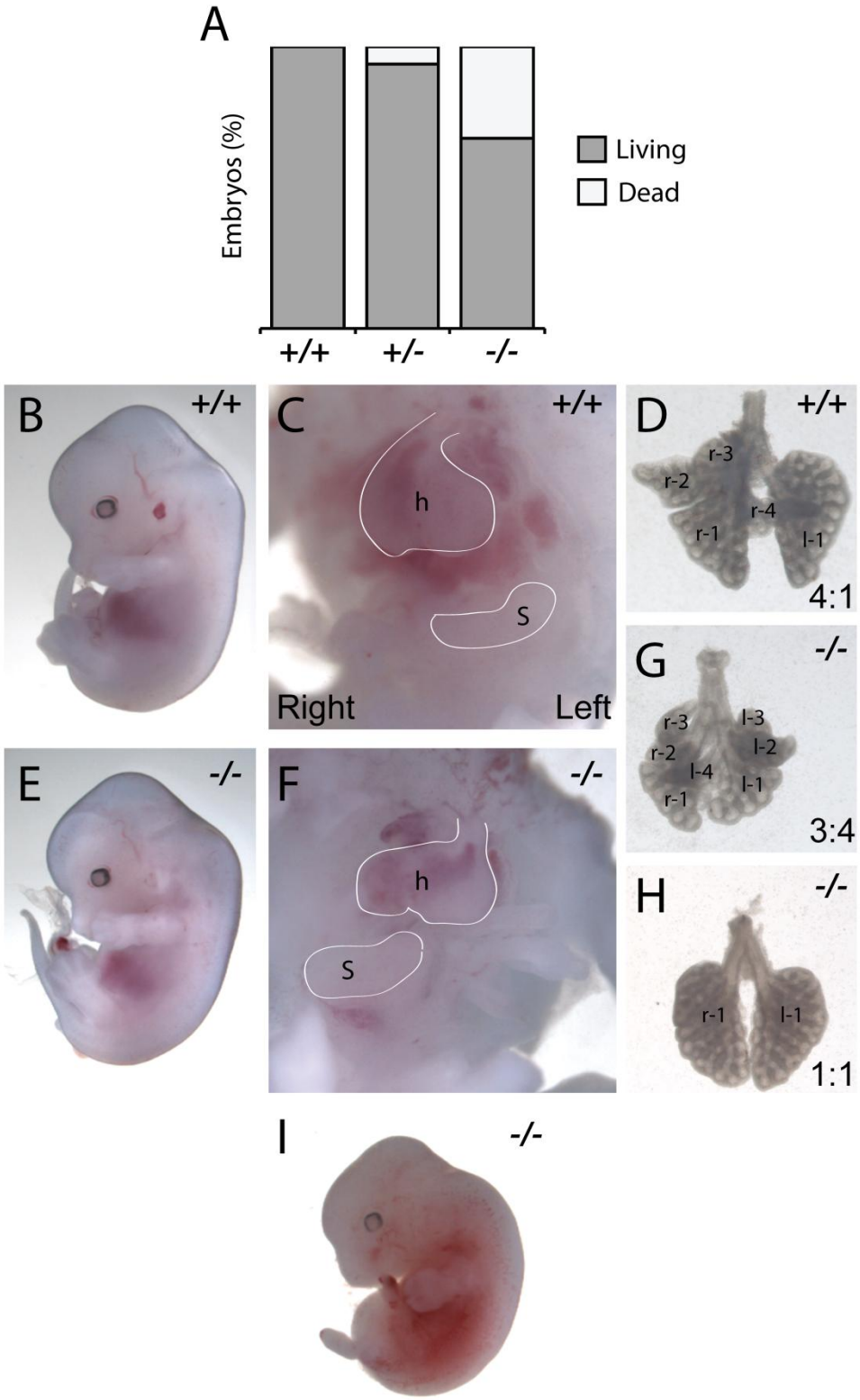

Figure 4.1. *Pkd1l1*$^{-/-}$ mutants exhibit gross situs defects

A Number of embryos of each genotype found at 13.5 dpc, either living or dead. All Pkd1l1$^{+/+}$ embryos were living (n=5/5), while 3/50 and 13/40 Pkd1l1$^{+/-}$ and Pkd1l1$^{-/-}$ embryos were found dead; the loss of homozygous mutant embryos was statistically significant (see text). **B** Wild-type whole embryo at 13.5 dpc showing **C** leftward heart apex and stomach positioning and **D** normal lung situs (4:1). **E** *Pkd1l1*$^{-/-}$ mutant embryo with **F** reversed heart apex and stomach positioning and **H** left pulmonary isomerism (1:1). **G** A second *Pkd1l1*$^{-/-}$ mutant embryo exhibiting partial right pulmonary isomerism (4:4). **I** A mutant embryo that had arreseted prior to dissection at 13.5 dpc. h - heart, s - stomach, l - left lung lobe, r - right lung lobe.

4.2.3. Node cilia are present and motile in *Pkd1l1*$^{-/-}$ mutants

The phenotype of *Pkd1l1*$^{-/-}$ mutants, with randomised lung situs, is similar to that of *iv/iv* mutants that have immotile node cilia. Indeed, embryos that have lost node cilia entirely often present with bilateral *Nodal* induction which would lead, most often, to left lung isomerism. Thus, we assayed for the presence of cilia in *Pkd1l1*$^{-/-}$ embryos by performing whole embryo immunofluorescence with anti-acetylated tubulin antibodies that mark the ciliary axoneme. This approach revealed that cilia were indeed present in *Pkd1l1*$^{-/-}$ embryos; the pattern of acetylated tubulin staining was not different to wild-type embryos (**Figure 4.2A,B**). However, it will be important to also perform scanning electron microscopy (SEM) to determine whether there are any more subtle structural defects in the cilia *Pkd1l1*$^{-/-}$ mutants.

To ascertain whether the node cilia of *Pkd1l1*$^{-/-}$ are motile, we performed high-speed video microscopy using differential interference contrast (DIC) optics, as described in **§3.2.2**. Cilia were found to be motile in both wild-type and *Pkd1l1*$^{-/-}$ mutants, with similar cilia beat frequency of around 10.5 revolutions per second (**Figure 4.2**).

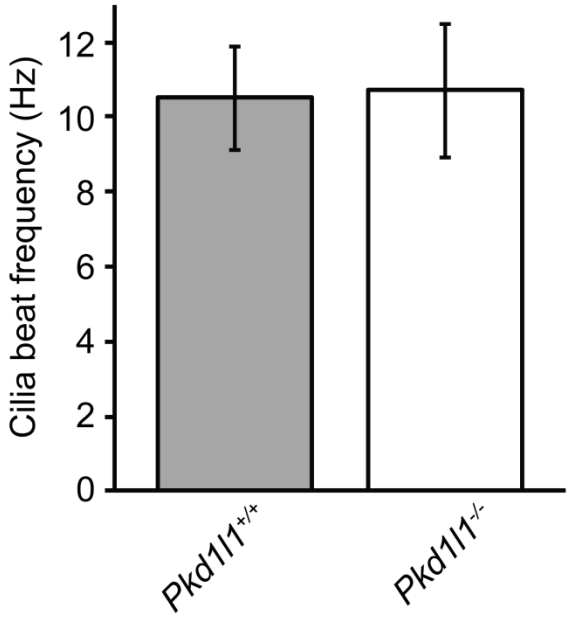

Figure 4.2. Node cilia rotate at the normal frequency in Pkd1l1-/- mutants

Ciliary rotation frequency was measured for wild-type and three mutant embryos, then at least 20 cilia per embryo were assessed for rotation frequency. Both wild-type and mutant embryos exhibited similar frequencies of cilia rotation, just over 10 times per second. Error bars represent standard deviation.

4.2.4. *Pitx2* expression bilaterally expressed in *Pkd1l1*$^{-/-}$ embryos

Given the discrepancy in phenotype between *Pkd1l1*$^{-/-}$ and *Pkd1l1*$^{rks/rks}$ mutants at 13.5 dpc, we wanted to assess the molecular basis of the *Pkd1l1*$^{-/-}$ phenotype. Thus, we determined the expression of the left-sided gene *Pitx2* in *Pkd1l1*$^{-/-}$ mutants. Strikingly, *Pitx2* was bilaterally expressed in the LPM in the majority of *Pkd1l1*$^{-/-}$ mutants (10/14) (**Figure 4.3B,C,E**). The remaining four mutants showed either left-sided or right-sided (**Figure 4.3D,E**) *Pitx2* expression (**Figure 4.3E**). Of the 10 mutants which exhibited bilateral *Pitx2* expression, the majority showed symmetrical expression between left and right (8/10) (**Figure 4.3B**). However, two mutants exhibited bilateral expression but had more extensive expression on the right hand side (2/10) (**Figure 4.3C**). Given that *Pitx2* is activated by Nodal, these results suggest that *Pkd1l1* is required to restrict Nodal pathway activity to the left LPM. Strikingly, this phenotype is opposite to the absent *Nodal/Lefty2/Pitx2* observed in *Pkd1l1*$^{rks/rks}$ mutants, reinforcing that idea that *Pkd1l1*^{rks} does not represent a null allele.

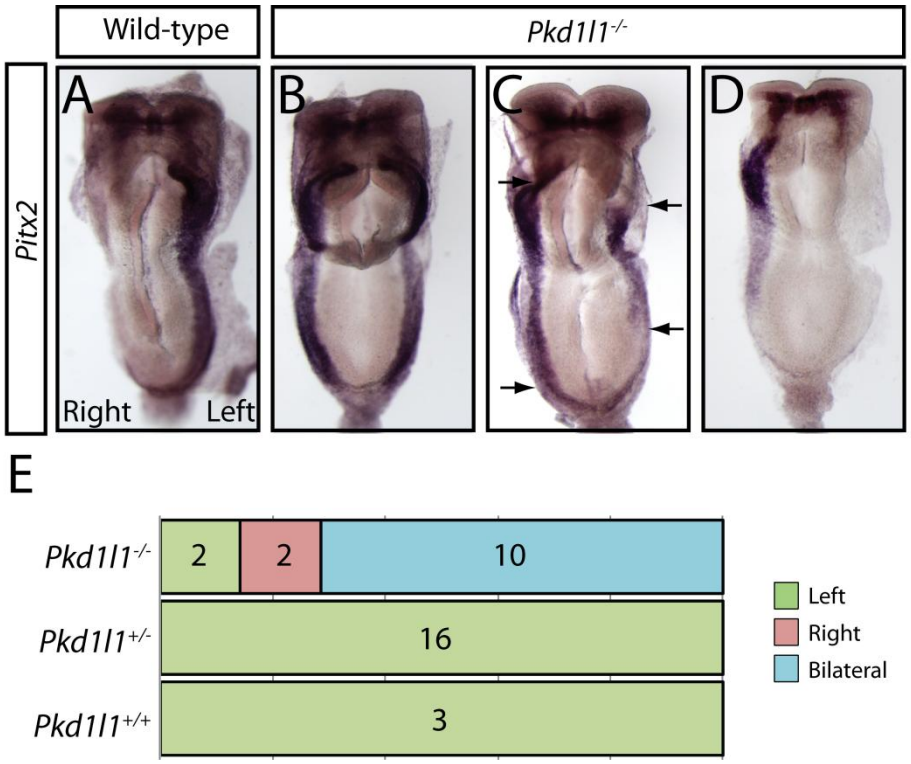

Figure 4.3. *Pitx2* expression is bilateral in *Pkd1l1*$^{-/-}$ mutants

A-D Whole mount in situ hybridisation for *Pitx2* in *Pkd1l1*$^{-/-}$ mutants, where *Pitx2* was most often bilateral (B,C), either symmetrically or with a bias (see arrows in C), or right-sided (D). **E** Number of embryos showing the indicated expression patterns.

4.2.5. The *Pkd1l1*^{rks} mutation disrupts an extracellular PKD domain

Based on the phenotypic differences between *Pkd1l1*$^{-/-}$ and *Pkd1l1*$^{rks/rks}$ mutants, after genetic background had been controlled, we reasoned that *Pkd1l1*^{rks} does not represent a simple null allele. Indeed, the ENU derived *Pkd1l1*^{rks} mutation causes an aspartic acid-to-glycine amino acid substitution at position 411 in the protein sequence (**§2.2.1**), and so would not be expected to disrupt protein expression itself. Pkd1l1 is a multi-pass transmembrane protein with a large extracellular N-terminal region (**Figure 4.4A**). This region contains two polycystic kidney disease (PKD) domains, approximately 90 amino acid domains composed largely of β-strands (Bycroft et al., 1999). The D411G point mutation in *Pkd1l1*^{rks} disrupts the second extracellular PKD domain of Pkd1l1 (**Figure 4.4A**). We therefore wondered how this mutation might affect the structure and function of this domain, and how this might impact upon the establishment of L-R asymmetry.

Firstly, the amino acid change itself is non-conservative. Aspartic acid is negatively charged and highly polar, whereas glycine is the smallest amino acid and is hydrophobic in character (**Figure 4.4C**). The *rks* mutation therefore represents a dramatic change in amino acid characteristics at the mutated residue. Amino acid conservation throughout evolution can give an indication of how essential a residue is for protein function. We therefore performed multi-species alignments of the second PKD domain of Pkd1l1 (Pkd1l1PKDd2) (**Figure 4.4B**). This revealed two interesting points: (1) the mutated aspartic acid has been highly conserved throughout evolution, being present in all organisms assessed apart from zebrafish where a conservative change to glutamic acid has occurred; and (2) the mutated aspartic acid (underlined) is part of the WNFGDG motif, the most highly conserved motif of the domain (Bycroft et al., 1999). Based on this, we would expect the D411G mutation to disrupt the function of the second PKD domain of Pkd1l1.

While no structural information exists for Pkd1l1PKDd2, previously the structure of a PKD domain from the Pkd1l1 homologue Pkd1 (Pkd1PKDd1) has been solved by nuclear magnetic resonance (NMR) spectroscopy (Bycroft et al., 1999). This revealed PKD domains to be composed of 7 β-strands (named A, B, C, C', E, F and G) which fold to form a β-sandwich structure. We used nFOLD3, an online tertiary structural prediction programme, to predict the structure of Pkd1l1PKDd2 based on other structures in the protein database. Not surprisingly, the structure we obtained was highly similar to the NMR-solved structure for Pkd1PKDd1 (**Figure 4.4A**), with 7 β-strands forming a β-sandwich structure. We then used nFOLD3 to predict the structure of Pkd1l1PKDd2 harbouring the *rks* D411G point mutation. In this case, the same overall structure was predicted but some secondary structural elements had been lost in the region of the mutation (**Figure 4.4A**, see asterisks in schematic); the software predicted that β-strand C' would not fold, while β-strand E would become shorter (**Figure 4.4A**). This apparent increase in disorder was backed up by a second prediction programme, DISOClust, which predicted an increase in residue disorder, characteristic of decreased secondary structural elements, in the centre of the domain where the *rks* mutation resides (**Figure 4.4D**). In conclusion, sequence alignments and structural predictions reveal the aspartic acid that is mutated in *Pkd1l1*^{rks} to be highly conserved and important for the PKD domain to retain structural integrity. This suggests that the D411G mutation in *Pkd1l1*^{rks} disrupts Pkd1l1 function by affecting

the structure and function of the second extracellular PKD domain, implicating this domain as essential for the establishment of L-R asymmetry.

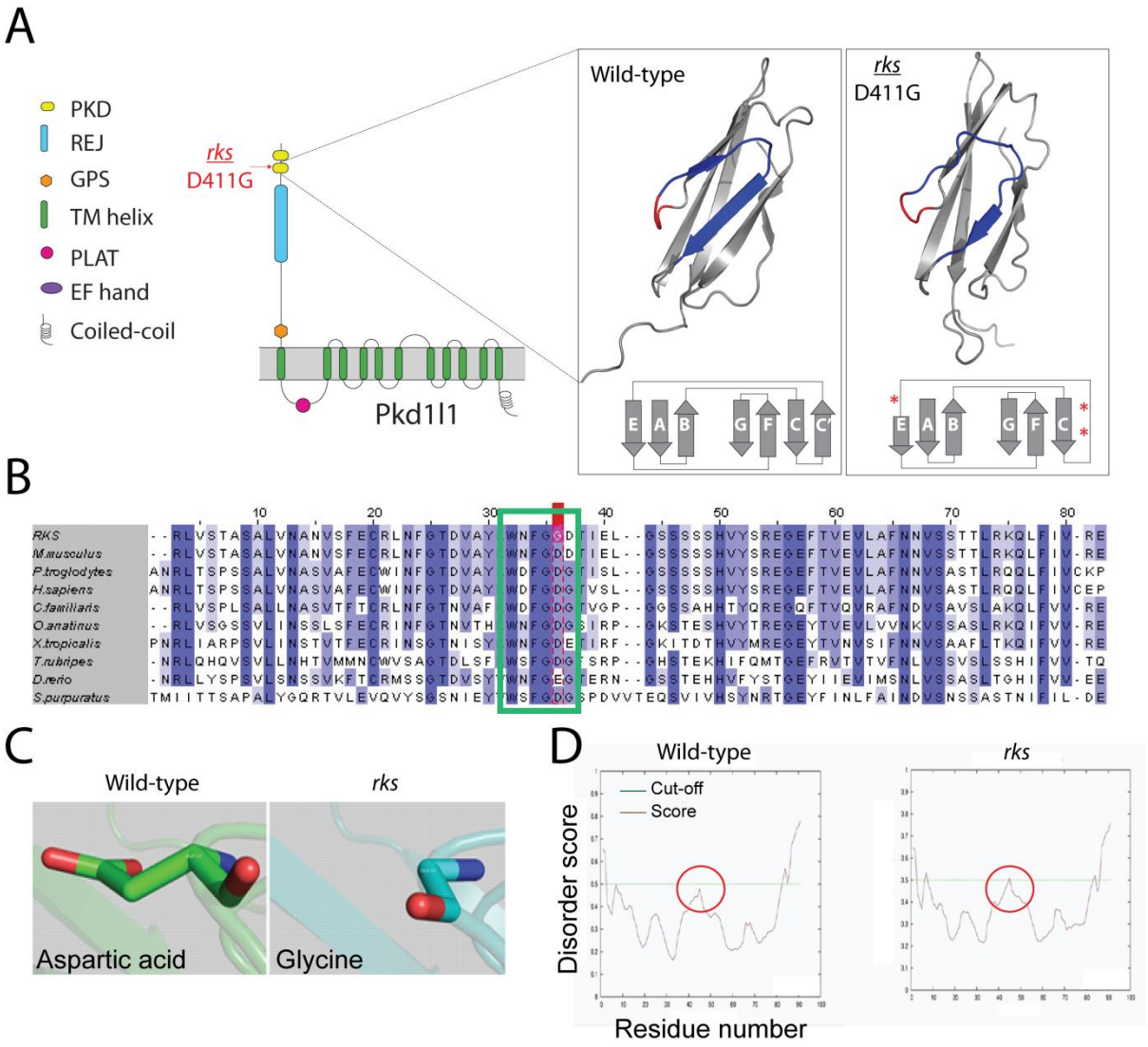

Figure 4.4. The *Pkd1l1*^{rks} mutation (D411G) disrupts an extracellular PKD domain

A Schematic of Pkd1l1 with annotated domains and the location of the *rks* mutation shown. Also shown are the structural models (with schematics) of the second PKD domain of Pkd1l1 (Pkd1l1PKDd2), with red denoting the mutated region and blue showing the region that has lost structure in the mutant (red asterisks in schematic). **B** Sequence alignment of Pkd1l1 with the *rks* mutation shown in red and the conserved WNFGDG region boxed. **C** Rendering of the mutated residue from the structural model shown in A, highlighting the change in characteristics including size between aspartic acid and glycine. **D** DISOclust disorder prediction for wild-type and *rks* PKD domain. Increased disorder is predicted in the region of the mutation, highlighted by the red circle.

4.2.6. Preliminary experiments to assess the mechanical strength of Pkd1l1 PKD domains

Several biological functions require proteins that are mechanically strong (i.e. resistant to unfolding under force) (Brockwell, 2007). Mechanical strength of proteins is principally determined by secondary structure and native topology, with β-sheet proteins unfolding at higher mechanical force than proteins composed mainly of α-helices (Forman and Clarke, 2007). Mechanical strength is further impacted by specific intramolecular interactions, such as hydrogen bonds and side-chain interactions that exist in a proteins native state (Best et al., 2003; Craig et al., 2004; Ng and Clarke, 2007). Immunoglobulin (Ig)-like domains, characterised by their β-sandwich structure, are particularly mechanically strong (Oberhauser and Carrion-Vazquez, 2008; Oberhauser et al., 1999; Oberhauser et al., 1998). The first PKD domain of Pkd1, which has a similar topology to Ig domains, was shown to be extremely resistant to unfolding under force (Forman and Clarke, 2007; Forman et al., 2005; Qian et al., 2005). These experiments used atomic force microscopy (AFM), applying force to the N and C termini of PKD domains. It has been argued that the mechanical strength of PKD domains is critical for Pkd1's function as a mechanosensor in kidney epithelial cells (Nauli et al., 2003); indeed, several human mutations in Pkd1's PKD domains that cause ADPKD have been shown to mechanically weaken those domains (**Figure 4.5A**; (Ma et al., 2009)) when incorporated into Pkd1PKDd1, the only domain that has been used for AFM to date.

Based on these notions, we predicted that the second PKD domain of Pkd1l1, in which the *Pkd1l1*^{rks} mutation resides, might be mechanically strong and that this strength may be affected by the *Pkd1l1*^{rks} mutation. To test this hypothesis, we set out to perform AFM experiments on both wild-type and mutant Pkd1l1PKDd2 domains.

4.2.6.1. A heterologous polyprotein construct for AFM

It is known that a construct containing simple repeats of Pkd1PKDd1 is not soluble (Forman et al., 2005; Qian et al., 2005). Thus, we used recombinant DNA techniques to engineer a heterologous polyprotein construct containing four domains (**Figure 4.5B**); three I27 domains from human titin (an I-set type Ig domain), and a single Pkd1l1PKDd2 domain. The titin I27 domains were used as they have been found previously to express well in bacteria and to aid in the

production of soluble protein product (Best et al., 2003; Forman et al., 2005; Qian et al., 2005). Furthermore, the I27 titin domain is known to unfold at around 180 pN, and so can act as an internal fingerprint during the AFM experiment. The PKD portion of the construct contains 78 amino acids, representing the entire PKD domain with little unstructured regions at the N- and C-termini. Furthermore, we included four alanine residues between the N- and C-termini of the PKD domain and the adjoining I27 domains; these small linkers allow each domain room enough to fold as an independent unit (Forman et al., 2005). The vector used for expression was pRSET-A (Invitrogen), which includes a 6xHis tag at the N-terminal side of the construct. We generated three such constructs, one wild-type PKDd2, one harbouring the *Pkd1l1*^{rks} domain (D34G in the construct), and one containing a D35S mutation that acts as a positive control as this mutation is known to reduce domain strength in Pkd1PKDd1 (Qian et al., 2005).

4.2.6.2. Purification of heterologous polyprotein and preliminary AFM

Constructs were expressed in bacteria and protein was then purified using a Ni column, as described previously ((Steward et al., 2002); see also **Experimental Procedures**). Separating protein by electrophoresis, then staining for total protein revealed bands of around 50 kDa (**Figure 4.5D**). This is likely to represent the purified heterologous polyprotein for two reasons: (1) the size is close to that predicted for the construct, and (2) the band is noticeably stronger when protein was purified from cells in which construct expression was induced by addition of IPTG (**Figure 4.5D**).

For AFM experiments, we collaborated with Andres Oberhauser (University of Texas). He performed AFM on all three polyproteins but was unable to find clear results (personal communication). For all three constructs, the AFM results were characteristic of unfolded domains, suggesting that the protein has denatured during the purification and not refolded. Thus, we have not yet been able to test whether the Pkd1l1PKDd2 domain is mechanically strong and whether such putative strength is weakened by the *Pkd1l1*^{rks} mutation.

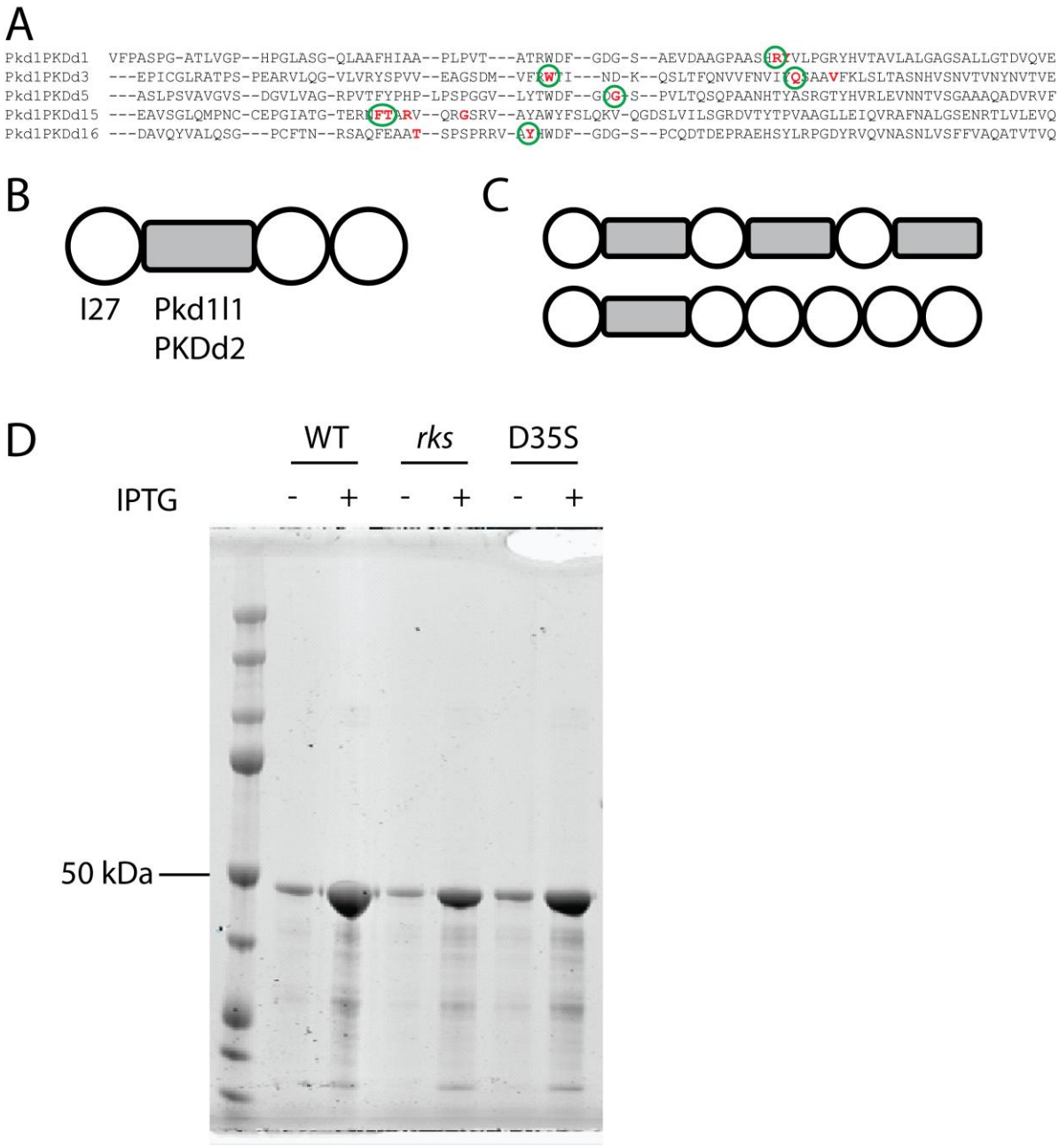

Figure 4.5. PKD domain constructs for atomic force microscopy

A Sequence alignments for five PKD domains from Pkd1. In red, mutations that cause ADPKD are shown. Green circles represent mutations that reduce PKD domain strength when incorporated in Pkd1PKDd1. **B-C** Schematic of AFM constructs showing PKD domains (grey) and I27 titin domains (white). **D** Expression (induced by IPTG) and purification of Pkd1l1PKDd2 wild-type and mutant constructs which are revealed at around 50 kDa by staining for protein.

4.2.6.3. Future tactics

There are several potential avenues for obtaining meaningful results from the AFM work. Firstly, it will be important to optimise the Ni-column purification of the polyproteins. Changing the elution conditions, especially the pH, will likely affect whether the proteins are denatured (Maria Buenavista, personal communication). Others have had success using different types of polyprotein constructs (**Figure 4.5C**) (Ma et al., 2009; Qian et al., 2005); thus, it may be fruitful to use a different arrangement of I27-PKD domains to encourage domain folding. However, it may be that the Pkd1l1PKDd2 is not amenable to the AFM technique: indeed, several other PKD domains from human PKD1 have been analysed by this technique, but only the first domain, Pkd1PKDd1, has been successful (Richard Sandford, personal communication). Thus, we are also planning to incorporate the *rks* mutation into a construct harbouring human Pkd1PKDd1. Wild-type versions of this construct are known to work well in the AFM experiments (Forman et al., 2005; Qian et al., 2005), and we should therefore be able to readily assess the effect of the *rks* point mutation on the strength of a PKD domain, even if it is not the PKD domain from Pkd1l1.

4.3. DISCUSSION

Engineered *Pkd1l1*$^{-/-}$ null mouse mutants were originally described by Vogel and colleagues (Vogel et al., 2010); analysed on a mixed 129:B6J genetic background, the authors observed that around 35% of the expected number of homozygous mice survived to adulthood. Since this is strikingly different to *Pkd1l1*$^{rks/rks}$ mutants, in which we observe 100% embryonic lethality on a C3H background, we decided to investigate the reason for this discrepancy. While being on a mixed genetic background did subtly alter the *Pkd1l1*$^{rks/rks}$ phenotype, this alone could not explain the differences between *Pkd1l1*$^{-/-}$ and *Pkd1l1*$^{rks/rks}$ mutants. For direct comparison with *Pkd1l1*^{rks}, we backcrossed *Pkd1l1*$^{-}$ to C3H for at least 4 generations; phenotypic analysis of these *Pkd1l1*$^{-/-}$ mutants revealed L-R defects that are strikingly different to *Pkd1l1*$^{rks/rks}$ mutants. Based on this, we reasoned that *Pkd1l1*^{rks} is likely to be a not a straight null allele of *Pkd1l1*. The D411G point mutation in *Pkd1l1*^{rks} is predicted to structurally and functionally disrupt the second of two extracellular PKD domains in the N terminal region of Pkd1l1. This likely prevents

the PKD domain from functioning, which may in turn hinder the sensation of fluid flow in the node.

4.3.1. *Pkd1l1*$^{-/-}$ and *Pkd1l1*$^{rks/rks}$ have distinct left-right defects

The fact that *Pkd1l1*$^{-/-}$ embryos exhibit a high proportion of reversed lung situs or left lung isomerism suggests that the normally left-restricted Nodal cascade is activated, likely in a randomised or bilateral fashion, in *Pkd1l1*$^{-/-}$ mutants. This is similar to the loss of leftward flow in *iv/iv* embryos (**Chapter three**); indeed, the 13.5 dpc phenotype of *iv/iv* and *Pkd1l1*$^{-/-}$ is more similar than is *Pkd1l1*$^{-/-}$ and *Pkd1l1*$^{rks/rks}$ (compare **Table 4-4** to **Table 4-5**). This unexpected finding demands a reconsideration of the model presented in **Figure 3.8D**. Based only on the *Pkd1l1*$^{rks/rks}$ phenotype, where the Nodal cascade is never induced in the LPM, we reasoned that mutation of *Pkd1l1* prevents the sensation of leftward flow and the downregulation of left-sided *Cerl2*, resulting in a failure to derepress left-sided Nodal; as a result, *Nodal* is not initiated in the left LPM. However, if the Nodal cascade is activated randomly/bilaterally in *Pkd1l1*$^{-/-}$ embryos, then we must add to this framework that Pkd1l1 normally acts to repress Nodal; this repression would then be relieved on the left side only as a consequence of the sensation of leftward flow by Pkd1l1. Another possibility to explain the phenotypic differences between *Pkd1l1*$^{-/-}$ and *Pkd1l1*$^{rks/rks}$ mutants is that a second protein can partially compensate to rescue Nodal activation when *Pkd1l1* is lost, but not when it is mutated. These two possibilities are considered at length in the general discussion (**Chapter six**).

4.3.2. The *Pkd1l1*$^{-/-}$ mouse phenotype is similar to the *Pkd1l1*^{abc} medaka fish mutant phenotype

During the course of this thesis, a medaka fish *Pkd1l1* mutant allele named *abc* was described (Kamura et al., 2011). The *abc* point missense mutation causes premature truncation of *Pkd1l1*, likely resulting in a null allele. Mutant fish exhibited randomised situs, while the expression of LPM *southpaw*, a fish *Nodal*, was left-sided (30%), right-sided (11%), bilateral (17%), or absent (43%) (Kamura et al., 2011). Such randomised activation is more similar to the likely *Pkd1l1*$^{-/-}$ molecular phenotype than it is to *Pkd1l1*$^{rks/rks}$, underlining the idea that *Pkd1l1*^{rks} represents a more complicated non-null allele.

4.3.3. A mechanosensitive PKD domain is likely disrupted by the *Pkd1l1*^{rks} mutation

The extracellular portion of Pkd1l1 contains two PKD domains. PKD domains are Ig-like β-sandwich folds that are remarkably mechanically strong (Bycroft et al., 1999; Forman et al., 2005; Qian et al., 2005). Using secondary and tertiary structural prediction programmes, we have ascertained that the *Pkd1l1*^{rks} point mutation likely structurally disrupts the second PKD domain of Pkd1l1, causing regions that normally form β-strands to become unstructured and disorderd. Since the secondary structural elements of PKD domains are crucial for their mechanical strength (Forman et al., 2009), we reasoned that the *Pkd1l1*^{rks} mutation likely results in reduced strength of the PKD domain. Furthermore, the D411G mutation in *Pkd1l1*^{rks} (underlined) disrupts a highly conserved WNFGDG motif within the PKD domain. Mutation of the neighbouring G residue (WNFGDG) to serine in the first PKD domain of Pkd1 results in a substantial weakening of the domain with the unfolding force being reduced from 180 pN in wild-type to 55 pN in the mutant (Ma et al., 2009). This clearly affects function, as this exact mutation is known to cause human ADPKD (pkdb.may.edu).

Pkd1 is argued to be a mechanosensitive protein, being required for flow sensation by kidney epithelial cells during kidney development and homeostasis (Nauli et al., 2003; Nauli and Zhou, 2004). Mutation of PKD domains affect such mechanosensation by Pkd1 (Ma et al., 2009). Pkd1l3 does not contain PKD domains; it is expressed in a subset of taste receptor cells and has been implicated in sour taste reception (Ishimaru et al., 2006; Ishimaru and Matsunami, 2009). Based on these two examples, it appears that PKD domains are present in Pkd-like proteins when the function is mechanosensation, whilst they are absent in the chemical sensor Pkd1l3. Thus, the fact that Pkd1l1 contains PKD domains whose mutation affects function, as *Pkd1l1*$^{rks/rks}$ mutants have severe L-R defects, heavily implicates Pkd1l1 as a sensor of mechanical force. This line of reasoning fits most coherently with the two-cilia hypothesis of nodal flow sensation, in which flow itself is directly sensed by mechanosensitive cilia in the node.

CHAPTER FIVE

Pkd1l1 and Pkd2 physically interact and the *Pkd2*^{lrm4} mutation disrupts Pkd2's localisation to node cilia

5.1. INTRODUCTION

The analysis of *Pkd1l1* and *Pkd2* mutant mice has revealed that both genes play a role in the establishment of L-R asymmetry. Furthermore, genetic analysis suggests that both Pkd1l1 and Pkd2 act downstream of leftward nodal flow but upstream of asymmetric gene expression, leading to the possibility that Pkd1l1 and Pkd2 act together in a complex. In kidney, Pkd1 and Pkd2 are known to form functional complexes, therefore we set out to test for a possible physical association between Pkd1l1 and Pkd2.

5.2. RESULTS

5.2.1. Pkd1l1 contains an intracellular coiled coil domain

Coiled coil domains can act as protein-protein interaction interfaces. Pkd1 and Pkd2 interact via intracellular C-terminal coiled coil domains (Hanaoka et al., 2000; Qian et al., 1997). Thus, we sought to ascertain whether mouse Pkd1l1 contained a coiled coil domain. The coiled coil prediction programme PCOILS predicted the existence of a coiled coil domain within Pkd1l1's intracellular C-terminus between amino acids 2540 and 2564 (**Figure 5.1A**). When represented as a heptad repeat, residues *a* and *d* of the 24 amino acid coiled coil were invariably hydrophobic in nature (**Figure 5.1C**); this is a characteristic feature of coiled coil domains. Furthermore, a helical wheel projection of the Pkd1l1 coiled coil sequence revealed distinct hydrophobic and polar surfaces (**Figure 5.1B**), with the former likely serving as a protein-protein interaction surface. The coiled coil region of mouse Pkd1l1 is well conserved in orthologous proteins. Thus, mouse Pkd1l1 contains a coiled coil domain within its intracellular C-terminus and this domain is likely to be of functional significance.

5.2.2. Generation and expression of Pkd1l1 and Pkd2 epitope-tagged constructs

To assess whether an interaction exists between Pkd1l1 and Pkd2, a Pkd1l1 construct containing the entire Pkd1l1 sequence attached to a C-terminal GFP tag was generated (**Figure 5.2A**). Overexpression of this construct in HEK 293T cells followed by immunoblotting with a GFP antibody, however, did not result in a band

of the expected size. Based on sequence, we predict the full length Pkd1l1-GFP protein to be around 460 kDa. Instead, we consistently observed a band at 80 kDa; this band was specific to transfected cells, and was enriched by GFP immunoprecipitation (**Figure 5.2B**). This is likely to represent a cleavage product. Based on the band size, we predict that the cleavage occurs intracellularly between the fifth and sixth transmembrane helices (**Figure 5.2A**; blue arrow). Interestingly, a recent report argues that Pkd1 is also cleaved between the fifth and sixth transmembrane helices (Woodward et al., 2011), suggesting that the putative Pkd1l1 cleavage we observe may be conserved in other Pkd1-like family members.

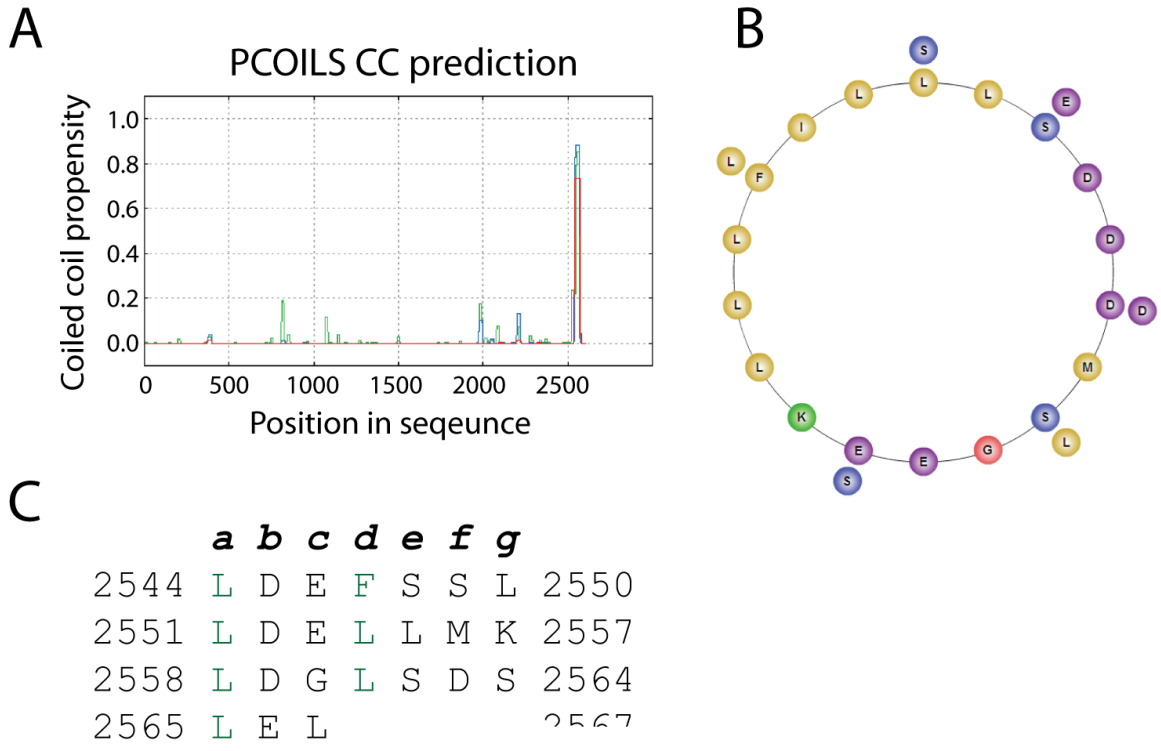

Figure 5.1. The Pkd1l1 protein contains a C-terminal coiled coil domain

A PCOILS coiled coil prediction software found a C-terminal region in Pkd1l1 with a high propensity to form a coiled coil domain. **B** The coiled coil region predicted in A, represented as a helical wheel projection. One surface is composed of hydrophobic amino acids (yellow); this likely represents a protein-protein interaction interface. **C** The coiled coil represented as a heptad repeat; amino acids in positions a and d are invariably hydrophobic, as is characteristic of a coil domain.

We also engineered a Pkd1l1 construct containing only the final 18 kDa of Pkd1l1 attached to a C-terminal GFP. This includes the final transmembrane helix as well as the coiled coil domain that we predict to be required to mediate protein-protein interaction (**Figure 5.2A**). Western blotting using an anti-GFP antibody after expression of Pkd1l1_CC-GFP in HEK 293T cells revealed a band at around 45 kDa that was specific to transfected cell lysates (**Figure 5.2D,E** - input lanes). The 45 kDa band is likely to represent Pkd1l1_CC-GFP for two reasons. First, the predicted molecular weight of Pkd1l1_CC-GFP is 45 kDa. Second, the band was absent from unstransfected or GFP empty vector-transfected lysates (**Figure 5.2D,E** – input lanes).

We also used an epitope-tagged Pkd2 expression constructs: Myc-PKD2 (Hanaoka et al., 2000). Expression of Myc-PKD2 in HEK 293T cells and subsequent Myc western blotting gave a specific band at 140 kDa; the approximate molecular weight of PKD2 (**Figure 5.2D,E** – input lanes). However, when expressed at higher levels, the Myc western blot also revealed higher molecular weight bands specific to Myc-PKD2 transfected cells (**Figure 5.2C** – input lanes). These bands are likely to represent oligomeric forms of PKD2 protein, as has been reported previously (Fogelgren et al., 2011; Hanaoka et al., 2000). Further confirmation that these bands represent PKD2 protein was obtained by performing a western blot using an anti-Pkd2 antibody (data not shown).

5.2.3. Pkd1l1 and Pkd2 interact via Pkd1l1's coiled coil domain

To test for an interaction between Pkd1l1 and Pkd2, we performed immunoprecipitation experiments from HEK 293T cell lysates after expression of Pkd1l1-GFP and Myc-PKD2. GFP immunoprecipitation purified both Pkd1l1-GFP (seen as a weak band at 80 kDa) and Myc-PKD2 (**Figure 5.2C**). As a control, only Myc-PKD2 was expressed; in this case, GFP immunoprecipitation did not purify Myc-PKD2, revealing a lack of non-specific binding (**Figure 5.2C**). The complementary experiments were also performed, using an anti-Myc antibody for immunoprecipitation; again, specific purification of both proteins was observed (**Figure 5.2C**). These results show that Pkd1l1 protein can interact with Pkd2, and that this interaction is mediated by the C-terminal cleavage product (**Figure 5.2A**).

Since Pkd1l1 contains a C-terminal CC domain, we predicted that this might be the element required for specific interaction with Pkd2. We therefore repeated the immunoprecipitation experiments using the Pkd1l1_CC-GFP construct. GFP immunoprecipitation enriched Pkd1l1_CC-GFP at 45 kDa and also co-purified Myc-PKD2 (**Figure 5.2D**). Conversely, Myc immunoprecipiation also co-purified Pkd1l1_CC-GFP along with Myc-PKD2 (**Figure 5.2D**). Negative controls were run alongside, and revealed a lack on non-specific immunoprecipitation (**Figure 5.2D**). Since the Pkd1l1_CC-GFP construct also contains the most C-terminal transmembrane helix, we needed to assess whether the Pkd1l1 CC domain itself was required for Pkd1l1-Pkd2 interaction. Thus, we mutated the CC at position 2554 in Pkd1l1. Amino acid 2554 is normally a leucine, a hydrophobic amino acid that forms part of the hydrophobic surface of the coil (**Figure 5.1B,C**). We mutated this residue to an aspartic acid, a polar amino acid which disrupted coil formation (PCOILS prediction). After expressing Pkd1l1_CC^{L2554D}-GFP and Myc-PKD2 in HEK 293T cells, we performed GFP and Myc immunoprecipitation. Though GFP and Myc immunoprecipitation purified Pkd1l1_CC^{L2554D}-GFP and Myc-PKD2, respectively, neither co-purified the other tagged protein (**Figure 5.2E**). These experiments were done alongside those using wild-type Pkd1l1_CC-GFP, and so the complete lack of co-purification with the mutant construct strongly suggested that disruption of the Pkd1l1 coiled coil domain prevents interaction with Pkd2, supporting the idea that Pkd1l1 and Pkd2 interact at the intracellular interface between their coiled coil domains.

As a final control experiment, we attempted to co-purify a Trim71-Flag (a gift from Victoria Patterson) protein with Pkd1l1_CC-GFP. Trim71 contains a large coiled coil domain (**Figure 5.2F**), and so this experiment tested whether the Pkd1l1 coil had any particular specificity for Pkd2 or whether it simply interacted with coiled coil domains in general. The Trim71-Flag protein was observed as a single band at the predicted molecular weight of 80 kDa. However, though GFP immunoprecipitation enriched Pkd1l1_CC-GFP, we found no evidence of Trim71-Flag co-precipitation (**Figure 5.2F**). This supports the idea that there exists some specificity between the Pkd1l1 CC and Pkd2, arguing that the Pkd1l1 CC is not simply sticky, being able to bind with other CC domains.

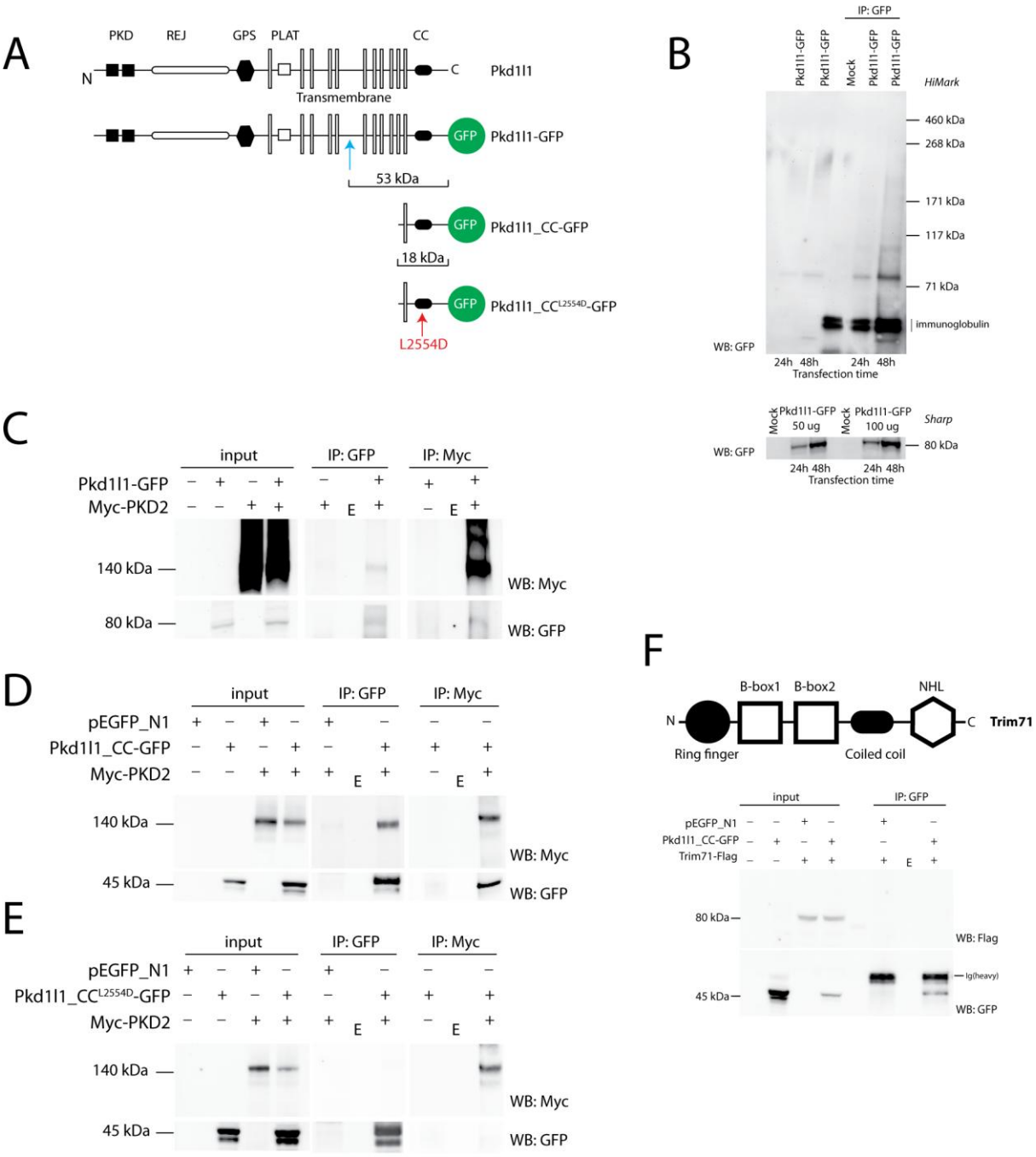

Figure 5.2. Pkd1l1 and Pkd2 physically interact

A Schematic of Pkd1l1 and the various constructs used for this work. A blue arrow shows the position of the predicted cleavage site. **B** Western blot of Pkd1l1-GFP input and after GFP IP, showing a cleavage product at around 80 kDa. **C-E** Myc and GFP IP experiments demonstrating interaction between Myc-PKD2 and the cleavage product of Pkd1l1 (C), as well as a shorter Pkd1l1 construct containing the coiled coil domain (D). Mutation of the coiled coil domain prevents interaction (E). **F** Pkd1l1 and Trim71 do not interact. Schematic of Trim71 structure showing a 31 amino acid coiled coil domain of similar length to to domain found in Pkd1l1. GFP IP experiments using Pkd1l1_CC-GFP and Trim71-Flag show they do not interact, with the Trim71-Flag band being visible at 80 kDa.

5.2.4. Pkd2 localises to primary cilia, including cilia within the node

To assess the sub-cellular localisation of Pkd2 we used a variety of approaches. To begin with, we transfected inner medullary collecting duct (IMCD3) cells with the Myc-PKD2 construct then performed Immunostaining using an anti-Myc antibody and an anti-Pkd2 antibody (YCE2). The two stains strongly co-localised throughout the cell (in a pattern reminiscent of the endoplasmic reticulum) and, to a lesser extent, in the nucleus (**Figure 5.3A**). However, differential interference contrast (DIC) revealed that the neighbouring untransfected cells were not stained by the YCE2 anti-Pkd2 antibody (**Figure 5.3A**). This suggests either that endogenous Pkd2 levels are low in IMCD3 cells and/or that the YCE2 antibody is not able to detect endogenous protein. Thus, we moved on to try other Pkd2 antibodies together with markers for various cellular locations.

Staining of non-transfected NIH-3T3 fibroblasts, a well-characterised cell line that grow cilia readily upon serum deprivation, revealed Pkd2 to localise to primary cilia (**Figure 5.3B,C**). Two Pkd2 antibodies were used: H-280 (**Figure 5.3B**) and D3 (**Figure 5.3C**), both from Santa Cruz, which appeared to recognise endogenous Pkd2. In these experiments, antibodies that recognise acetylated alpha-tubulin (Ac-tub) and glutamylated tubulin (Glu-tub), both markers of the ciliary axoneme, were used. Pkd2 localised in punctae along the axoneme, but also appeared in some cells to be concentrated near the base (**Figure 5.3B**; asterisk). Strikingly, Pkd2 localised strongly at the tip of the majority of cilia visualised (staining at the tip was always stronger than staining along the axoneme) (**Figure 5.3B,C**). This staining of the tip was most obvious when Glu-tub was used as a counterstain because the concentration of Glu-tub is known to decrease along the axoneme with close to none being found at the tip (**Figure 5.3C**) (Pathak et al., 2011). Since these antibodies detect endogenous Pkd2 in cilia in a culutred cells, we reasoned that these would be useful for assessing Pkd2 localisation within emrbyos.

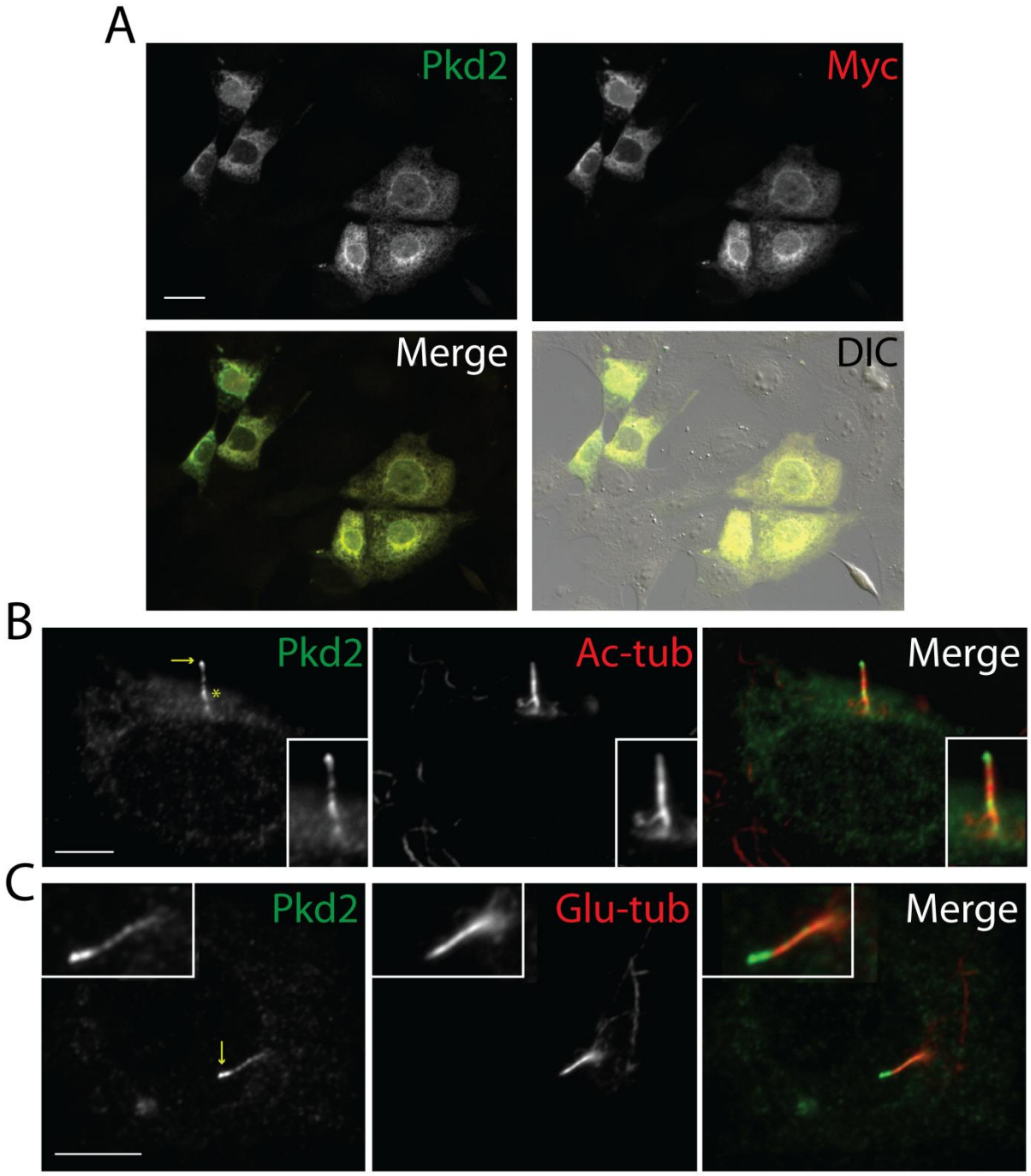

Figure 5.3 Pkd2 localises to the cilium of NIH-3T3 cells

A Non-ciliated IMCD3 cells were transfected with Myc-PKD2 then immunostained for Pkd2 using the YCE2 antibody and counter-stained for Myc. Pkd2 and Myc staining strikingly overlapped, suggesting both antibodies recognise the same protein species. However, untransfected cells revealed by DIC showed no staining with the YCE2 antibody. Thus, YCE2 does not recognise endogenous Pkd2. Scale bar: 10 um. **B-C** NIH-3T3 cells were immostained for endogenous Pkd2 (green; B: H280 and C: D3) and either **A** acetylated alpha-tubulin (Ac-tub; red) or **B** glutamylated tubulin (Glu-tub; red), both microtubule modifications that mark the ciliary axoneme. Pkd2 staining was observed in a punctate fashion along the ciliary axoneme and at a domain near the base of the cilium (asterisk) in some cells. Strong Pkd2 localisation was evident at the ciliary tips (arrows). Scale bar: 5um

5.2.5. The *Pkd2^{lrm4}* mutation disrupts Pkd2's ciliary localisation

The *Pkd2^{lrm4}* point mutation results in an glutamic acid to glycine substitution at amino acid 442, which lies in the first extracellular loop between transmembrane helix 1 and 2 (**Figure 5.4A**). In zebrafish, two antibodies are known to bind epitopes in this transmembrane loop and both are known to block Pkd2 channel function (Schottenfeld et al., 2007). Thus, we initially predicted that the E442G mutation in *Pkd2^{lrm4}* might destroy Pkd2's Ca^{2+} channel function. However, it has recently been demonstrated that Pkd2^{lrm4} protein retains Ca^{2+} channel activity (Yoshiba et al., 2012). Instead, we found that the Pkd2^{lrm4} mutation disrupts the localisation of Pkd2 to cilia within the node. Using the H280 antibody optimised in NIH-3T3 cells (**Figure 5.3B**), we found Pkd2 to localise to nearly all cilia within the node (**Figure 5.4B**), as previously described (McGrath et al., 2003). We quantified the number of Pkd2 positive cilia from three embryos, finding that 234 of a total 236 counted cilia (99.2%) contained Pkd2. In contrast, staining of *Pkd2$^{lrm4/lrm4}$* mutant embryos revealed that Pkd2 no longer localised to node cilia in mutants (**Figure 5.6C**). Of 247 cilia counted from three *Pkd2$^{lrm4/lrm4}$* embryos, none contained Pkd2. Thus, the Pkd2^{lrm4} point mutation prevents Pkd2 from localising to cilia in the node, a finding also made by Hamada and colleagues (Yoshiba et al., 2012). Given the L-R defects prevalent in *Pkd2$^{lrm4/lrm4}$* mutants (**Chapter two**), this finding argues that Pkd2 is only functional within cilia during the determination of L-R asymmetry.

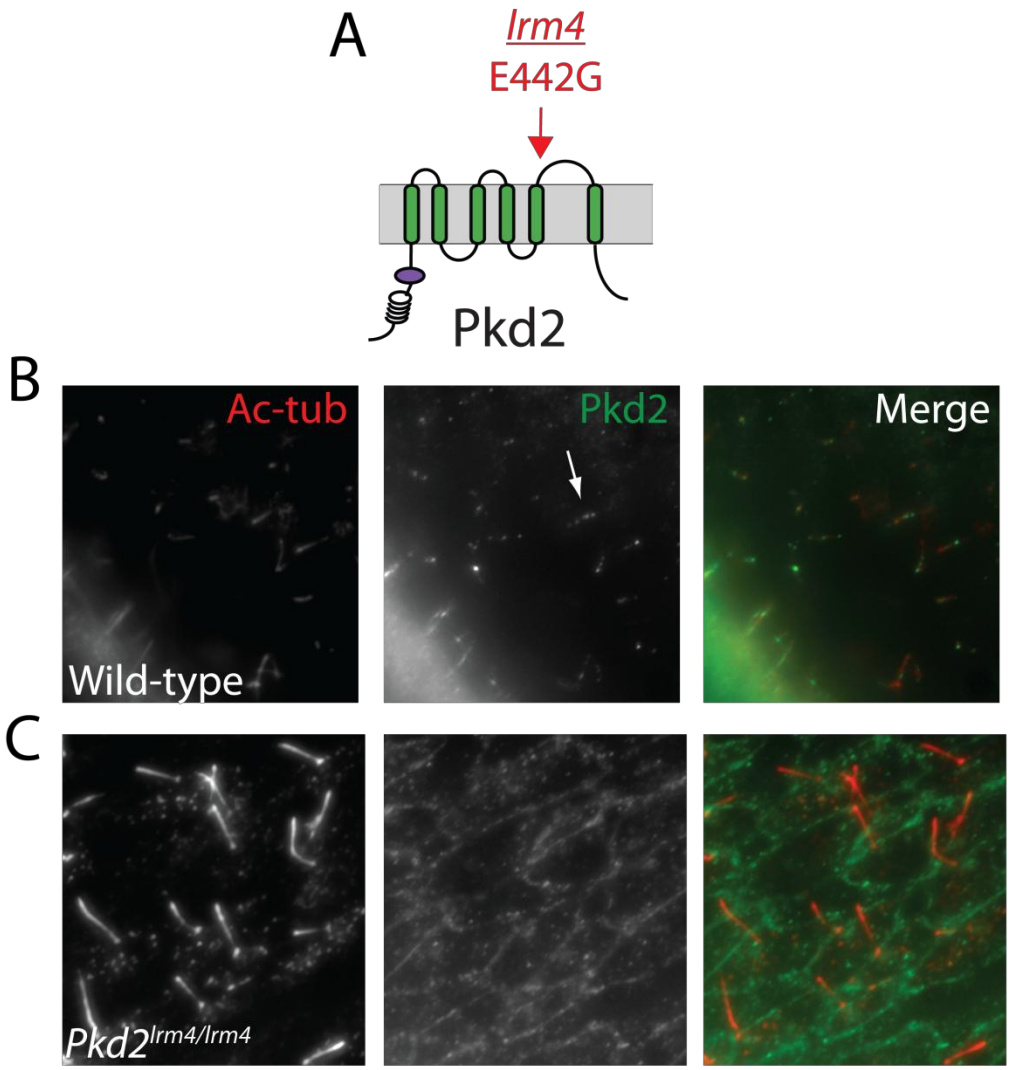

Figure 5.4 Pkd2 localisation to node cilia is disrupted by the E442G mutation in lrm4

A Schematic of Pkd2 protein showing six transmembrane helices, and an intracellular coiled coil domain and EF-hand domain at the C-terminus. Also shown is the position of the E442G mutation. **B-C** Pkd2 staining of embryos at 8.5 dpc reveals Pkd2 to localise to node cilia in a punctate fashion (arrow) in wild-type embryos (B). However, Pkd2 is not present in the node cilia of *Pkd2*$^{lrm4/lrm4}$ mutants (C). Cilia are marked by Ac-tub staining.

5.3. DISCUSSION

In this chapter, an interaction between Pkd1l1 and Pkd2, mediated by Pkd1l1's intracellular coiled coil (CC) domain, has been demonstrated. Furthermore, it has been shown that Pkd2's normal localisation to cilia within the node is disrupted in the *Pkd2*$^{lrm4/lrm4}$ mutant, thereby providing a mechanism of how the *Pkd2*^{lrm4} mutation results in severe L-R defects. This also suggests that Pkd2 localisation to node cilia is essential for Pkd2's function in L-R determination, conclusions that have also been shown by others (Yoshiba et al., 2012). Unfortunately, owing to the absence of a working antibody, we have been unable to assess to localisation of Pkd1l1 within embryos. However, Kamura and colleagues have shown that Pkd1l1 localises to all cilia in the medaka fish Kupffer's vesicle (KV). Though yet to be determined, this makes it likey that Pkd1l1 localises to cilia in the mouse node.

5.3.1. Complexes of sensory polycystin proteins

Over the last decade, members of the polycystin family of proteins have been found to have roles in sensation. Usually, polycystin proteins function in complexes. For example, Pkd1 and Pkd2 interact and co-localise to kidney epithelial cells where they are thought to sense the force of fluid flow (Hanoaka et al., 2000; Nauli et al., 2003). Indeed, mutation of either *PKD1* or *PKD2* in human causes autosomal dominant polycystic kidney disease (ADPKD) (pkdb.mayo.edu). Similarly, Pkd1l3 and Pkd2l1 are known to interact and co-localise to a subset of taste receptor cells where they are argued to function in sour taste reception (Ishimaru et al., 2006; Ishimaru and Matsunami, 2009). In *C. elegans*, the Pkd1 orthologue *lov-1* and the Pkd2 orthologue are both expressed in adult male sensory neurons, though it is not known whether the protein products interact in vivo (Barr et al., 2001; Barr and Sternberg, 1999). Thus, it appears a common theme that two polycystin proteins, one Pkd1-like protein and one Pkd2-like protein, function together as sensory complexes.

Our data support this notion. We provide evidence that the C-terminal portion of Pkd1l1 can physically interact with Pkd2. Indeed, we map the site of interaction to Pkd1l1's intracellular CC domain. Similar findings were reported by others (Kamura

et al., 2011). However, these data do not rule out the possibility that Pkd1l1 makes further contacts with Pkd2 beyond the CC, for example within the transmembrane domains. Furthermore, Kerry-Lyn Riley has shown that Pkd1l1 can localise to primary cilia in IMCD3 cells (data not shown; (Field et al., 2011)), while Kamura and colleagues reported co-localisation of Pkd1l1 and Pkd2 in KV cilia in medaka fish (Kamura et al., 2011). However, both out data and that of Kamura et al., fall short of demonstrating in vivo interaction between Pkd1l1 and Pkd2 within cilia. Nevertheless, these data do support a model in which Pkd1l1 and Pkd2 interact physically in cilia within the L-R coordinator of mammals and fish where they act as sensory complexes required to detect leftward flow.

5.3.2. Pkd2's ciliary localisation is required for L-R determination

Pkd2^{lrm4} protein harbours an E442G amino acid substitution that lies in the first extracellular loop of the protein and would not be likely to prevent production of the protein. Indeed, others have shown that Pkd2^{lrm4} protein retains Ca^{2+} channel activity (Yoshiba et al., 2012). Here, we make the surprising discovery that Pkd2 no longer localises to node cilia in *Pkd2$^{lrm4/lrm4}$* mutants, an observation also reported by others (Yoshiba et al., 2012). These data suggest that suggest that the role of Pkd2 during L-R determination is played within cilia.

Why Pkd2^{lrm4} protein fails to localise to node cilia is unknown. Pkd2 contains an N-terminal ciliary localisation signal, however, the Pkd2^{lrm4} mutation resides within an extracellular loop and is unlikely to affect this signal. Moreover, mutation of the ciliary localisation signal does not prevent Pkd2 from localising to node cilia (Yoshiba et al., 2012). This confusing finding emphasises how little we known about the trafficking of Pkd2 to node cilia. It will be interesting to assess Pkd2 localisation in *Pkd1l1$^{-/-}$* embryos. This will test whether Pkd1l1 is required for Pkd2 localisation to cilia as a situation in which the two interact before being loaded into cilia can be envisioned.

Chapter Six

Coda: On the concordance of organ situs in left-right mutants

In humans, the complete reversal of situs (called situs inversus totalis) is compatible with a healthy life, though the condition is not asymptomatic; it has recently been shown to increase the risk of congenital heart disease (CHD) (Ramsdell, 2005). However, significant morbidity and mortality is associated with perturbations in laterality that result in discordant orientation of organ systems, called heterotaxia, and complex CHD (Bisgrove et al., 2003). Nevertheless, the concordant asymmetric development between different organs is not well understood. In this thesis, we have assessed the phenotypes of four mouse mutants: *Pkd1l1*$^{rks/rks}$, *Pkd2*$^{lrm4/lrm4}$, *iv/iv* and *Pkd1l1*$^{-/-}$ at 13.5 dpc, particularly noting overt stomach and heart positioning, both normally leftward, and lung situs. For three of these mutants, extensive molecular analysis of the LPM and midline markers has also been performed, allowing us to make some conclusions about the link between asymmetric gene cascades and organ concordance.

Heart and stomach positioning were each scored in three possible categories: left (L), central (C), or right (R). Thus, individual embryos were placed into one of 9 possible categories (a 3x3 table) in which three categories represent heart-stomach concordance (LL, CC, and RR) while the other six represent discordance (e.g. LR, RC) between heart and stomach positions. As a simple measure of discordance, we applied the Discordance Index (*DI*) (Bisgrove et al., 2000), defined as:

Wild-type embryos, in which stomach and heart apex position is always leftwards, have a *DI* = 0. Similarly, if all embryos exhibited an entirely discordant phenotype, the *DI* would equal 1. Thus, *DI* is a unitless measure with values of increasing discordance ranging from 0 to 1.

The heart and stomach were not always positioned to the same side of the embryo in the mutants assessed in this thesis. For example, see the *Pkd1l1*$^{rks/rks}$ mutant in **Figure 2.2G**, in which heart positioning is reversed, while the stomach retains a central position. Indeed, for *Pkd1l1*$^{rks/rks}$, 11/28 of individual embryos

exhibited heart-stomach discordance, while 17/45 *Pkd2*$^{lrm4/lrm4}$ mutants demonstrated discordance between heart and stomach positioning (**Figure 6.1A**). Thus, the heart-stomach *DI* for *Pkd1l1*$^{rks/rks}$ and *Pkd2*$^{lrm4/lrm4}$ is 0.39 and 0.38, respectively (**Figure 6.1B**). In contrast, the majority of *iv/iv* and *Pkd1l1*$^{-/-}$ embryos exhibit a high level of heart-stomach concordance (**Figure 6.1A**), with their *DI*'s being 0.10 and 0.12, respectively (**Figure 6.1B**). Thus, *Pkd1l1*$^{rks/rks}$ and *Pkd2*$^{lrm4/lrm4}$ mutants fall into a 'high discordance' category, while *iv/iv* and *Pkd1l1*$^{-/-}$ mutants have 'low discordance'. Statistical testing revealed the differences between these categories to be significant (**Figure 6.1B**).

It is not surprising that *Pkd1l1*$^{rks/rks}$ and *Pkd2*$^{lrm4/lrm4}$ mutants have high discordance, as both mutants have the same molecular phenotype, with loss of the left-sided Nodal pathway. This data, therefore, shows that in the absence of left-sided Nodal signals, heart and stomach direction randomise independently of each other, suggesting that each organ anlagen receives and responds to the L-R pathway independently. In the absence of signalling, each makes a random decision and the final outcome is the sum of independent L-R decisions with respect to each other, a situation that resembles human heterotaxia. Thus, in the absence of the LPM Nodal cascade, the positioning of the heart and stomach are: (1) randomised; and (2) independent of one another.

The lower discordance in *iv/iv* mutants can be explained by the fact that these mutants do activate the Nodal cascade, albeit in a randomised or, most often, bilateral fashion. One would predict that left or right sided *Pitx2* expression would lead to concordant stomach and heart positions, being normal or reversed, respectively. Similarly, those embryos which have bilateral expression with a strong bias to one side might be expected to show concordant heart/stomach positions. Finally, some *iv/iv* mutants showed symmetrical bilateral *Pitx2* expression, with no discernible difference between left and right; 26% of *iv/iv* mutants showed this expression pattern between the 4-7 somite stages (**Figure 3.5**). In these embryos, the most obvious expectation would be randomised stomach and heart positioning. Since heart and stomach positioning were never central in *iv/iv* mutants (and were rarely central in the other mutants) (**Figure 6.1A**), it can be argued that half of the embryos showing bilaterally symmetric *Pitx2* would develop to have discordant stomach/heart positioning. Thus, the *Pitx2* expression pattern of *iv/iv* mutants predicts that around 13% of embryos would exhibit a heart-stomach discordant

phenotype. This prediction is remarkably close to the 10% of embryos that exhibit such discordance at 13.5 dpc.

These preliminary data suggest that overt morphological phenotype can be predicted from molecular L-R marker expression. This might be useful in elucidating the cause of human laterality disorders, where molecular analysis of embryos is not possible.

A

Pkd1l1$^{rks/rks}$

Stomach \ Heart	Left	Centre	Right
Left	11	1	7
Centre	0	0	0
Right	3	0	6

Pkd2$^{lrm4/lrm4}$

Stomach \ Heart	Left	Centre	Right
Left	18	1	10
Centre	1	0	2
Right	2	1	10

iv/iv

Stomach \ Heart	Left	Centre	Right
Left	28	0	0
Centre	0	0	0
Right	7	0	32

Pkd1l1$^{-/-}$

Stomach \ Heart	Left	Centre	Right
Left	8	0	2
Centre	0	0	1
Right	0	1	16

B

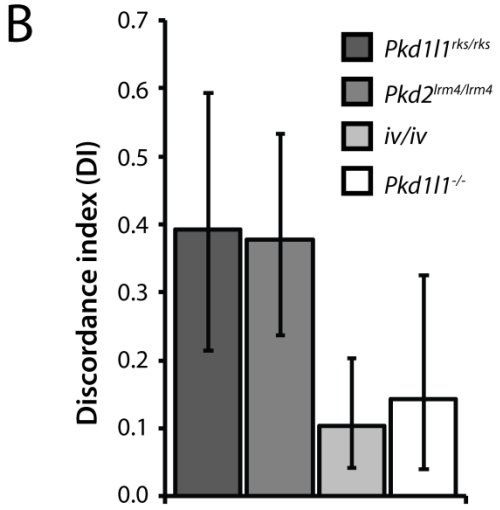

Figure 6.1. Heart-stomach concordance in various left-right mutants

A Tables showing the numbers of embryos in the various phenotypic categories, with the diagonal categories (green) being the concordant ones. **B** Plot of discordance index for four mutants, with the binomial confidence intervals given as error bars.

Chapter Seven

Discussion

7.1. Summary of findings

At the outset of this thesis, I set out to characterise two ENU-induced mouse mutants, *Pkd1l1*^{rks} and *Pkd2*^{lrm4} (Bogani et al., 2009; Ermakov et al., 2009; Field et al., 2011; Patterson et al., 2009). The findings that both mutants exhibit nearly identical L-R defects when assessed on the same genetic background supports the model that Pkd1l1 and Pkd2 act together, or in closely related pathways, during L-R determination. Furthermore, I have shown that Pkd1l1 and Pkd2 physically interact, an association mediated by Pkd1l1's intracellular coiled coil domain.

Pkd1l1$^{rks/rks}$ mutant embryos exhibit right lung isomerism as they do not express the left-sided LPM *Nodal/Lefty/Pitx2* cascade. This led to the notion that Pkd1l1 is required for the activation of LPM Nodal signalling. However, the phenotype of *Pkd1l1*$^{-/-}$ mutants required a revision of this framework. Remarkably, a high proportion of *Pkd1l1*$^{-/-}$ mutants embryos exhibit left pulmonary isomerism and show bilateral *Pitx2* expression; the complete opposite phenotype of *Pkd1l1*$^{rks/rks}$. This finding suggests that *Pkd1l1* is in fact required to restrict Nodal signalling to the left side of the embryo. It is likely that the phenotypic differences between *Pkd1l1*$^{-/-}$ and *Pkd1l1*$^{rks/rks}$ mutants result from differences in the kinds of alleles these represent; clearly *Pkd1l1*^{rks} is not a simple loss of function allele, discussed further below.

Pkd1l1 is expressed throughout the notochord and the ventral layer of the node in the mouse embryo at the time when L-R determination occurs. This suggests a role for *Pkd1l1* in the node itself, though we cannot formally rule out a function in the notochord for *Pkd1l1* in L-R symmetry breaking. Both node cilia structure and motility are, however, normal in *Pkd1l1*$^{rks/rks}$ and *Pkd1l1*$^{-/-}$ mutants, implying that the severe L-R defects observed are not a consequence of altered leftward flow. Using genetic epistasis tests, we also find that *Pkd1l1* acts downstream of leftward flow. Given Pkd1l1's close homology to a known sensory protein, Pkd1, these findings fit most cohesively with a model in which Pkd1l1 is required in the node for the sensation of leftward flow. In support of this, the perinodal gene *Cerl2*, normally repressed on the left side by the action of flow, remains symmetrical in *Pkd1l1*$^{rks/rks}$ mutants.

The consequence of mutation of Pkd2 has also been investigated. *Pkd2*$^{lrm4/lrm4}$ mutants, also derived from a forward genetics screen (Ermakov et al.,

2009), exhibit a phenotype almost identical to *Pkd1l1*$^{rks/rks}$, with right pulmonary isomerism and loss of the left sided Nodal cascade. Furthermore, *Pkd2*$^{lrm4/lrm4}$ mutants also have structurally normal and motile node cilia, while *Pkd2* acts downstream of leftward flow. Together with the finding that Pkd1l1 and Pkd2 physically interact, these data suggest a model in which Pkd1l1-Pkd2 complexes act to sense leftward flow in the node.

7.2. *Pkd1l1* and *Pkd2* mutants

The consequences of loss or mutation of *Pkd1l1* and *Pkd2* genes have now been assessed in the mouse and fish (zebrafish and medaka fish) (Bisgrove et al., 2005; Ermakov et al., 2009; Field et al., 2011; Kamura et al., 2011; Pennekamp et al., 2002; Schottenfeld et al., 2007; Vogel et al., 2010). Here, the results from these studies are summarised.

7.2.1. Loss of *Pkd1l1* in mouse and medaka fish

Mouse null *Pkd1l1* mutants (MGI - *Pkd1l1*^{tm1Lex}) were originally described by Vogel and colleagues; on a mixed 129;B6 background, around 35% of the expected number of *Pkd1l1*$^{-/-}$ mutants survived to adulthood and around one third of these mutants exhibited situs inversus of the viscera (Vogel et al., 2010). In this thesis, we found a similar survivability after backcrossing to C3H for at least 4 generations. However, this analysis was extended, demonstrating that embryonic situs was also perturbed in *Pkd1l1*$^{-/-}$ embryos. For example, the ratio of right:left lung lobes, normally 4:1, was often perturbed, with situs inversus (1:4) and especially left isomerism (1:1) phenotypes being prominent. These data are consistent with some randomisation, but mainly bilateral activation of the normally left-restricted Nodal cascade. Indeed, preliminary molecular analyses suggest that the Nodal cascade, assayed by *Pitx2* expression, is indeed usually bilateral in *Pkd1l1*$^{-/-}$ mutants.

The consequences of loss of *Pkd1l1* have also been assessed in medaka fish. The *Pkd1l1*^{abc} medaka mutant was identified in an ENU screen as a mutant affecting L-R asymmetry (Kamura et al., 2011). Heart and liver positioning was randomised in *Pkd1l1*^{abc} mutants while *southpaw* was either left-sided (30%), right-sided (11%), bilateral (17%), or absent (43%); similar results were obtained for *lefty* expression (Kamura et al., 2011). The expression of *charon* around the KV,

normally repressed on the left side downstream of flow, was symmetrical in *Pkd1l1*^{abc} mutants (Kamura et al., 2011). These defects were not caused by aberrant leftward flow, as flow in the KV was normal in *Pkd1l1*^{abc} mutants (Kamura et al., 2011).

These data suggest an evolutionarily conserved role for *Pkd1l1* during the establishment of L-R asymmetry. Indeed, in both mouse and medaka fish *Pkd1l1* expression is restricted to the node and KV, respectively, and is not expressed in the LPM (Field et al., 2011; Kamura et al., 2011).

7.2.2. *Pkd1l1*$^{rks/rks}$ mutants

Pkd1l1^{rks} derived from an ENU screen and encodes a D411G amino acid point mutation that resides in an extracellular PKD domain of Pkd1l1 protein. Mutants exhibit normal cilia motility in the node but fail to repress left-sided crown cell *Cerl2* and, likely as a result, do not initiate the left-sided *Nodal/Lefty/Pitx2* cascade. This results in a fully penetrant right pulmonary isomerism in *Pkd1l1*$^{rks/rks}$ mutants. These results are strikingly different, indeed opposite, to the phenotype for *Pkd1l1*$^{-/-}$ mutants. We have ruled out genetic background differences as a cause of this discrepancy and instead favour the idea that *Pkd1l1*^{rks} represents a more complicated *Pkd1l1* allele that is not a simple null.

7.2.3. Loss of *Pkd2* in mouse and fish

In the mouse, *Pkd2*$^{-/-}$ mutant embryos exhibit right pulmonary isomerism and loss of left LPM *Nodal* expression in the majority of cases (Pennekamp et al., 2002; Yoshiba et al., 2012). However mutants exhibit a high proportion of bilateral LPM *Pitx2* expression (Pennekamp et al., 2002; Yoshiba et al., 2012), perhaps explained by low level *Nodal* expression in the LPM which has not been detected by in situ hybridisation. Furthermore, *Pkd1l1*$^{-/-}$ embryos have structurally normal cilia and generate robust leftward flow in the node, but left-sided *Cerl2* expression is not repressed (Yoshiba et al., 2012). Since Pkd2 is a cation channel and is required for the left-sided Ca^{2+} elevation observed in mouse embryos (McGrath et al., 2003), it is thought that flow activates Pkd2, permitting a cellular Ca^{2+} response, resulting in the repression of left-sided *Cerl2* (Yoshiba et al., 2012). However, a direct link between Ca^{2+} signalling and asymmetric gene expression has not been established.

In the zebrafish and medaka fish, *Pkd2* is also required for the establishment of L-R asymmetry (Bisgrove et al., 2005; Kamura et al., 2011; Schottenfeld et al., 2007). Morpholino knock-down of zebrafish *pkd2* caused randomisation of the zebrafish Nodal *southpaw* (Bisgrove et al., 2005), with left, right, bilateral, and absent patterns of expression being evident in approximately equal ratios. In medaka fish, a *pkd2* morpholino induced similar defects in the positioning of the visceral organs to mutation of *pkd1l1*, though no assessment of the Nodal cascade was performed (Kamura et al., 2011). Finally, a zebrafish mutant *pkd2* allele termed *curly up* (*cup*), which is presumed to be a molecular null, also causes severe L-R defects (Schottenfeld et al., 2007). In these mutants, both *southpaw* and *pitx2* are expressed bilaterally but restricted to the posterior LPM (Schottenfeld et al., 2007), leading to the proposal that *pkd2* is required to restrict *southpaw* to the left LPM but also for the propagation of signal into the anterior LPM tissue (Schottenfeld et al., 2007). In contrast, Bisgrove and colleagues find that specifically knocking down *pkd2* in the dorsal forerunner cells (DFCs), precursors of the KV, is sufficient to induce L-R defects that are equivalent to the global knock-down (Bisgrove et al., 2005). Thus, it is presently not clear what the role of *pkd2* is in fish L-R development, with Burdine and colleagues arguing that 'the requirement for *pkd2* in L-R patterning is conserved, but the role of *pkd2* might not be' (Schottenfeld et al., 2007).

7.2.4. *Pkd2$^{lrm4/lrm4}$* mutants

Pkd2^{lrm4} encodes an ENU-induced E442G point mutation in the extracellular loop between the first two transmembrane helices (Ermakov et al., 2009). Since antibodies that recognise epitopes in this region are known to block channel function (Schottenfeld et al., 2007), it seemed likely that the Pkd2^{lrm4} protein is non-functional as a Ca^{2+} channel. However, we have shown that Pkd2^{lrm4} protein is instead not able to localise to node cilia. Others have also made these observations, while it has further been shown that Pkd2^{lrm4} is still able to function as a Ca^{2+} channel (Yoshiba et al., 2012). The *Pkd2$^{lrm4/lrm4}$* mutants themselves exhibit right pulmonary isomerism owing to a loss of left-sided *Nodal* signalling, whilst *Cerl2* expression is not downregulated on the left side. These data suggest that Pkd2-mediated *Cerl2* repression requires Pkd2 to localise to primary cilia, the likely site of Pkd2 function during establishment of L-R asymmetry.

7.3. Interactions between genes controlling the generation and sensation of nodal flow

Loss of *Pkd1l1*, a strong candidate to be the sensor of nodal flow, results in randomised positioning of the heart and stomach, and affects the lobation pattern of the lungs. Indeed, in the absence of ability to sense leftward flow, the normally left-restricted Nodal cascade activates bilaterally. However, the phenotype of *Pkd1l1*$^{rks/rks}$ mutants is strikingly different to *Pkd1l1*$^{-/-}$ mutants. In chapter five, I argued that the Pkd1l1^{rks} mutation renders the protein insensitive to leftward flow, owing to the structural disruption of an extracellular polyscytic kidney disease (PKD) domain, likely crucial for flow sensing (Forman et al., 2005; Ma et al., 2009; Qian et al., 2005), in mutants. In contrast to *Pkd1l1*$^{-/-}$ mutants, *Pkd1l1*$^{rks/rks}$ embryos never activate the LPM Nodal cascade; even randomised stochastic activation is lost in these embryos. How can we explain the discrepancies between *Pkd1l1*$^{-/-}$ and *Pkd1l1*$^{rks/rks}$? More generally, how can we integrate the data in this thesis, as well as other published findings, into a coherent model of the establishment of L-R asymmetry?

7.3.1. Might there be a second flow-sensing molecule?

One possibility is that a second protein capable of sensing nodal flow, as well as Pkd1l1, exists in the node. In this scenario, complete loss of *Pkd1l1* can be partially compensated by the action of this second protein. In contrast, *Pkd1l1*$^{rks/rks}$ mutants cannot be rescued because mutant Pkd1l1 protein is likely to be present in *Pkd1l1*$^{rks/rks}$ mutants, interfering with any potential compensation perhaps by binding to all available Pkd2.

A potential candidate protein to act in a compensatory fashion would be the Pkd1l1-related protein Pkd1. Pkd1 is a known mechanosensitive protein that, along with Pkd2, forms a flow-sensitive cation channel complex in the cilia of kidney epithelial cells (Hanaoka et al., 2000; Nauli et al., 2003; Qian et al., 1997). Some support for this model exists in that Pkd1 has previously been reported to localise to node cilia in mouse (Nakaya et al., 2005). However, L-R defects have been specifically searched for in *Pkd1*$^{-/-}$ embryos and not found (Karcher et al., 2005). It is possible that loss of *Pkd1* alone is not sufficient to cause L-R defects but that it still partially compensates when *Pkd1l1* is lost. We are currently testing this possibility

by generating *Pkd1*$^{-/-}$;*Pkd1l1*$^{-/-}$ double mutant embryos; if *Pkd1* does have a low-level role in nodal flow sensation, then we might expect to see complete loss of LPM Nodal induction in double mutants, similar to the situation in *Pkd1l1*$^{rks/rks}$ embryos. However, theoretical considerations may not favour this model. Given that leftward flow is normal in *Pkd1l1* mutants in mouse and fish embryos, it seems unlikely that a low level compensation could account for the bilateral/randomised situs seen in mutants lacking *Pkd1l1*. We might instead expect normal situs in embryos where the compensation has been sufficient, and loss of Nodal induction (leading to right pulmonary isomerism) in those in which compensation has not been sufficient. The existence of reversed and bilateral LPM *Pitx2* patterns in mutants lacking *Pkd1l1* is hard to explain within this framework.

7.3.2. Flow relieves Pkd1l1-mediated inhibition of the left-sided Nodal cascade: a genetic model

Instead, our data support a model in which flow, Pkd1l1, Pkd2, Cerl2, and Nodal are linked by multiple repressive interactions (**Figure 7.1A**). Loss of *Pkd1l1* results in ectopic, often bilateral, activation of the normally left-restricted Nodal cascade. Therefore, *Pkd1l1* must normally act to inhibit *Nodal* activity, restricting it the left side. Since loss of *Pkd2* has the opposite phenotype with loss of left-sided Nodal signals and right pulmonary isomerism (Pennekamp et al., 2002; Yoshiba et al., 2012), *Pkd1l1* and *Pkd2* must have opposing effects in terms of *Nodal* activity. Though we have not yet tested whether *Pkd2* acts genetically downstream of *Pkd1l1*, we believe it most likely will given the nature of the proteins (Pkd1l1 being a sensor, and Pkd2 being a channel that is opened downstream of sensing). We are currently testing this by generating and phenotyping *Pkd1l1*$^{-/-}$;*Pkd2*$^{lrm4/lrm4}$ double mutant embryos. Finally, *Cerl2*, which normally represses *Nodal* but is itself repressed on the left side by flow, must act downstream of both *Pkd1l1* and *Pkd2* because its expression remains symmetrical in *Pkd1l1*$^{rks/rks}$ and *Pkd2*$^{lrm4/lrm4}$ (this thesis) as well as in *Pkd2*$^{-/-}$ embryos (Yoshiba et al., 2012).

These findings can be integrated into a genetic model (**Figure 7.1A**). In wild-type embryos, leftward flow acts to repress Pkd1l1, thereby relieving repression of Pkd2. Owing to the repressive effect of Pkd2 on Cerl2, identified in this thesis but also demonstrated by others recently (Yoshiba et al., 2012), Cerl2 is inhibited on the

left side resulting in a derepression of Nodal. In contrast, on the right side Pkd1l1 is not repressed by flow and so the pathway operates in reverse, with Cerl2 remaining high on the right and Nodal not being derepressed. This results in a greater amount of active Nodal on the left side of the node, likely favouring activation of the Nodal cascade in the left LPM rather than the right.

Can this model explain the phenotypes described in this thesis? Within the framework described in **Figure 7.1**, *Pkd1l1*$^{rks/rks}$ mutants can be understood in the following way: though flow is normal, Pkd1l1^{rks} is insensitive to its presence, owing to disruption of an extracellular PKD domain, and so cannot be repressed. However, Pkd1l1^{rks} protein is still likely to be present in node cilia and perform its inhibition of Pkd2. This results in Cerl2 not being repressed on the left side and therefore Nodal not being activated, the result of which is a loss of node *Nodal* asymmetry and absence of the LPM *Nodal* cascade (**Figure 7.1B**). Similarly, the phenotype of *Pkd2*$^{lrm4/lrm4}$ mutants can be explained if we suppose that the Pkd2^{lrm4} mutant protein is no longer able to repress Cerl2 (**Figure 7.1C**). This is likely since Pkd2^{lrm4} protein does not localise to node cilia, which is the site at which the role of Pkd2 in L-R determination is known to be (Yoshiba et al., 2012).

The phenotype of *Pkd1l1*$^{-/-}$ mutants can also be explained by this genetic model. In this case, the flow sensor has been completely lost and so, even though leftward flow is normal, it cannot impart any L-R information to the embryo. What is different here compared to *Pkd1l1*^{rks}, however, is that the repression of Pkd2 by Pkd1l1 has also been lost. Thus, Pkd2 is more active on both sides of the node, resulting in repression of Cerl2 bilaterally and an increase in Nodal (**Figure 7.1D**). This situation favours bilateral activation of the Nodal cascade, the phenotype most often seen in *Pkd1l1*$^{-/-}$ mutants.

Currently, we are testing this genetic model by generating *Pkd1l1*$^{-/-}$*;Pkd2*$^{lrm4/lrm4}$ double mutant embryos to ask in what order these two genes act on the L-R pathway. The model shown in **Figure 7.1** predicts that the phenotype of such double mutants would resemble *Pkd2*$^{lrm4/lrm4}$ single mutants with loss of LPM *Nodal* and right lung isomerism. It might also be interesting to generate *Pkd1l1*$^{-/-}$*;Cerl2*$^{-/-}$ double mutants to clarify the epistatic relationship between these two genes, as has recently been done of *Pkd2* and *Cerl2* (Yoshiba et al., 2012). However, the similar phenotype of *Pkd1l1*$^{-/-}$ and *Cerl2*$^{-/-}$ embryos might make such an experiment difficult

to analyse; a very high n number would be required to distinguish sutble phenotypic differences.

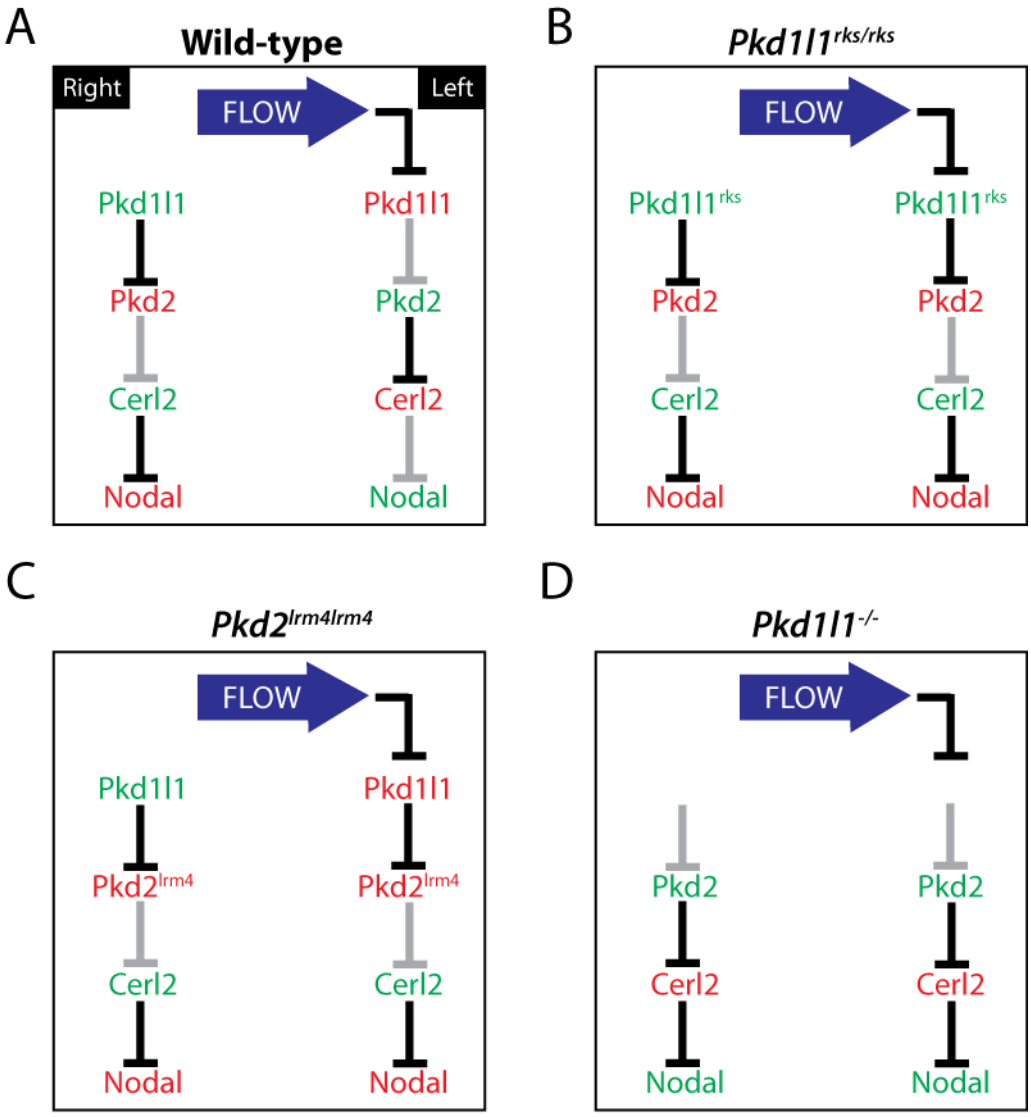

Figure 7.1 Model of the interactions between genes controlling the generation and sensation of leftward flow (see text for details)

7.4. How might Pkd1l1 sense leftward flow?

If Pkd1l1 is the sensor of asymmetric flow in the node, the pertinent question becomes: how, at the molecular level, does Pkd1l1 sense flow? Two possibilities are that Pkd1l1 senses an asymmetrically distributed molecule that is secreted symmetrically into the node (chemosensation) or that Pkd1l1 is a direct sensor of

the force of leftward flow (mechanosensation). These two possibilities are discussed here in light of several pieces of evidence.

7.4.1. Polycystin proteins as sensors: the PKD domain points to mechanosensation

Various members of the polycystin family of proteins are known to have sensory roles. Pkd1 and Pkd2 form complexes in the primary cilia on the surface of kidney epithelial cells (Hanaoka et al., 2000; Nauli et al., 2003; Nauli and Zhou, 2004), where they are argued to act as sensors of fluid flow, eliciting a downstream Ca^{2+} response which inhibits the formation of kidney cysts (Harris and Torres, 2009; Nauli et al., 2003). Pkd1l3 and Pkd2l1 both co-localise to a subset of taste receptor cells where they are required for bitter taste sensation (Ishimaru et al., 2006; Ishimaru and Matsunami, 2009). PkdREJ (receptor for egg jelly) localises to the murine sperm head where it is argued to respond to the zona pellucida matrix thereby triggering the acrosome reaction (Butscheid et al., 2006; Hughes et al., 1999; Sutton et al., 2006). The *C. elegans* Pkd1 and Pkd2 orthologues are both expressed in adult male sensory neurons and are required for mating behaviour, implying their function as sensors (Barr et al., 2001; Barr and Sternberg, 1999).

The *Pkd1l1*^{rks} mutation disrupts the second extracellular PKD domain of Pkd1l1. Owing to their strength and their role in the sensation of fluid flow within Pkd1 protein in the kidney, PKD domains are argued to be essential for mechanosensation (Forman and Clarke, 2007; Forman et al., 2005; Forman et al., 2009; Ma et al., 2009; Oberhauser and Carrion-Vazquez, 2008; Qian et al., 2005). Given that Pkd1, a well-characterised mechanosensor, and Pkd1l1 are the only characterised Pkd1-like polycystins to contain PKD domains, we believe that the finding that L-R defects are caused by disrupting a Pkd1l1 PKD domain favours a role for Pkd1l1 in mechanosensation. It is surprising, therefore, that Kamura and colleagues argue that the extracellular portion of Pkd1 and Pkd1l1 are very different; based on this they conclude that if Pkd1 is a mechanosensor, it is likely that Pkd1l1 is not (Kamura et al., 2011). On the contrary, the extracellular domains of Pkd1 and Pkd1l1 are more similar to each other than to any of the other Pkd1-like family members at the sequence level (Michelle Simon, personal communication), while the existence of PKD domains in these two proteins strongly favours a common

mechanistic function. It is worth noting that Pkd1l2 contains a single PKD domain (Li et al., 2003), however the function of this protein is currently unknown (Mackenzie et al., 2009; Yuasa et al., 2004), and so is not informative for this discussion.

It is an interesting curiosity that Pkd1 contains 15 PKD domains in its extracellular region while Pkd1l1 only contains two (Yuasa et al., 2002). It is tempting to speculate that differences in the forces of fluid flow between the node and kidney are reflected in the number of PKD domains required for mechanosensation.

7.4.2. Two populations of cilia in the node

Based on the lack of L-R dynein (Lrd) expression in peripheral node cilia in the mouse, it was argued that there are two populations of cilia in the node: a central motile subset and a peripherally localised immotile subset on the surface of crown cells (McGrath et al., 2003). Recently, Yoshiba and colleagues have demonstrated that only these lateral-most cilia, most of which are indeed immotile, are required for the sensation of artificial flow (Yoshiba et al., 2012). The 'two-cilia' model was initially described as motile cilia generating flow which is then mechanically sensed by the immotile cilia (McGrath et al., 2003; Tabin and Vogan, 2003) Part of the appeal of this model was that is provided an explanation for the discrepancy in phenotype between mutants lacking cilia motility (*iv/iv*) and those lacking cilia entirely (*Kif3a* or *Kif3b*). Mutants with immotile cilia generally exhibit randomised LPM Nodal signalling (Collignon et al., 1996; Norris and Robertson, 1999; Okada et al., 1999; Supp et al., 1997), while mutant lacking cilia show bilateral pathway activity (Huangfu et al., 2003; Marszalek et al., 1999; Nonaka et al., 1998; Takeda et al., 1999). The idea was that sensory cilia are still present in *iv/iv* mutants and so could still sense random flow fluctuations, resulting in randomised Nodal pathway induction. Mutants lacking cilia, however, could not sense even randomised signals, and so no left- or right-sided only expression patterns would be observed (Tabin, 2005; Tabin and Vogan, 2003). However, the bilateral expression seen in mutants lacking cilia could also be the result of several other factors. Firstly, mutants lacking cilia also have severe midline defects and so likely do not express robust levels of *Lefty1*; loss of the midline barrier would therefore favour bilateral activation. Secondly, it is known that Hedgehog signalling is required to make both the left and

right LPM tissues competent to initiate *Nodal* expression (Tsiairis and McMahon, 2009). Thus, loss of cilia would affect Hedgehog pathway function, resulting in alterations (though not necessarily diminishing) the likelihood of *Nodal* induction. Thus, the differences in phenotype between mutants lacking motile cilia and mutants lacking cilia entirely does not favour either the mechanosensation or the chemosensation models. It might, therefore, be more useful in the future to refer to the 'two-cilia' model in terms of there being motile and sensory populations of cilia at the node, and not using the term to invoke whether the sensory cilia are detecting flow itself or a chemical determinant biased by the flow.

Intriguingly, Kamura and colleagues have failed to detect any immotile cilia in the medaka fish KV, even after extensive analsysis (Kamura et al., 2011). It could be motile cilia are also acting to detect flow/chemicals within the KV. Indeed, it is an emerging notion that motile cilia have sensory functions (Bloodgood, 2010). For example, human airway epithelial cells can sense bitter compounds through T2R receptors localised on motile cilia (Shah et al., 2009). Furthermore, the sensory proteins Pkd1l1 and Pkd2 localise to all KV cilia in medaka fish (Kamura et al., 2011). Thus, the 'two-cilia' model may only apply in mammals, and we may need to invoke a 'one-cilia' model in the fish. Interestingly, though the sub-cellular localisation of Pkd1l1 in the node remains to be determined, Pkd2 is known to localise to all node cilia (McGrath et al., 2003). Whilst speculation, this observation may suggest that motile node cilia also have sensory function.

7.4.3. Two cilia are enough to break L-R symmetry

Recently, it has been demonstrated that as few as two rotating cilia in the mouse node are sufficient to break L-R symmetry (Shinohara et al., 2012). The authors suggest that whilst this observation does not rigorously distinguish the two models of flow sensation, it does favour the mechanosensation hypothesis. The node is a low Reynolds number environment (Cartwright et al., 2004), in which viscosity dominates over inertia. Thus, the flow generated by two rotating cilia would be expected to be local, making it difficult to reconcile with the hypothesis that a chemical determinant is moved long range across the node. In contrast, the authors argue that mechanical force could be theoretically transmitted at the speed of sound from the rotating cilia to the edge of the node (Shinohara et al., 2012). Indeed, in

embryos with two rotating cilia, there were still immotile sensory cilia at the node periphery, though their numbers were reduced (Shinohara et al., 2012).

7.4.4. Is flow sensing alone sufficient to distinguish left from right?

Some have argued that the force of leftward flow would be insufficient to induce a response in peripheral immotile cilia (Cartwright et al., 2008; Cartwright et al., 2004; Okada et al., 2005). However, theoretical studies in which both active rotating and passive immotile cilia are modelled, incorporating parameters such as measured flow rates, suggest that passive cilia would be significantly deflected (Chen et al., 2009; Chen et al., 2011). Indeed, artificial deflection of cilia to a similar magnitude as that predicted for node cilia, was sufficient to induce a Ca^{2+} response (Praetorius et al., 2003). A second issue is that some have argued that the forces in the node would be symmetrical, having no L-R difference (Okada et al., 2005). Whilst this issue is not settled, it seems unlikely that both left sided and right sided sensory cilia are under the same force. This is because the rotating cilia drive leftward flow in a small plane just above the surface of cilia. In contrast, the return rightward flow (which is what would be affecting right-sided cilia) involves much slower movement of a larger body of liquid.

7.4.5. Can a morphogen be biased by the flow?

Another interesting aspect of the system is whether a morphogen molecule can be asymmetrically distributed by flow. Theoretical and biophysical work suggests that a morphogen around 40-50 kDa would retain an asymmetrical steady-state in the node cavity (Okada et al., 2005). However, the identity of such a transported molecular determinant remains to be established. We might expect such a morphogen to be produced in the node, while its loss should result in the lack of *Nodal* expression in the LPM. To date, no strong candidate has emerged, though there are several possibilities.

Sonic hedgehog (Shh) and retinoic acid (RA) are argued to be carried by membrane-sheathed nodal vesicular parcels (NVPs) to the left side (Tanaka et al., 2005). However, there is no evidence for asymmetric Shh signalling in the mouse node, with typical Shh targets being expressed symmetrically. Thus, the Hirokawa model suggests that an asymmetrical but non-canonical Shh pathway is operative at

the node; a suggestion that has remained unsubstantiated by experimental data. However, there is some circumstantial evidence from other systems for such a model: it has been demonstrated that hedgehog proteins are carried by lipoprotein particles (Queiroz et al., 2010), and that Shh signalling leads to a Ca^{2+} response in the developing spinal cord (Belgacem and Borodinsky, 2011). There is some debate about the role of RA in L-R asymmetry but it appears not to be involved in the early phases of L-R determination in mouse (Kawakami et al., 2005; Tanaka et al., 2005; Vermot and Pourquie, 2005; Wasiak and Lohnes, 1999). Instead being required to protect somites from asymmetric signals as they develop symmetrically at either side of the midline (Dubrulle and Pourquie, 2004; Vermot and Pourquie, 2005; Vilhais-Neto et al., 2010; Vilhais-Neto and Pourquie, 2008).

Another candidate morphogen that could be transported by the flow is Wnt3a. Loss of *Wnt3a* results in L-R defects (Nakaya et al., 2005), while Wnt3a protein is known to be carried by lipoprotein particles (Neumann et al., 2009) and can evoke a Ca^{2+} response in hippocampal neurons (Avila et al., 2010). It will be interesting to determine where *Wnt3a* is expressed and whether Wnt3a protein is secreted into the node cavity. However, *Nodal* is expressed bilaterally in *Wnt3a*$^{-/-}$ mutants (Nakaya et al., 2005), rather than being absent as we might expect if Wnt3a is the morphogen which activates left sided pathways.

Intriguingly, Pkd proteins themselves can be carried by large exosome-like vesicles (Hogan et al., 2009), opening the possibility that Pkd1l1/Pkd2 complexes are transported by flow in the node (Hirokawa et al., 2012). How this possibility fits within the chemosensation vs mechanosensation arguments, however, is not clear.

In summary, whilst there are some candidate morphogens that could be transported leftward by the flow, perhaps in an NVP-mediated process, the majority of the theoretical and experimental evidence supports the mechanosensation hypothesis of flow sensation.

7.5. Future directions

The data presented in this thesis favour a model in which cilial Pkd1l1-Pkd2 protein complexes sense leftward flow in the node cavity to elicit chemical changes (Ca^{2+} and *Cerl2* gene expression) in the crown cells around the node periphery (**Figure 7.1**). Several outstanding questions remain: (1) how is leftward flow sensed;

mechanosensation of the force of flow or chemical sensation of a determinant molecule; (2) how does leftward flow result in the opening of Pkd2 channels? Are flow-induced conformational changes induced through Pkd1l1? (3) What is the association between left-sided Ca^{2+} elevation and changes in gene expression? The answering of such questions will require several experimental approaches invoking genetics, biophysics and structural biology.

It will also be important to ascertain the evolutionary conservation of such a 'Pkd1l1-Pkd2' mechanism. Clearly both *Pkd1l1* and *Pkd2* are required for L-R determination in zebrafish and medaka fish, as well as the mouse; are these proteins also needed in amphibians or birds? Since L-R determination in the chick embryo appears to not utilise a flow-based mechanism, it might be that Pkd1l1 and Pkd2 are dispensable. However, it could also be the case that as L-R determination mechanisms have diverged in the chick, the requirement for polycystin proteins has been retained.

More broadly, it will be important to study the downstream consequences of Pkd1l1/Pkd2 function during L-R establishment. The conserved left-sided Nodal cascade has been well studied in several organisms. However, some genes are expressed solely on the right side (Murray and Gridley, 2006a; Murray and Gridley, 2006b), while others are expressed in the left LPM in a Nodal-independent manner (Stevens et al., 2010). We still do not understand how these genes are expressed asymemtrically and what their downstream functions might be with respect to asymmetric organogenesis. L-R asymmetrical development is completed with the asymmetric morphogenesis of the organs and vasculature. However, this is the area in which we know the least. Apart from a few examples, we know very little about how asymmetric signals drive asymmetric morphogenesis. Though some general principles of asymmetric morphogenesis have emerged (**§1.2**), a more complete understanding of the mechanisms involved will require several experimental appraoches in multiple organisms, focusing on one organ at a time.

Chapter Eight

Experimental procedures

8.1. Mice

Animals were maintained according to the Medical Research Council's guidance in 'Responsibility in the Use of Animals for Medical Research' (July 1993), and in accordance with the Animals (Scientific Procedures) Act, 1986. With the exception of *iv/iv* (see below), all lines were maintained as heterozygotes in a controlled light-dark cycle, with dark set as between 7pm and 7am.

For genotyping, genomic DNA was crudely extracted from ear biopsies, tail clips, and embryonic material, by incubation in 90 µl of 50 mM NaOH for 1 hour at 95°C. The reaction was cooled, neutralised by addition of 10 µl of 1 M Tris-HCl pH 4.5, then diluted with ddH_2O. This DNA preparation was then used for genotyping PCRs, described for each line below, with the primer sequences given in **Table 8-1**.

8.1.1. Situs inversus viscerum (*iv*)

The *iv* locus arose as a spontaneous point mutation in the Dynein axonemal heavy chain 11 gene *Dnahc11*; *iv* mice contain an A-to-G mutation in exon 47 of *Dnahc11*, resulting in a glutamate-to-lysine amino acid substitution (Supp et al., 1997). Mice were maintained by continued backcrossing to C3H/HeH, as well as by *+/iv* x *+/iv* intercrosses to produce *iv/iv* adults. To genotype, 108 base pairs of exon 47 flanking the mutation were amplified by PCR using the biotinylated iv_F_Biotin and iv_R primers. The PCR set-up was as follows: 5 µl MasterMix (Qiagen); 1 µl 10 µM iv_F_Biotin and iv_R; 1 µl of genomic DNA; 2 µl ddH_2O. PCR was carried out using the following parameters: 95°C for 5 mins followed by 44 cycles of 95°C 15 s, 60°C 30 s, and 72°C 15 s with a final extension of 72°C for 5 mins. PCR product was subjected to pyrosequencing using the reverse sequencing primer iv_SeqR.

8.1.2. Pkd2^{lrm4}

Left-right mutant 4 (*lrm4*) mice contain an A-to-G transversion in exon 7 of *Pkd2* (Ermakov et al., 2009). The mutation was genotyped by a PCR-pyrosequencing method. 125 bp flanking the mutation at nucleotide 1408 were amplified by PCR using the biotinylated forward primer lrm4_F_Biotin and the reverse primer lrm4_R. The PCR set-up was as follows: 5 µl MasterMix (Qiagen); 0.1 µl 100 µM lrm4_F_Biotin and lrm4_R; 1 µl genomic DNA; 4.8 µl ddH_2O. PCR was carried out using the following protocol: 95°C for 5 mins followed by 44 cycles of 95°C 15 s,

60°C 30 s, and 72°C 15 s with a final extension 72°C for 5 mins. Pyrosequencing of the PCR product was performed using the reverse sequencing primer lrm4_SeqR. The line was maintained by continual backcrossing to C3H/HeH.

8.1.3. Pkd1l1^{rks}

Rikishi (*rks*) mice contain an A-to-G transversion at nucleotide 1232 in exon 8 of *Pkd1l1* (Field et al., 2011), resulting in an aspartic acid-to-glycine amino acid substitution at residue 411. PCR was used to amplify a region of exon 8 containing the mutation using primers rks_F_Biotin and rks_R and the following set-up: 5 µl MasterMix (Qiagen); 1 µl each of 10 µM rks_F_Biotin and rks_R; 1 µl genomic DNA; 2 µl ddH_2O. PCR was carried out using: 95°C for 5 mins followed by 44 cycles of 95°C 15 s, 59°C 30 s, and 72°C 15 s followed by an extension step at 72°C for 5 mins. PCR product was subjected to pyrosequencing using the reverse primer rks_SeqR. The line was maintained by continual backcrossing to C3H/HeH.

Timed mates were generated through overnight matings, with noon on the day of the copulation plug being discovered designated as 0.5 days post coitum (dpc). Pregnant females were sacrificed by cervical dislocation and the uterus was removed. Embryos older than 10.5 dpc were culled according to Home Office mandates. Embryos were dissected in PBS supplemented with 10% fetal bovine serum (FBS) under a Leica MZ6 microscope and processed according to downstream function.

8.1.4. Riboprobe synthesis mRNA whole mount in situ hybridisation (WISH)

Embryos were terminated by immersion in ice-cold fixative (4% PFA in PBS) and incubated overnight at 4°C. Embryos were rinsed in PBS, then dehydrated through a MeOH series (25%, 50%, 75%, and 100% MeOH in PBS) and stored in 100% MeOH at -20°C until WISH.

The following riboprobes were used in this thesis: *Nodal*, *Lefty1/2*, *Pitx2*, *Pkd1l1*, *Shh*, and *Foxa2*. For riboprobe synthesis, plasmids were linearised with appropriate restriction enzyme and buffer (NEB); digests were assessed by gel electrophoresis to check digest completion. DNA was then precipitated (0.15 M sodium acetate, 66% ethanol, -20°C for 1 hour), centrifuged (13,000 rpm for 10 minutes at 4°C), then washed with 70% ethanol. Pellets were air-dried and

resuspended in RNase-free water. Transcription (37°C, 2 hours) from the linearised plasmid incorporated digoxygenin-labelled dUTP (1 x transcription buffer (Roche), 1 x digoxygenin labelling mix (Roche), 1 µg linearised plasmid, 20 units of RNase inhibitor (Invitrogen), 10 units of T7 or T3 RNA polymerase (Roche) in a 20 µl reaction). Transcription efficiency was assessed by analysing a 1 µl aliquot on an electrophoresis gel; the RNA band is expected to be 10 times as intense as the plasmid band, indicating probe concentration is 10 µg/µl. Probe was then precipitated using 100 µl TE, 10 µl 4 M LiCl and 300 µl ethanol and incubated at -20°C for 2 hours. Probe was pelleted (13,000 g, 20 minutes, 4°C), washed with 70% ethanol to remove salt and immediately resuspended in RNase-free TE, then aliquoted and stored at -80°C.

For WISH, embryos were rehydrated to PBT (0.1% Tween-20 in PBS), bleached (6% H_2O_2 in PBT, 40 minutes), treated with proteinase K (10 µg/ml, 10 minutes, RT) followed by glycine (2mg/ml) then washed in PBS, re-fixed for 20 minutes (0.2% glutaraldehyde in 4% PFA in PBS), washed again in PBS then incubated in prehybridisation solution for at least 4 hours at 70°C before being incubated in 0.1 µg/ml digoxygenin-labelled riboprobe in hybridisation solution overnight at 70°C. Embryos were then washed twice in solution I for 30 minutes at 70°C, twice in solution II for 30 minutes at 70°C, incubated in Tris buffered saline with Tween-20 (TBST) for at least 30 minutes at room temperature, then blocked with 10% sheep serum in TBST for at least 2.5 hours at room temperature. Anti-digoxygenin alkaline phosphatise antibody (anti-DIG-AP) (Roche) (1:500) was incubated at 4°C for at least 1 hour in pre-absorbing solution (embryo powder, 1% sheep serum in TBST) before centrifugation at 3000 rpm for 10 minutes. Supernatant was made to volume with 1% sheep serum in TBST and applied to embryos (4°C, overnight). Embryos were then washed with 6-8 changes of TBST for 24 hours, equilibrated in NTMT, and incubated with nitro-blue tetrazolium chloride (NBT) and 5-bromo-4-chloro-3'-indolyphosphate phosphotoluidine (BCIP) salt (20 µl/ml in TBST) and washed in PBT. The coloured reaction was stopped by post-fixing embryos in PFA for 1 hour at room temperature. Photographs were taken using a Leica MZ16 microscope.

8.1.5. X-gal staining of embryos

For assessment of *LacZ* expression embryos were stained with X-gal. Dissected embryos were fixed (1% PFA, 0.2% glutaraldehyde, 2 mM $MgCl_2$, 5 mM EGTA, 0.02% Nonidet P-40 (NP-40) in PBS) for 30 minutes on ice, washed three times (0.02% NP-40 in PBS, 5 minutes) then incubated in X-gal stain solution (5 mM $K_3Fe(CN)_6$, 5 mM $K_4Fe(CN)_6$, 2 mM $MgCl_2$, 0.01% deoxycholate, 0.02% NP-40, 1 mg/ml X-gal in PBS) at 37^oC until colour developed sufficiently. The colour reaction was stopped with three PBS washes and post-fixing in 4% PFA for 20 minutes at room temperature. Stained embryos were stored short-term in 0.4% PFA in PBS at 4^oC, then photographed with a Leica MZ16 microscope.

8.1.6. High-speed video microscopy

For cilia beat analysis, embryos were dissected in 199 medium (Gibco), then flat-mounted on a microscope slide under a coverslip. High-speed videa capture (100 frames per second) was performed under differential interference contrast (DIC) optics (Leica 2500 microscope) using a 63 x NA 0.9 objective. At least 3 wild-type and mutant embryos were analysed frame-by frame using ImageJ; between 20-30 cilia per node were counted for 5 rotations to calculate rotation frequency. Yolk sacs were collected for genotyping.

8.1.7. Scanning electron microscopy

Embryos were dissected at 8.5 dpc under PBS and fixed in 0.1 M sodium cacodylate in 2.5% glutaraldehyde in PBS for 1 hour at room temperature, washed twice in 0.1 M sodium cacodylate for 5 minutes then dehydrated through an ethanol series. Finally, embryos were washed twice in glass vials with acetone then stored at 4^oC in acetone. Embryos were critically point dired using an EMI-Tech K850 dryer then sputter coated with gold particles using a Polaron SEM Coating Unit E5100. Scanning electron microscopy was performed with a JEOL JSM 6500F.

8.2. Molecular biology

8.2.1. Gel electrophoresis

Nucleic acids mixed with loading buffer (1 x TE pH 8.0, 10% glycerol, 0.08% Orange G) were loaded into 0.7-2% Agarose (Invitrogen) gels made in TBE containing 1:10,000 ethidium bromide. A 1 kb Plus DNA Ladder (Invitrogen) was loaded to assess product sizes. Gels were electrophoresed for 20-50 minutes at around 90 V then visualised using a Gel Doc system (BioRad).

8.2.2. Purification of PCR products

PCR products were purified directly using the QIAquick PCR Purification kit (Qiagen) according to manufactureres instructions. Alternatively, product was purified from agarose gels after electrophoresis using the QIAquick Gel Extraction kit (Qiagen) according to the kits instructions.

8.2.3. DNA sequencing

Purified DNA was sequenced by GATC using either standard construct primers or primers targeted to the sequence of interest. Sequences were analysed by BLAST (Ensembl) and by sequence alignment (VectorNTI).

8.2.4. Transformation of plasmid DNA

Plasmid DNA was transformed into chemically competent DH5α *E. coli* cells. Around 10 ng of plasmid DNA was added to 25-50 µl of cells then incubated on ice for 30 minutes. Cells were then heat shocked at 42°c for 45 seconds, cooled on ice for 2 minutes, then grown in 1 ml of pre-warmed LB media at 37°C for 1 hour with shaking at 225 rpm. Cells were then spread on LB-agar selective plates containing appropriate antibiotic and incubated overnight at 37°C.

8.2.5. DNA preparation from colonies

Either 3 ml or 50 ml cultures were grown from colonies in LB medium containing antibiotic. DNA from these cultures was prepared using either a Miniprep kit (Qiagen) or a Midiprep kit (Qiagen), following manufacturer's instructions. DNA

concentration was determined by assessing absorbance at 260 nm using a Nanodrop ND-8000 (Thermo Scientific).

8.2.6. Restriction enzyme digestion

Restriction endonucleases were from NEB and were used with the recommended buffer and incubation temperature using the rule that 1 unit of restriction enzyme fully digests 1 µg of DNA in 1 hour. Digests were routinely performed with the following set-up: 2 µl purified DNA (around 200 ng/µl), 1 µl 10 x restriction enzyme buffer (NEB), 1 µl restriction enzyme (10 U/µl) (NEB), and 6 µl H_2O. The success of restriction digestion was determined by DNA gel electrohoresis.

8.2.7. Dephosphorylation of vector DNA

To prevent DNA strands from self-ligating and to aid construct-insert ligation efficiency, 5' phosphates were removed from DNA ends by dephosphorylation using a recombinant rAPid alkaline phosphatase (Roche) following manufacturer's instructions. A typical reaction set-up was: 5 µl vector DNA (around 200 ng/µl), 2 µl 10 x rAPid alkaline phosphatase buffer (Roche), 1 µl rAPid alkaline phosphatase (1 U) (Roche), 12 µl H_2O. Reactions were incubated at 37°C for 10 minutes; at the end of this period rAPid alkaline phosphatase was inactivated by incubation of the reaction at 75°C for 2 minutes.

8.2.8. Ligation of vector and insert

Positive and negative control ligation reactions were performed alongside each ligation reaction. Reactions were performed using an approximate molar ratio of 3:1 insert fragment to vector using T4 DNA ligase (Roche) with a typical set-up of: 1 µl vector DNA (50 ng/µl), 6 µl insert DNA fragment (25 ng/µl), 2 µl 5 x DNA Dilution Buffer (Roche), 10 µl 2 x T4 DNA Ligation Buffer (Roche) and 1 µl T4 DNA ligase (Roche). Ligations were incuabated at room temperature for 15 minutes for sticky 5' overhang DNA ends and for 1 hour for blunt DNA ends.

8.3. Protein biochemistry

8.3.1. Protein extraction and quantitation

Protein from cultured cells was prepared using Nonidet P40 (NP40) lysis buffer (150 mM NaCl, 50 mM Tris-HCl (pH 8) and 1% NP40 in PBS containing 1 x Proteinase Inhibitor (Roche)). Cells were scraped off plates in lysis buffer then transferred to eppendorf tubes, incubated on ice for 30 minutes then centrifuged at 13,000 rpm (4°C); the surpernatant was pipetted off the pellet and transferred to a fresh cool eppendorf tube. Protein was quantified using Bradford reagent with BSA (NEB) as standards.

8.3.2. Immunoprecipiation

Immunoprecipitations (IPs) were performed with 0.4 mg pre-cleared protein lysate per IP, using anti-myc (Sigma, C3956) and anti-GFP (Roche 11 814 460 001) antibodies bound to Protein G Sepharose beads (Sigma). IPs were performed for 1 hour at 4°C with rotation; beads were then washed 5 times with ice-cold PBS. Precipitated protein-bead complexes were boiled at 100°C for 10 minutes prior to resolution by SDS-PAGE.

8.3.3. Western blotting

Protein samples were denatured at 70°C for 10 minutes in SDS-PAGE Buffer (1 x LBS loading buffer (Invitrogen), 1 x reducing agent (Invitrogen) in H_2O). NuPAGE 3-8% Tris-Acetate or 4-12% Bis-Tris polyacrylamide gels (Invitrogen) were used in electrophoresis tanks with 1 x MOPS buffer (Invitrogen) and antioxidant (Invitrogen). HiMark Prestained Protein Standard (Invitrogen) or SeeBlue Plus2 Prestained Standard (Invitrogen) were used as size ladders, and gels were electrophoresed at 100-150 V for 1-2 hours. Protein was transferred from gels to nitocellulose membranes using the iBLOT system (Invitrogen); membranes were then blocked by incubation with 5% milk in PBT either at room temerpature for 1 hour or overnight at 4°C. After blocking, membranes were incubated in primary antibody of appropriate concentration in 2-5% milk in PBT overnight at 4°C, washed in PBT (three times, 10 minutes each), incubated in fluorescent secondary antibodies in 5% milk in PBT for 1 hour at room temperature in the dark, washed in PBT (four times, seven minutes

each in the dark), then left to dry in the dark. Protein was detected on blots using the Odessey system.

8.4. Tissue culture

Human Embryonic Kidney (HEK 293T) cells were grown in Dulbecco's Modified Eagle's Medium with Glutamax (DMEM) (Gibco), while Inner Medullary Collecting Duct (IMCD3) cells were grown in DMEM: Nutrient mixture F-12 (Gibco). Both media were supplemented with 1% penecilin-streptomycin (Gibco) and 10% foetal bovine serum (FBS) (Gibco).

8.4.1. Waking cells

Aliquots frozen on liquid nitrogen were rapid thawed at 37°C with gentle shaking, transferred to fresh tubes, centrifuged at 1000 g for 5 minutes, resuspended in fresh pre-warmed media, transferred onto plates and incubated overnight (37°C, 5% CO_2).

8.4.2. Splitting cells

Spent media was aspirated away and cells were rinsed in warm PBS. 2.5% Trypsin-EDTA (Gibco) was used to de-attach cells (assessed by light microscopy), then was inactivated by addition of an equal volume of culture media. Suspended cells were then transferred to tubes, centrifgued at 1000 g for 5 minutes; pellets were resuspended in 10 ml media, then pipetted into plates or flasks for culture.

8.4.3. Freezing cells

For long term storage, cells were trypsinised, centrifuged (1000 g for 5 minutes), then pellets were resuspended in freezing medium (Gibco) at 1 ml/million cells. Cells were aliquoted into 1.5 ml cryotubes (Nunc), flash frozen on dry ice/isopropanol and stored at -70°C in a polystyrene insert box overnight before being transferred to liquid nitrogen for long term storage.

8.4.4. Counting cells

Media was aspirated away, cells were washed in pre-warmed PBS, then trypsinised, centrifuged, and resuspended as described above. 50 µl of cell suspension was applied to a haemocytometer and cells were counted by light microscopy with n cells in a defined square being equivalent to n x 10^4 cells/ml. Specific numbers of cells were plated for transfection the next morning: 6 well plate – 1.5 million/well; 9 cm^2 dish – 2.5 million/dish; 8 chamber slide – 20,000/chamber.

8.4.5. Transfection of constructs

Constructs were transfected into cells grown to 50-70% confluence using JetPEI (Polyplus Transfection) according to manufacturer's instructions.

8.4.6. Immunocytofluorescence

Coverslips with cells grown on them were washed 3 times in PBS, fixed in ice cold 100% methanol for 3 minutes, rinsed twice in PBS, permeated in 0.1% Triton-X100 for 3 minutes, rinsed in PBS then blocked for 2 hours in 1% goat serum in PBS. Cells were then incubated in primary antibody for 30 minutes to 1 hour, washed for 1 hour in PBS, the incubated in secondary antibody for 30 minutes. Finally, cells were washed 3 times with PBS. Coverslips containing cells were mounted (cell side down)

References

Adachi, H., Saijoh, Y., Mochida, K., Ohishi, S., Hashiguchi, H., Hirao, A. and Hamada, H. (1999). Determination of left/right asymmetric expression of nodal by a left side-specific enhancer with sequence similarity to a lefty-2 enhancer. *Genes Dev* 13, 1589-600.

Afzelius, B. A. (1976). A human syndrome caused by immotile cilia. *Science* 193, 317-9.

Andersson, O., Reissmann, E., Jornvall, H. and Ibanez, C. F. (2006). Synergistic interaction between Gdf1 and Nodal during anterior axis development. *Dev Biol* 293, 370-81.

Antic, D., Stubbs, J. L., Suyama, K., Kintner, C., Scott, M. P. and Axelrod, J. D. (2010). Planar cell polarity enables posterior localization of nodal cilia and left-right axis determination during mouse and Xenopus embryogenesis. *PLoS One* 5, e8999.

Ashe, H. L. and Briscoe, J. (2006). The interpretation of morphogen gradients. *Development* 133, 385-94.

Avila, M. E., Sepulveda, F. J., Burgos, C. F., Moraga-Cid, G., Parodi, J., Moon, R. T., Aguayo, L. G., Opazo, C. and De Ferrari, G. V. (2010). Canonical Wnt3a modulates intracellular calcium and enhances excitatory neurotransmission in hippocampal neurons. *J Biol Chem* 285, 18939-47.

Badano, J. L., Mitsuma, N., Beales, P. L. and Katsanis, N. (2006). The ciliopathies: an emerging class of human genetic disorders. *Annu Rev Genomics Hum Genet* 7, 125-48.

Baker, K. and Beales, P. L. (2009). Making sense of cilia in disease: the human ciliopathies. *Am J Med Genet C Semin Med Genet* 151C, 281-95.

Bangs, F., Antonio, N., Thongnuek, P., Welten, M., Davey, M. G., Briscoe, J. and Tickle, C. (2011). Generation of mice with functional inactivation of talpid3, a gene first identified in chicken. *Development* 138, 3261-72.

Barr, M. M., DeModena, J., Braun, D., Nguyen, C. Q., Hall, D. H. and Sternberg, P. W. (2001). The Caenorhabditis elegans autosomal dominant polycystic kidney disease gene homologs lov-1 and pkd-2 act in the same pathway. *Curr Biol* 11, 1341-6.

Barr, M. M. and Sternberg, P. W. (1999). A polycystic kidney-disease gene homologue required for male mating behaviour in C. elegans. *Nature* 401, 386-9.

Beddington, R. S. and Robertson, E. J. (1999). Axis development and early asymmetry in mammals. *Cell* 96, 195-209.

Belgacem, Y. H. and Borodinsky, L. N. (2011). Sonic hedgehog signaling is decoded by calcium spike activity in the developing spinal cord. *Proc Natl Acad Sci U S A* 108, 4482-7.

Bell, E., Munoz-Sanjuan, I., Altmann, C. R., Vonica, A. and Brivanlou, A. H. (2003). Cell fate specification and competence by Coco, a maternal BMP, TGFbeta and Wnt inhibitor. *Development* 130, 1381-9.

Bellomo, D., Lander, A., Harragan, I. and Brown, N. A. (1996). Cell proliferation in mammalian gastrulation: the ventral node and notochord are relatively quiescent. *Dev Dyn* 205, 471-85.

Ben, J., Elworthy, S., Ng, A. S., van Eeden, F. and Ingham, P. W. (2011). Targeted mutation of the talpid3 gene in zebrafish reveals its conserved requirement for ciliogenesis and Hedgehog signalling across the vertebrates. *Development* 138, 4969-78.

Berbari, N. F., O'Connor, A. K., Haycraft, C. J. and Yoder, B. K. (2009). The primary cilium as a complex signaling center. *Curr Biol* 19, R526-35.

Best, R. B., Fowler, S. B., Herrera, J. L., Steward, A., Paci, E. and Clarke, J. (2003). Mechanical unfolding of a titin Ig domain: structure of transition state revealed by combining atomic force microscopy, protein engineering and molecular dynamics simulations. *J Mol Biol* 330, 867-77.

Beyer, T., Danilchik, M., Thumberger, T., Vick, P., Tisler, M., Schneider, I., Bogusch, S., Andre, P., Ulmer, B., Walentek, P. et al. (2012a). Serotonin Signaling Is Required for Wnt-Dependent GRP Specification and Leftward Flow in Xenopus. *Curr Biol* 22, 33-9.

Beyer, T., Thumberger, T., Schweickert, A. and Blum, M. (2012b). Connexin26-mediated transfer of laterality cues in Xenopus. *Biology Open* 1, 473-481.

Bisgrove, B. W., Essner, J. J. and Yost, H. J. (2000). Multiple pathways in the midline regulate concordant brain, heart and gut left-right asymmetry. *Development* 127, 3567-79.

Bisgrove, B. W., Morelli, S. H. and Yost, H. J. (2003). Genetics of human laterality disorders: insights from vertebrate model systems. *Annu Rev Genomics Hum Genet* 4, 1-32.

Bisgrove, B. W., Snarr, B. S., Emrazian, A. and Yost, H. J. (2005). Polaris and Polycystin-2 in dorsal forerunner cells and Kupffer's vesicle are required for specification of the zebrafish left-right axis. *Dev Biol* 287, 274-88.

Blacque, O. E., Cevik, S. and Kaplan, O. I. (2008). Intraflagellar transport: from molecular characterisation to mechanism. *Front Biosci* 13, 2633-52.

Bloodgood, R. A. (2009). From central to rudimentary to primary: the history of an underappreciated organelle whose time has come. The primary cilium. *Methods Cell Biol* 94, 3-52.

Bloodgood, R. A. (2010). Sensory reception is an attribute of both primary cilia and motile cilia. *J Cell Sci* 123, 505-9.

Blum, M., Andre, P., Muders, K., Schweickert, A., Fischer, A., Bitzer, E., Bogusch, S., Beyer, T., van Straaten, H. W. and Viebahn, C. (2007). Ciliation and gene expression distinguish between node and posterior notochord in the mammalian embryo. *Differentiation* 75, 133-46.

Blum, M., Weber, T., Beyer, T. and Vick, P. (2009). Evolution of leftward flow. *Semin Cell Dev Biol* 20, 464-71.

Boettger, T., Wittler, L. and Kessel, M. (1999). FGF8 functions in the specification of the right body side of the chick. *Curr Biol* 9, 277-80.

Bogani, D., Siggers, P., Brixey, R., Warr, N., Beddow, S., Edwards, J., Williams, D., Wilhelm, D., Koopman, P., Flavell, R. A. et al. (2009). Loss of mitogen-activated protein kinase kinase kinase 4 (MAP3K4) reveals a requirement for MAPK signalling in mouse sex determination. *PLoS Biol* 7, e1000196.

Bolker, J. A. (1993). Gastrulation and mesoderm morphogenesis in the white sturgeon. *J Exp Zool* 266, 116-31.

Borovina, A., Superina, S., Voskas, D. and Ciruna, B. (2010). Vangl2 directs the posterior tilting and asymmetric localization of motile primary cilia. *Nat Cell Biol* 12, 407-12.

Boulter, C., Mulroy, S., Webb, S., Fleming, S., Brindle, K. and Sandford, R. (2001). Cardiovascular, skeletal, and renal defects in mice with a targeted disruption of the Pkd1 gene. *Proc Natl Acad Sci U S A* 98, 12174-9.

Brennan, J., Lu, C. C., Norris, D. P., Rodriguez, T. A., Beddington, R. S. and Robertson, E. J. (2001). Nodal signalling in the epiblast patterns the early mouse embryo. *Nature* 411, 965-9.

Brennan, J., Norris, D. P. and Robertson, E. J. (2002). Nodal activity in the node governs left-right asymmetry. *Genes Dev* 16, 2339-44.

Britz-Cunningham, S. H., Shah, M. M., Zuppan, C. W. and Fletcher, W. H. (1995). Mutations of the Connexin43 gap-junction gene in patients with heart malformations and defects of laterality. *N Engl J Med* 332, 1323-9.

Brockwell, D. J. (2007). Probing the mechanical stability of proteins using the atomic force microscope. *Biochem Soc Trans* 35, 1564-8.

Brokaw, C. J. (2005). Computer simulation of flagellar movement IX. Oscillation and symmetry breaking in a model for short flagella and nodal cilia. *Cell Motil Cytoskeleton* 60, 35-47.

Brown, N. A., McCarthy, A. and Wolpert, L. (1990). The development of handed asymmetry in aggregation chimeras of situs inversus mutant and wild-type mouse embryo. *Development* 110, 949-54.

Brown, N. A. and Wolpert, L. (1990). The development of handedness in left/right asymmetry. *Development* 109, 1-9.

Burdine, R. D. and Schier, A. F. (2000). Conserved and divergent mechanisms in left-right axis formation. *Genes Dev* 14, 763-76.

Burn, S. F., Boot, M. J., de Angelis, C., Doohan, R., Arques, C. G., Torres, M. and Hill, R. E. (2008). The dynamics of spleen morphogenesis. *Dev Biol* 318, 303-11.

Burn, S. F. and Hill, R. E. (2009). Left-right asymmetry in gut development: what happens next? *Bioessays* 31, 1026-37.

Butscheid, Y., Chubanov, V., Steger, K., Meyer, D., Dietrich, A. and Gudermann, T. (2006). Polycystic kidney disease and receptor for egg jelly is a plasma membrane protein of mouse sperm head. *Mol Reprod Dev* 73, 350-60.

Bycroft, M., Bateman, A., Clarke, J., Hamill, S. J., Sandford, R., Thomas, R. L. and Chothia, C. (1999). The structure of a PKD domain from polycystin-1: implications for polycystic kidney disease. *Embo J* 18, 297-305.

Cartwright, J. H., Piro, N., Piro, O. and Tuval, I. (2007). Embryonic nodal flow and the dynamics of nodal vesicular parcels. *J R Soc Interface* 4, 49-55.

Cartwright, J. H., Piro, N., Piro, O. and Tuval, I. (2008). Fluid dynamics of establishing left-right patterning in development. *Birth Defects Res C Embryo Today* 84, 95-101.

Cartwright, J. H., Piro, O. and Tuval, I. (2004). Fluid-dynamical basis of the embryonic development of left-right asymmetry in vertebrates. *Proc Natl Acad Sci U S A* 101, 7234-9.

Caspary, T., Larkins, C. E. and Anderson, K. V. (2007). The graded response to Sonic Hedgehog depends on cilia architecture. *Dev Cell* 12, 767-78.

Chang, H., Zwijsen, A., Vogel, H., Huylebroeck, D. and Matzuk, M. M. (2000). Smad5 is essential for left-right asymmetry in mice. *Dev Biol* 219, 71-8.

Chen, D., Norris, D. and Ventikos, Y. (2009). The active and passive ciliary motion in the embryo node: a computational fluid dynamics model. *J Biomech* 42, 210-6.

Chen, D., Norris, D. and Ventikos, Y. (2011). Ciliary behaviour and mechano-transduction in the embryonic node: computational testing of hypotheses. *Med Eng Phys* 33, 857-67.

Chen, Y. and Schier, A. F. (2001). The zebrafish Nodal signal Squint functions as a morphogen. *Nature* 411, 607-10.

Chen, Y. and Schier, A. F. (2002). Lefty proteins are long-range inhibitors of squint-mediated nodal signaling. *Curr Biol* 12, 2124-8.

Cheng, S. K., Olale, F., Bennett, J. T., Brivanlou, A. H. and Schier, A. F. (2003). EGF-CFC proteins are essential coreceptors for the TGF-beta signals Vg1 and GDF1. *Genes Dev* 17, 31-6.

Cheng, S. K., Olale, F., Brivanlou, A. H. and Schier, A. F. (2004). Lefty blocks a subset of TGFbeta signals by antagonizing EGF-CFC coreceptors. *PLoS Biol* 2, E30.

Chiang, C., Litingtung, Y., Lee, E., Young, K. E., Corden, J. L., Westphal, H. and Beachy, P. A. (1996). Cyclopia and defective axial patterning in mice lacking Sonic hedgehog gene function. *Nature* 383, 407-13.

Chilvers, M. A., Rutman, A. and O'Callaghan, C. (2003). Ciliary beat pattern is associated with specific ultrastructural defects in primary ciliary dyskinesia. *J Allergy Clin Immunol* 112, 518-24.

Chinoy, M. R. (2003). Lung growth and development. *Front Biosci* 8, d392-415.

Collignon, J., Varlet, I. and Robertson, E. J. (1996). Relationship between asymmetric nodal expression and the direction of embryonic turning. *Nature* 381, 155-8.

Craig, D., Gao, M., Schulten, K. and Vogel, V. (2004). Tuning the mechanical stability of fibronectin type III modules through sequence variations. *Structure* 12, 21-30.

Cui, C., Little, C. D. and Rongish, B. J. (2009). Rotation of organizer tissue contributes to left-right asymmetry. *Anat Rec (Hoboken)* 292, 557-61.

Danos, M. C. and Yost, H. J. (1995). Linkage of cardiac left-right asymmetry and dorsal-anterior development in Xenopus. *Development* 121, 1467-74.

Danos, M. C. and Yost, H. J. (1996). Role of notochord in specification of cardiac left-right orientation in zebrafish and Xenopus. *Dev Biol* 177, 96-103.

Davidson, B. P., Kinder, S. J., Steiner, K., Schoenwolf, G. C. and Tam, P. P. (1999). Impact of node ablation on the morphogenesis of the body axis and the lateral asymmetry of the mouse embryo during early organogenesis. *Dev Biol* 211, 11-26.

Davis, N. M., Kurpios, N. A., Sun, X., Gros, J., Martin, J. F. and Tabin, C. J. (2008). The chirality of gut rotation derives from left-right asymmetric changes in the architecture of the dorsal mesentery. *Dev Cell* 15, 134-45.

De Robertis, E. M. and Sasai, Y. (1996). A common plan for dorsoventral patterning in Bilateria. *Nature* 380, 37-40.

Dubrulle, J. and Pourquie, O. (2004). Coupling segmentation to axis formation. *Development* 131, 5783-93.

Eggenschwiler, J. T. and Anderson, K. V. (2007). Cilia and developmental signaling. *Annu Rev Cell Dev Biol* 23, 345-73.

Ermakov, A., Stevens, J. L., Whitehill, E., Robson, J. E., Pieles, G., Brooker, D., Goggolidou, P., Powles-Glover, N., Hacker, T., Young, S. R. et al. (2009). Mouse mutagenesis identifies novel roles for left-right patterning genes in pulmonary, craniofacial, ocular, and limb development. *Dev Dyn* 238, 581-94.

Esser, A. T., Smith, K. C., Weaver, J. C. and Levin, M. (2006). Mathematical model of morphogen electrophoresis through gap junctions. *Dev Dyn* 235, 2144-59.

Essner, J. J., Amack, J. D., Nyholm, M. K., Harris, E. B. and Yost, H. J. (2005). Kupffer's vesicle is a ciliated organ of asymmetry in the zebrafish embryo that initiates left-right development of the brain, heart and gut. *Development* 132, 1247-60.

Ezratty, E. J., Stokes, N., Chai, S., Shah, A. S., Williams, S. E. and Fuchs, E. (2011). A role for the primary cilium in Notch signaling and epidermal differentiation during skin development. *Cell* 145, 1129-41.

Feistel, K. and Blum, M. (2006). Three types of cilia including a novel 9+4 axoneme on the notochordal plate of the rabbit embryo. *Dev Dyn* 235, 3348-58.

Field, S., Riley, K. L., Grimes, D. T., Hilton, H., Simon, M., Powles-Glover, N., Siggers, P., Bogani, D., Greenfield, A. and Norris, D. P. (2011). Pkd1l1 establishes left-right asymmetry and physically interacts with Pkd2. *Development* 138, 1131-42.

Fliegauf, M., Benzing, T. and Omran, H. (2007). When cilia go bad: cilia defects and ciliopathies. *Nat Rev Mol Cell Biol* 8, 880-93.

Fogelgren, B., Lin, S. Y., Zuo, X., Jaffe, K. M., Park, K. M., Reichert, R. J., Bell, P. D., Burdine, R. D. and Lipschutz, J. H. (2011). The exocyst protein Sec10 interacts with Polycystin-2 and knockdown causes PKD-phenotypes. *PLoS Genet* 7, e1001361.

Follit, J. A., Tuft, R. A., Fogarty, K. E. and Pazour, G. J. (2006). The intraflagellar transport protein IFT20 is associated with the Golgi complex and is required for cilia assembly. *Mol Biol Cell* 17, 3781-92.

Follit, J. A., Xu, F., Keady, B. T. and Pazour, G. J. (2009). Characterization of mouse IFT complex B. *Cell Motil Cytoskeleton* 66, 457-68.

Forman, J. R. and Clarke, J. (2007). Mechanical unfolding of proteins: insights into biology, structure and folding. *Curr Opin Struct Biol* 17, 58-66.

Forman, J. R., Qamar, S., Paci, E., Sandford, R. N. and Clarke, J. (2005). The remarkable mechanical strength of polycystin-1 supports a direct role in mechanotransduction. *J Mol Biol* 349, 861-71.

Forman, J. R., Yew, Z. T., Qamar, S., Sandford, R. N., Paci, E. and Clarke, J. (2009). Non-native interactions are critical for mechanical strength in PKD domains. *Structure* 17, 1582-90.

Friedman, M. (2008). The evolutionary origin of flatfish asymmetry. *Nature* 454, 209-12.

Fukumoto, T., Kema, I. P. and Levin, M. (2005). Serotonin signaling is a very early step in patterning of the left-right axis in chick and frog embryos. *Curr Biol* 15, 794-803.

Gaio, U., Schweickert, A., Fischer, A., Garratt, A. N., Muller, T., Ozcelik, C., Lankes, W., Strehle, M., Britsch, S., Blum, M. et al. (1999). A role of the cryptic gene in the correct establishment of the left-right axis. *Curr Biol* 9, 1339-42.

Germain, S., Howell, M., Esslemont, G. M. and Hill, C. S. (2000). Homeodomain and winged-helix transcription factors recruit activated Smads to distinct promoter elements via a common Smad interaction motif. *Genes Dev* 14, 435-51.

Gierer, A. and Meinhardt, H. (1972). A theory of biological pattern formation. *Kybernetik* 12, 30-9.

Goetz, S. C. and Anderson, K. V. (2010). The primary cilium: a signalling centre during vertebrate development. *Nat Rev Genet* 11, 331-44.

Gourronc, F., Ahmad, N., Nedza, N., Eggleston, T. and Rebagliati, M. (2007). Nodal activity around Kupffer's vesicle depends on the T-box transcription factors Notail and Spadetail and on Notch signaling. *Dev Dyn* 236, 2131-46.

Grande, C. and Patel, N. H. (2009a). Lophotrochozoa get into the game: the nodal pathway and left/right asymmetry in bilateria. *Cold Spring Harb Symp Quant Biol* 74, 281-7.

Grande, C. and Patel, N. H. (2009b). Nodal signalling is involved in left-right asymmetry in snails. *Nature* 457, 1007-11.

Gros, J., Feistel, K., Viebahn, C., Blum, M. and Tabin, C. J. (2009). Cell movements at Hensen's node establish left/right asymmetric gene expression in the chick. *Science* 324, 941-4.

Hanaoka, K., Qian, F., Boletta, A., Bhunia, A. K., Piontek, K., Tsiokas, L., Sukhatme, V. P., Guggino, W. B. and Germino, G. G. (2000). Co-assembly of polycystin-1 and -2 produces unique cation-permeable currents. *Nature* 408, 990-4.

Harris, P. C. and Torres, V. E. (2009). Polycystic kidney disease. *Annu Rev Med* 60, 321-37.

Hashimoto, H., Rebagliati, M., Ahmad, N., Muraoka, O., Kurokawa, T., Hibi, M. and Suzuki, T. (2004). The Cerberus/Dan-family protein Charon is a negative regulator of Nodal signaling during left-right patterning in zebrafish. *Development* 131, 1741-53.

Hashimoto, M. and Hamada, H. (2010). Translation of anterior-posterior polarity into left-right polarity in the mouse embryo. *Curr Opin Genet Dev* 20, 433-7.

Hashimoto, M., Shinohara, K., Wang, J., Ikeuchi, S., Yoshiba, S., Meno, C., Nonaka, S., Takada, S., Hatta, K., Wynshaw-Boris, A. et al. (2010). Planar polarization of node cells determines the rotational axis of node cilia. *Nat Cell Biol* 12, 170-6.

Hejnol, A. and Martindale, M. Q. (2008a). Acoel development indicates the independent evolution of the bilaterian mouth and anus. *Nature* 456, 382-6.

Hejnol, A. and Martindale, M. Q. (2008b). Acoel development supports a simple planula-like urbilaterian. *Philos Trans R Soc Lond B Biol Sci* 363, 1493-501.

Held, L. I. (2009). Quirks of Human Anatomy: An Evo-Devo Look at the Human Body.

Hirokawa, N., Tanaka, Y. and Okada, Y. (2012). Cilia, KIF3 molecular motor and nodal flow. *Curr Opin Cell Biol*.

Hogan, M. C., Manganelli, L., Woollard, J. R., Masyuk, A. I., Masyuk, T. V., Tammachote, R., Huang, B. Q., Leontovich, A. A., Beito, T. G., Madden, B. J. et al.

(2009). Characterization of PKD protein-positive exosome-like vesicles. *J Am Soc Nephrol* 20, 278-88.

Hojo, M., Takashima, S., Kobayashi, D., Sumeragi, A., Shimada, A., Tsukahara, T., Yokoi, H., Narita, T., Jindo, T., Kage, T. et al. (2007). Right-elevated expression of charon is regulated by fluid flow in medaka Kupffer's vesicle. *Dev Growth Differ* 49, 395-405.

Hou, J., Yashiro, K., Okazaki, Y., Saijoh, Y., Hayashizaki, Y. and Hamada, H. (2004). Identification of a novel left-right asymmetrically expressed gene in the mouse belonging to the BPI/PLUNC superfamily. *Dev Dyn* 229, 373-9.

Huangfu, D., Liu, A., Rakeman, A. S., Murcia, N. S., Niswander, L. and Anderson, K. V. (2003). Hedgehog signalling in the mouse requires intraflagellar transport proteins. *Nature* 426, 83-7.

Hughes, J., Ward, C. J., Aspinwall, R., Butler, R. and Harris, P. C. (1999). Identification of a human homologue of the sea urchin receptor for egg jelly: a polycystic kidney disease-like protein. *Hum Mol Genet* 8, 543-9.

Icardo, J. M. and Ojeda, J. L. (1984). Effects of colchicine on the formation and looping of the tubular heart of the embryonic chick. *Acta Anat (Basel)* 119, 1-9.

Ishikawa, H. and Marshall, W. F. (2011). Ciliogenesis: building the cell's antenna. *Nat Rev Mol Cell Biol* 12, 222-34.

Ishimaru, Y., Inada, H., Kubota, M., Zhuang, H., Tominaga, M. and Matsunami, H. (2006). Transient receptor potential family members PKD1L3 and PKD2L1 form a candidate sour taste receptor. *Proc Natl Acad Sci U S A* 103, 12569-74.

Ishimaru, Y. and Matsunami, H. (2009). Transient receptor potential (TRP) channels and taste sensation. *J Dent Res* 88, 212-8.

Izraeli, S., Lowe, L. A., Bertness, V. L., Campaner, S., Hahn, H., Kirsch, I. R. and Kuehn, M. R. (2001). Genetic evidence that Sil is required for the Sonic Hedgehog response pathway. *Genesis* 31, 72-7.

Izraeli, S., Lowe, L. A., Bertness, V. L., Good, D. J., Dorward, D. W., Kirsch, I. R. and Kuehn, M. R. (1999). The SIL gene is required for mouse embryonic axial development and left-right specification. *Nature* 399, 691-4.

Kamura, K., Kobayashi, D., Uehara, Y., Koshida, S., Iijima, N., Kudo, A., Yokoyama, T. and Takeda, H. (2011). Pkd1l1 complexes with Pkd2 on motile cilia and functions to establish the left-right axis. *Development* 138, 1121-9.

Kanai-Azuma, M., Kanai, Y., Gad, J. M., Tajima, Y., Taya, C., Kurohmaru, M., Sanai, Y., Yonekawa, H., Yazaki, K., Tam, P. P. et al. (2002). Depletion of definitive gut endoderm in Sox17-null mutant mice. *Development* 129, 2367-79.

Karcher, C., Fischer, A., Schweickert, A., Bitzer, E., Horie, S., Witzgall, R. and Blum, M. (2005). Lack of a laterality phenotype in Pkd1 knock-out embryos correlates with absence of polycystin-1 in nodal cilia. *Differentiation* 73, 425-32.

Kawakami, Y., Raya, A., Raya, R. M., Rodriguez-Esteban, C. and Izpisua Belmonte, J. C. (2005). Retinoic acid signalling links left-right asymmetric patterning and bilaterally symmetric somitogenesis in the zebrafish embryo. *Nature* 435, 165-71.

Kawasumi, A., Nakamura, T., Iwai, N., Yashiro, K., Saijoh, Y., Belo, J. A., Shiratori, H. and Hamada, H. (2011). Left-right asymmetry in the level of active Nodal protein produced in the node is translated into left-right asymmetry in the lateral plate of mouse embryos. *Dev Biol* 353, 321-30.

Kile, B. T. and Hilton, D. J. (2005). The art and design of genetic screens: mouse. *Nat Rev Genet* 6, 557-67.

Kimmel, C. B. (1996). Was Urbilateria segmented? *Trends Genet* 12, 329-31.

King, T., Beddington, R. S. and Brown, N. A. (1998). The role of the brachyury gene in heart development and left-right specification in the mouse. *Mech Dev* 79, 29-37.

Kondo, S. and Miura, T. (2010). Reaction-diffusion model as a framework for understanding biological pattern formation. *Science* 329, 1616-20.

Kramer-Zucker, A. G., Olale, F., Haycraft, C. J., Yoder, B. K., Schier, A. F. and Drummond, I. A. (2005). Cilia-driven fluid flow in the zebrafish pronephros, brain and Kupffer's vesicle is required for normal organogenesis. *Development* 132, 1907-21.

Krebs, L. T., Iwai, N., Nonaka, S., Welsh, I. C., Lan, Y., Jiang, R., Saijoh, Y., O'Brien, T. P., Hamada, H. and Gridley, T. (2003). Notch signaling regulates left-right asymmetry determination by inducing Nodal expression. *Genes Dev* 17, 1207-12.

Kreiling, J. A., Balantac, Z. L., Crawford, A. R., Ren, Y., Toure, J., Zchut, S., Kochilas, L. and Creton, R. (2008). Suppression of the endoplasmic reticulum calcium pump during zebrafish gastrulation affects left-right asymmetry of the heart and brain. *Mech Dev* 125, 396-410.

Kurpios, N. A., Ibanes, M., Davis, N. M., Lui, W., Katz, T., Martin, J. F., Izpisua Belmonte, J. C. and Tabin, C. J. (2008). The direction of gut looping is established by changes in the extracellular matrix and in cell:cell adhesion. *Proc Natl Acad Sci U S A* 105, 8499-506.

Le Good, J. A., Joubin, K., Giraldez, A. J., Ben-Haim, N., Beck, S., Chen, Y., Schier, A. F. and Constam, D. B. (2005). Nodal stability determines signaling range. *Curr Biol* 15, 31-6.

Lenhart, K. F., Lin, S. Y., Titus, T. A., Postlethwait, J. H. and Burdine, R. D. (2011). Two additional midline barriers function with midline lefty1 expression to maintain asymmetric Nodal signaling during left-right axis specification in zebrafish. *Development* 138, 4405-10.

Levin, M. (1998). Left-right asymmetry and the chick embryo. *Semin Cell Dev Biol* 9, 67-76.

Levin, M. (2003). Motor protein control of ion flux is an early step in embryonic left-right asymmetry. *Bioessays* 25, 1002-10.

Levin, M., Johnson, R. L., Stern, C. D., Kuehn, M. and Tabin, C. (1995). A molecular pathway determining left-right asymmetry in chick embryogenesis. *Cell* 82, 803-14.

Levin, M. and Mercola, M. (1998a). The compulsion of chirality: toward an understanding of left-right asymmetry. *Genes Dev* 12, 763-9.

Levin, M. and Mercola, M. (1998b). Gap junctions are involved in the early generation of left-right asymmetry. *Dev Biol* 203, 90-105.

Levin, M., Thorlin, T., Robinson, K. R., Nogi, T. and Mercola, M. (2002). Asymmetries in H+/K+-ATPase and cell membrane potentials comprise a very early step in left-right patterning. *Cell* 111, 77-89.

Li, A., Tian, X., Sung, S. W. and Somlo, S. (2003). Identification of two novel polycystic kidney disease-1-like genes in human and mouse genomes. *Genomics* 81, 596-608.

Lim, Y. S., Chua, C. E. and Tang, B. L. (2011). Rabs and other small GTPases in ciliary transport. *Biol Cell* 103, 209-21.

Logan, M., Pagan-Westphal, S. M., Smith, D. M., Paganessi, L. and Tabin, C. J. (1998). The transcription factor Pitx2 mediates situs-specific morphogenesis in response to left-right asymmetric signals. *Cell* 94, 307-17.

Lowe, L. A., Supp, D. M., Sampath, K., Yokoyama, T., Wright, C. V., Potter, S. S., Overbeek, P. and Kuehn, M. R. (1996). Conserved left-right asymmetry of nodal expression and alterations in murine situs inversus. *Nature* 381, 158-61.

Ma, L., Xu, M., Forman, J. R., Clarke, J. and Oberhauser, A. F. (2009). Naturally occurring mutations alter the stability of polycystin-1 polycystic kidney disease (PKD) domains. *J Biol Chem* 284, 32942-9.

Mackenzie, F. E., Romero, R., Williams, D., Gillingwater, T., Hilton, H., Dick, J., Riddoch-Contreras, J., Wong, F., Ireson, L., Powles-Glover, N. et al. (2009). Upregulation of PKD1L2 provokes a complex neuromuscular disease in the mouse. *Hum Mol Genet* 18, 3553-66.

Maisonneuve, C., Guilleret, I., Vick, P., Weber, T., Andre, P., Beyer, T., Blum, M. and Constam, D. B. (2009). Bicaudal C, a novel regulator of Dvl signaling abutting RNA-processing bodies, controls cilia orientation and leftward flow. *Development* 136, 3019-30.

Mani, R., St Onge, R. P., Hartman, J. L. t., Giaever, G. and Roth, F. P. (2008). Defining genetic interaction. *Proc Natl Acad Sci U S A* 105, 3461-6.

Manner, J. (2001). Does an equivalent of the "ventral node" exist in chick embryos? A scanning electron microscopic study. *Anat Embryol (Berl)* 203, 481-90.

Marjoram, L. and Wright, C. (2011). Rapid differential transport of Nodal and Lefty on sulfated proteoglycan-rich extracellular matrix regulates left-right asymmetry in Xenopus. *Development* 138, 475-85.

Marques, S., Borges, A. C., Silva, A. C., Freitas, S., Cordenonsi, M. and Belo, J. A. (2004). The activity of the Nodal antagonist Cerl-2 in the mouse node is required for correct L/R body axis. *Genes Dev* 18, 2342-7.

Marszalek, J. R., Ruiz-Lozano, P., Roberts, E., Chien, K. R. and Goldstein, L. S. (1999). Situs inversus and embryonic ciliary morphogenesis defects in mouse

mutants lacking the KIF3A subunit of kinesin-II. *Proc Natl Acad Sci U S A* 96, 5043-8.

Massague, J., Seoane, J. and Wotton, D. (2005). Smad transcription factors. *Genes Dev* 19, 2783-810.

McGrath, J., Somlo, S., Makova, S., Tian, X. and Brueckner, M. (2003). Two populations of node monocilia initiate left-right asymmetry in the mouse. *Cell* 114, 61-73.

Meno, C., Saijoh, Y., Fujii, H., Ikeda, M., Yokoyama, T., Yokoyama, M., Toyoda, Y. and Hamada, H. (1996). Left-right asymmetric expression of the TGF beta-family member lefty in mouse embryos. *Nature* 381, 151-5.

Meno, C., Shimono, A., Saijoh, Y., Yashiro, K., Mochida, K., Ohishi, S., Noji, S., Kondoh, H. and Hamada, H. (1998). lefty-1 is required for left-right determination as a regulator of lefty-2 and nodal. *Cell* 94, 287-97.

Meno, C., Takeuchi, J., Sakuma, R., Koshiba-Takeuchi, K., Ohishi, S., Saijoh, Y., Miyazaki, J., ten Dijke, P., Ogura, T. and Hamada, H. (2001). Diffusion of nodal signaling activity in the absence of the feedback inhibitor Lefty2. *Dev Cell* 1, 127-38.

Meyers, E. N. and Martin, G. R. (1999). Differences in left-right axis pathways in mouse and chick: functions of FGF8 and SHH. *Science* 285, 403-6.

Miller, D. J. and Ball, E. E. (2009). The gene complement of the ancestral bilaterian - was Urbilateria a monster? *J Biol* 8, 89.

Muller, P., Rogers, K. W., Jordan, B. M., Lee, J. S., Robson, D., Ramanathan, S. and Schier, A. F. (2012). Differential diffusivity of Nodal and Lefty underlies a reaction-diffusion patterning system. *Science* 336, 721-4.

Murdoch, J. N. and Copp, A. J. (2010). The relationship between sonic Hedgehog signaling, cilia, and neural tube defects. *Birth Defects Res A Clin Mol Teratol* 88, 633-52.

Murray, S. A. and Gridley, T. (2006a). Snail1 gene function during early embryo patterning in mice. *Cell Cycle* 5, 2566-70.

Murray, S. A. and Gridley, T. (2006b). Snail family genes are required for left-right asymmetry determination, but not neural crest formation, in mice. *Proc Natl Acad Sci U S A* 103, 10300-4.

Nakamura, T. and Hamada, H. (2012). Left-right patterning: conserved and divergent mechanisms. *Development* 139, 3257-62.

Nakamura, T., Mine, N., Nakaguchi, E., Mochizuki, A., Yamamoto, M., Yashiro, K., Meno, C. and Hamada, H. (2006). Generation of robust left-right asymmetry in the mouse embryo requires a self-enhancement and lateral-inhibition system. *Dev Cell* 11, 495-504.

Nakaya, M. A., Biris, K., Tsukiyama, T., Jaime, S., Rawls, J. A. and Yamaguchi, T. P. (2005). Wnt3a links left-right determination with segmentation and anteroposterior axis elongation. *Development* 132, 5425-36.

Nauli, S. M., Alenghat, F. J., Luo, Y., Williams, E., Vassilev, P., Li, X., Elia, A. E., Lu, W., Brown, E. M., Quinn, S. J. et al. (2003). Polycystins 1 and 2 mediate mechanosensation in the primary cilium of kidney cells. *Nat Genet* 33, 129-37.

Nauli, S. M. and Zhou, J. (2004). Polycystins and mechanosensation in renal and nodal cilia. *Bioessays* 26, 844-56.

Neumann, S., Coudreuse, D. Y., van der Westhuyzen, D. R., Eckhardt, E. R., Korswagen, H. C., Schmitz, G. and Sprong, H. (2009). Mammalian Wnt3a is released on lipoprotein particles. *Traffic* 10, 334-43.

Ng, S. P. and Clarke, J. (2007). Experiments suggest that simulations may overestimate electrostatic contributions to the mechanical stability of a fibronectin type III domain. *J Mol Biol* 371, 851-4.

Nonaka, S., Shiratori, H., Saijoh, Y. and Hamada, H. (2002). Determination of left-right patterning of the mouse embryo by artificial nodal flow. *Nature* 418, 96-9.

Nonaka, S., Tanaka, Y., Okada, Y., Takeda, S., Harada, A., Kanai, Y., Kido, M. and Hirokawa, N. (1998). Randomization of left-right asymmetry due to loss of nodal cilia generating leftward flow of extraembryonic fluid in mice lacking KIF3B motor protein. *Cell* 95, 829-37.

Nonaka, S., Yoshiba, S., Watanabe, D., Ikeuchi, S., Goto, T., Marshall, W. F. and Hamada, H. (2005). De novo formation of left-right asymmetry by posterior tilt of nodal cilia. *PLoS Biol* 3, e268.

Norris, D. P., Brennan, J., Bikoff, E. K. and Robertson, E. J. (2002). The Foxh1-dependent autoregulatory enhancer controls the level of Nodal signals in the mouse embryo. *Development* 129, 3455-68.

Norris, D. P. and Grimes, D. T. (2012). Mouse models of ciliopathies: the state of the art. *Dis Model Mech* 5, 299-312.

Norris, D. P. and Robertson, E. J. (1999). Asymmetric and node-specific nodal expression patterns are controlled by two distinct cis-acting regulatory elements. *Genes Dev* 13, 1575-88.

Oberhauser, A. F. and Carrion-Vazquez, M. (2008). Mechanical biochemistry of proteins one molecule at a time. *J Biol Chem* 283, 6617-21.

Oberhauser, A. F., Marszalek, P. E., Carrion-Vazquez, M. and Fernandez, J. M. (1999). Single protein misfolding events captured by atomic force microscopy. *Nat Struct Biol* 6, 1025-8.

Oberhauser, A. F., Marszalek, P. E., Erickson, H. P. and Fernandez, J. M. (1998). The molecular elasticity of the extracellular matrix protein tenascin. *Nature* 393, 181-5.

Oh, E. C. and Katsanis, N. (2012). Cilia in vertebrate development and disease. *Development* 139, 443-8.

Oh, S. P. and Li, E. (1997). The signaling pathway mediated by the type IIB activin receptor controls axial patterning and lateral asymmetry in the mouse. *Genes Dev* 11, 1812-26.

Okabe, N., Xu, B. and Burdine, R. D. (2008). Fluid dynamics in zebrafish Kupffer's vesicle. *Dev Dyn* 237, 3602-12.

Okada, Y., Nonaka, S., Tanaka, Y., Saijoh, Y., Hamada, H. and Hirokawa, N. (1999). Abnormal nodal flow precedes situs inversus in iv and inv mice. *Mol Cell* 4, 459-68.

Okada, Y., Takeda, S., Tanaka, Y., Izpisua Belmonte, J. C. and Hirokawa, N. (2005). Mechanism of nodal flow: a conserved symmetry breaking event in left-right axis determination. *Cell* 121, 633-44.

Oki, S., Hashimoto, R., Okui, Y., Shen, M. M., Mekada, E., Otani, H., Saijoh, Y. and Hamada, H. (2007). Sulfated glycosaminoglycans are necessary for Nodal signal

transmission from the node to the left lateral plate in the mouse embryo. *Development* 134, 3893-904.

Pathak, N., Austin, C. A. and Drummond, I. A. (2011). Tubulin tyrosine ligase-like genes ttll3 and ttll6 maintain zebrafish cilia structure and motility. *J Biol Chem* 286, 11685-95.

Patterson, K. D., Drysdale, T. A. and Krieg, P. A. (2000). Embryonic origins of spleen asymmetry. *Development* 127, 167-75.

Patterson, V. L., Damrau, C., Paudyal, A., Reeve, B., Grimes, D. T., Stewart, M. E., Williams, D. J., Siggers, P., Greenfield, A. and Murdoch, J. N. (2009). Mouse hitchhiker mutants have spina bifida, dorso-ventral patterning defects and polydactyly: identification of Tulp3 as a novel negative regulator of the Sonic hedgehog pathway. *Hum Mol Genet* 18, 1719-39.

Pearce, J. J., Penny, G. and Rossant, J. (1999). A mouse cerberus/Dan-related gene family. *Dev Biol* 209, 98-110.

Pennekamp, P., Karcher, C., Fischer, A., Schweickert, A., Skryabin, B., Horst, J., Blum, M. and Dworniczak, B. (2002). The ion channel polycystin-2 is required for left-right axis determination in mice. *Curr Biol* 12, 938-43.

Philippe, H., Brinkmann, H., Copley, R. R., Moroz, L. L., Nakano, H., Poustka, A. J., Wallberg, A., Peterson, K. J. and Telford, M. J. (2011). Acoelomorph flatworms are deuterostomes related to Xenoturbella. *Nature* 470, 255-8.

Piccolo, S., Agius, E., Leyns, L., Bhattacharyya, S., Grunz, H., Bouwmeester, T. and De Robertis, E. M. (1999). The head inducer Cerberus is a multifunctional antagonist of Nodal, BMP and Wnt signals. *Nature* 397, 707-10.

Piedra, M. E., Icardo, J. M., Albajar, M., Rodriguez-Rey, J. C. and Ros, M. A. (1998). Pitx2 participates in the late phase of the pathway controlling left-right asymmetry. *Cell* 94, 319-24.

Praetorius, H. A., Frokiaer, J., Nielsen, S. and Spring, K. R. (2003). Bending the primary cilium opens Ca2+-sensitive intermediate-conductance K+ channels in MDCK cells. *J Membr Biol* 191, 193-200.

Praetorius, H. A. and Spring, K. R. (2003). Removal of the MDCK cell primary cilium abolishes flow sensing. *J Membr Biol* 191, 69-76.

Qian, F., Germino, F. J., Cai, Y., Zhang, X., Somlo, S. and Germino, G. G. (1997). PKD1 interacts with PKD2 through a probable coiled-coil domain. *Nat Genet* 16, 179-83.

Qian, F., Wei, W., Germino, G. and Oberhauser, A. (2005). The nanomechanics of polycystin-1 extracellular region. *J Biol Chem* 280, 40723-30.

Queiroz, K. C., Tio, R. A., Zeebregts, C. J., Bijlsma, M. F., Zijlstra, F., Badlou, B., de Vries, M., Ferreira, C. V., Spek, C. A., Peppelenbosch, M. P. et al. (2010). Human plasma very low density lipoprotein carries Indian hedgehog. *J Proteome Res* 9, 6052-9.

Ramsdell, A. F. (2005). Left-right asymmetry and congenital cardiac defects: getting to the heart of the matter in vertebrate left-right axis determination. *Dev Biol* 288, 1-20.

Randall, R. A., Howell, M., Page, C. S., Daly, A., Bates, P. A. and Hill, C. S. (2004). Recognition of phosphorylated-Smad2-containing complexes by a novel Smad interaction motif. *Mol Cell Biol* 24, 1106-21.

Rankin, C. T., Bunton, T., Lawler, A. M. and Lee, S. J. (2000). Regulation of left-right patterning in mice by growth/differentiation factor-1. *Nat Genet* 24, 262-5.

Raya, A. and Izpisua Belmonte, J. C. (2008). Insights into the establishment of left-right asymmetries in vertebrates. *Birth Defects Res C Embryo Today* 84, 81-94.

Raya, A., Kawakami, Y., Rodriguez-Esteban, C., Buscher, D., Koth, C. M., Itoh, T., Morita, M., Raya, R. M., Dubova, I., Bessa, J. G. et al. (2003). Notch activity induces Nodal expression and mediates the establishment of left-right asymmetry in vertebrate embryos. *Genes Dev* 17, 1213-8.

Raya, A., Kawakami, Y., Rodriguez-Esteban, C., Ibanes, M., Rasskin-Gutman, D., Rodriguez-Leon, J., Buscher, D., Feijo, J. A. and Izpisua Belmonte, J. C. (2004). Notch activity acts as a sensor for extracellular calcium during vertebrate left-right determination. *Nature* 427, 121-8.

Rebagliati, M. R., Toyama, R., Fricke, C., Haffter, P. and Dawid, I. B. (1998). Zebrafish nodal-related genes are implicated in axial patterning and establishing left-right asymmetry. *Dev Biol* 199, 261-72.

Reiter, J. F. (2008). A cilium is not a cilium is not a cilium: signaling contributes to ciliary morphological diversity. *Dev Cell* 14, 635-6.

Ryan, A. K., Blumberg, B., Rodriguez-Esteban, C., Yonei-Tamura, S., Tamura, K., Tsukui, T., de la Pena, J., Sabbagh, W., Greenwald, J., Choe, S. et al. (1998). Pitx2 determines left-right asymmetry of internal organs in vertebrates. *Nature* 394, 545-51.

Saijoh, Y., Adachi, H., Sakuma, R., Yeo, C. Y., Yashiro, K., Watanabe, M., Hashiguchi, H., Mochida, K., Ohishi, S., Kawabata, M. et al. (2000). Left-right asymmetric expression of lefty2 and nodal is induced by a signaling pathway that includes the transcription factor FAST2. *Mol Cell* 5, 35-47.

Saijoh, Y., Oki, S., Ohishi, S. and Hamada, H. (2003). Left-right patterning of the mouse lateral plate requires nodal produced in the node. *Dev Biol* 256, 160-72.

Saijoh, Y., Oki, S., Tanaka, C., Nakamura, T., Adachi, H., Yan, Y. T., Shen, M. M. and Hamada, H. (2005). Two nodal-responsive enhancers control left-right asymmetric expression of Nodal. *Dev Dyn* 232, 1031-6.

Sakuma, R., Ohnishi Yi, Y., Meno, C., Fujii, H., Juan, H., Takeuchi, J., Ogura, T., Li, E., Miyazono, K. and Hamada, H. (2002). Inhibition of Nodal signalling by Lefty mediated through interaction with common receptors and efficient diffusion. *Genes Cells* 7, 401-12.

Sampath, K., Rubinstein, A. L., Cheng, A. M., Liang, J. O., Fekany, K., Solnica-Krezel, L., Korzh, V., Halpern, M. E. and Wright, C. V. (1998). Induction of the zebrafish ventral brain and floorplate requires cyclops/nodal signalling. *Nature* 395, 185-9.

Sarmah, B., Latimer, A. J., Appel, B. and Wente, S. R. (2005). Inositol polyphosphates regulate zebrafish left-right asymmetry. *Dev Cell* 9, 133-45.

Sarmah, B., Winfrey, V. P., Olson, G. E., Appel, B. and Wente, S. R. (2007). A role for the inositol kinase Ipk1 in ciliary beating and length maintenance. *Proc Natl Acad Sci U S A* 104, 19843-8.

Satir, P. and Christensen, S. T. (2007). Overview of structure and function of mammalian cilia. *Annu Rev Physiol* 69, 377-400.

Saund, R. S., Kanai-Azuma, M., Kanai, Y., Kim, I., Lucero, M. T. and Saijoh, Y. (2012). Gut endoderm is involved in the transfer of left-right asymmetry from the node to the lateral plate mesoderm in the mouse embryo. *Development* 139, 2426-35.

Schier, A. F. (2009). Nodal morphogens. *Cold Spring Harb Perspect Biol* 1, a003459.

Schneider, I., Houston, D. W., Rebagliati, M. R. and Slusarski, D. C. (2008). Calcium fluxes in dorsal forerunner cells antagonize beta-catenin and alter left-right patterning. *Development* 135, 75-84.

Schneider, L., Clement, C. A., Teilmann, S. C., Pazour, G. J., Hoffmann, E. K., Satir, P. and Christensen, S. T. (2005). PDGFRalphaalpha signaling is regulated through the primary cilium in fibroblasts. *Curr Biol* 15, 1861-6.

Schottenfeld, J., Sullivan-Brown, J. and Burdine, R. D. (2007). Zebrafish curly up encodes a Pkd2 ortholog that restricts left-side-specific expression of southpaw. *Development* 134, 1605-15.

Schweickert, A., Vick, P., Getwan, M., Weber, T., Schneider, I., Eberhardt, M., Beyer, T., Pachur, A. and Blum, M. (2010). The nodal inhibitor Coco is a critical target of leftward flow in Xenopus. *Curr Biol* 20, 738-43.

Schweickert, A., Weber, T., Beyer, T., Vick, P., Bogusch, S., Feistel, K. and Blum, M. (2007). Cilia-driven leftward flow determines laterality in Xenopus. *Curr Biol* 17, 60-6.

Shah, A. S., Ben-Shahar, Y., Moninger, T. O., Kline, J. N. and Welsh, M. J. (2009). Motile cilia of human airway epithelia are chemosensory. *Science* 325, 1131-4.

Shen, M. M. (2007). Nodal signaling: developmental roles and regulation. *Development* 134, 1023-34.

Shinohara, K., Kawasumi, A., Takamatsu, A., Yoshiba, S., Botilde, Y., Motoyama, N., Reith, W., Durand, B., Shiratori, H. and Hamada, H. (2012). Two rotating cilia in the node cavity are sufficient to break left-right symmetry in the mouse embryo. *Nat Commun* 3, 622.

Shiratori, H., Sakuma, R., Watanabe, M., Hashiguchi, H., Mochida, K., Sakai, Y., Nishino, J., Saijoh, Y., Whitman, M. and Hamada, H. (2001). Two-step regulation of

left-right asymmetric expression of Pitx2: initiation by nodal signaling and maintenance by Nkx2. *Mol Cell* 7, 137-49.

Shiratori, H., Yashiro, K., Shen, M. M. and Hamada, H. (2006). Conserved regulation and role of Pitx2 in situs-specific morphogenesis of visceral organs. *Development* 133, 3015-25.

Shook, D. R., Majer, C. and Keller, R. (2004). Pattern and morphogenesis of presumptive superficial mesoderm in two closely related species, Xenopus laevis and Xenopus tropicalis. *Dev Biol* 270, 163-85.

Shu, X., Huang, J., Dong, Y., Choi, J., Langenbacher, A. and Chen, J. N. (2007). Na,K-ATPase alpha2 and Ncx4a regulate zebrafish left-right patterning. *Development* 134, 1921-30.

Singla, V. and Reiter, J. F. (2006). The primary cilium as the cell's antenna: signaling at a sensory organelle. *Science* 313, 629-33.

Song, H., Hu, J., Chen, W., Elliott, G., Andre, P., Gao, B. and Yang, Y. (2010). Planar cell polarity breaks bilateral symmetry by controlling ciliary positioning. *Nature* 466, 378-82.

Stevens, J., Ermakov, A., Braganca, J., Hilton, H., Underhill, P., Bhattacharya, S., Brown, N. A. and Norris, D. P. (2010). Analysis of the asymmetrically expressed Ablim1 locus reveals existence of a lateral plate Nodal-independent left sided signal and an early, left-right independent role for nodal flow. *BMC Dev Biol* 10, 54.

Steward, A., Toca-Herrera, J. L. and Clarke, J. (2002). Versatile cloning system for construction of multimeric proteins for use in atomic force microscopy. *Protein Sci* 11, 2179-83.

Sulik, K., Dehart, D. B., Iangaki, T., Carson, J. L., Vrablic, T., Gesteland, K. and Schoenwolf, G. C. (1994). Morphogenesis of the murine node and notochordal plate. *Dev Dyn* 201, 260-78.

Supp, D. M., Brueckner, M., Kuehn, M. R., Witte, D. P., Lowe, L. A., McGrath, J., Corrales, J. and Potter, S. S. (1999). Targeted deletion of the ATP binding domain of left-right dynein confirms its role in specifying development of left-right asymmetries. *Development* 126, 5495-504.

Supp, D. M., Witte, D. P., Potter, S. S. and Brueckner, M. (1997). Mutation of an axonemal dynein affects left-right asymmetry in inversus viscerum mice. *Nature* 389, 963-6.

Sutherland, M. J. and Ware, S. M. (2009). Disorders of left-right asymmetry: heterotaxy and situs inversus. *Am J Med Genet C Semin Med Genet* 151C, 307-17.

Sutton, K. A., Jungnickel, M. K., Ward, C. J., Harris, P. C. and Florman, H. M. (2006). Functional characterization of PKDREJ, a male germ cell-restricted polycystin. *J Cell Physiol* 209, 493-500.

Tabin, C. (2005). Do we know anything about how left-right asymmetry is first established in the vertebrate embryo? *J Mol Histol* 36, 317-23.

Tabin, C. J. (2006). The key to left-right asymmetry. *Cell* 127, 27-32.

Tabin, C. J. and Vogan, K. J. (2003). A two-cilia model for vertebrate left-right axis specification. *Genes Dev* 17, 1-6.

Takeda, S., Yonekawa, Y., Tanaka, Y., Okada, Y., Nonaka, S. and Hirokawa, N. (1999). Left-right asymmetry and kinesin superfamily protein KIF3A: new insights in determination of laterality and mesoderm induction by kif3A-/- mice analysis. *J Cell Biol* 145, 825-36.

Tanaka, Y., Okada, Y. and Hirokawa, N. (2005). FGF-induced vesicular release of Sonic hedgehog and retinoic acid in leftward nodal flow is critical for left-right determination. *Nature* 435, 172-7.

Taschner, M., Bhogaraju, S. and Lorentzen, E. (2012). Architecture and function of IFT complex proteins in ciliogenesis. *Differentiation* 83, S12-22.

Tsiairis, C. D. and McMahon, A. P. (2009). An Hh-dependent pathway in lateral plate mesoderm enables the generation of left/right asymmetry. *Curr Biol* 19, 1912-7.

Tuson, M., He, M. and Anderson, K. V. (2011). Protein kinase A acts at the basal body of the primary cilium to prevent Gli2 activation and ventralization of the mouse neural tube. *Development* 138, 4921-30.

Ul Hassan, A., Hassan, G., Khan, S. H., Rasool, Z. and Abida, A. (2009). Ciliopathy with special emphasis on kartageners syndrome. *Int J Health Sci (Qassim)* 3, 65-9.

Verhey, K. J., Dishinger, J. and Kee, H. L. (2011). Kinesin motors and primary cilia. *Biochem Soc Trans* 39, 1120-5.

Vermot, J. and Pourquie, O. (2005). Retinoic acid coordinates somitogenesis and left-right patterning in vertebrate embryos. *Nature* 435, 215-20.

Vilhais-Neto, G. C., Maruhashi, M., Smith, K. T., Vasseur-Cognet, M., Peterson, A. S., Workman, J. L. and Pourquie, O. (2010). Rere controls retinoic acid signalling and somite bilateral symmetry. *Nature* 463, 953-7.

Vilhais-Neto, G. C. and Pourquie, O. (2008). Retinoic acid. *Curr Biol* 18, R191-2.

Vincent, S. D., Norris, D. P., Le Good, J. A., Constam, D. B. and Robertson, E. J. (2004). Asymmetric Nodal expression in the mouse is governed by the combinatorial activities of two distinct regulatory elements. *Mech Dev* 121, 1403-15.

Viotti, M., Niu, L., Shi, S. H. and Hadjantonakis, A. K. (2012). Role of the gut endoderm in relaying left-right patterning in mice. *PLoS Biol* 10, e1001276.

Vogel, P., Read, R., Hansen, G. M., Freay, L. C., Zambrowicz, B. P. and Sands, A. T. (2010). Situs inversus in Dpcd/Poll-/-, Nme7-/- , and Pkd1l1-/- mice. *Vet Pathol* 47, 120-31.

Vonica, A. and Brivanlou, A. H. (2007). The left-right axis is regulated by the interplay of Coco, Xnr1 and derriere in Xenopus embryos. *Dev Biol* 303, 281-94.

Walentek, P., Beyer, T., Thumberger, T., Schweickert, A. and Blum, M. (2012). ATP4a is required for Wnt-dependent Foxj1 expression and leftward flow in Xenopus left-right development. *Cell Rep* 1, 516-27.

Wallingford, J. B. and Mitchell, B. (2011). Strange as it may seem: the many links between Wnt signaling, planar cell polarity, and cilia. *Genes Dev* 25, 201-13.

Wandelt, J. and Nagy, L. M. (2004). Left-right asymmetry: more than one way to coil a shell. *Curr Biol* 14, R654-6.

Wang, G., Cadwallader, A. B., Jang, D. S., Tsang, M., Yost, H. J. and Amack, J. D. (2011). The Rho kinase Rock2b establishes anteroposterior asymmetry of the ciliated Kupffer's vesicle in zebrafish. *Development* 138, 45-54.

Wang, G., Manning, M. L. and Amack, J. D. (2012). Regional cell shape changes control form and function of Kupffer's vesicle in the zebrafish embryo. *Dev Biol* 370, 52-62.

Wann, A. K., Zuo, N., Haycraft, C. J., Jensen, C. G., Poole, C. A., McGlashan, S. R. and Knight, M. M. (2012). Primary cilia mediate mechanotransduction through control of ATP-induced Ca2+ signaling in compressed chondrocytes. *Faseb J* 26, 1663-71.

Wasiak, S. and Lohnes, D. (1999). Retinoic acid affects left-right patterning. *Dev Biol* 215, 332-42.

Williams, P. H., Hagemann, A., Gonzalez-Gaitan, M. and Smith, J. C. (2004). Visualizing long-range movement of the morphogen Xnr2 in the Xenopus embryo. *Curr Biol* 14, 1916-23.

Woodward, O. M., Li, Y., Yu, S., Greenwell, P., Wodarczyk, C., Boletta, A., Guggino, W. B. and Qian, F. (2011). Identification of a polycystin-1 cleavage product, P100, that regulates store operated Ca entry through interactions with STIM1. *PLoS One* 5, e12305.

Wu, G., Markowitz, G. S., Li, L., D'Agati, V. D., Factor, S. M., Geng, L., Tibara, S., Tuchman, J., Cai, Y., Park, J. H. et al. (2000). Cardiac defects and renal failure in mice with targeted mutations in Pkd2. *Nat Genet* 24, 75-8.

Yamamoto, M., Mine, N., Mochida, K., Sakai, Y., Saijoh, Y., Meno, C. and Hamada, H. (2003). Nodal signaling induces the midline barrier by activating Nodal expression in the lateral plate. *Development* 130, 1795-804.

Yan, Y. T., Gritsman, K., Ding, J., Burdine, R. D., Corrales, J. D., Price, S. M., Talbot, W. S., Schier, A. F. and Shen, M. M. (1999). Conserved requirement for EGF-CFC genes in vertebrate left-right axis formation. *Genes Dev* 13, 2527-37.

Yin, Y., Bangs, F., Paton, I. R., Prescott, A., James, J., Davey, M. G., Whitley, P., Genikhovich, G., Technau, U., Burt, D. W. et al. (2009). The Talpid3 gene (KIAA0586) encodes a centrosomal protein that is essential for primary cilia formation. *Development* 136, 655-64.

Yoder, B. K., Hou, X. and Guay-Woodford, L. M. (2002). The polycystic kidney disease proteins, polycystin-1, polycystin-2, polaris, and cystin, are co-localized in renal cilia. *J Am Soc Nephrol* 13, 2508-16.

Yoshiba, S., Shiratori, H., Kuo, I. Y., Kawasumi, A., Shinohara, K., Nonaka, S., Asai, Y., Sasaki, G., Belo, J. A., Sasaki, H. et al. (2012). Cilia at the Node of Mouse Embryos Sense Fluid Flow for Left-Right Determination via Pkd2. *Science*.

Yuasa, T., Takakura, A., Denker, B. M., Venugopal, B. and Zhou, J. (2004). Polycystin-1L2 is a novel G-protein-binding protein. *Genomics* 84, 126-38.

Yuasa, T., Venugopal, B., Weremowicz, S., Morton, C. C., Guo, L. and Zhou, J. (2002). The sequence, expression, and chromosomal localization of a novel polycystic kidney disease 1-like gene, PKD1L1, in human. *Genomics* 79, 376-86.

Zariwala, M. A., Omran, H. and Ferkol, T. W. (2011). The emerging genetics of primary ciliary dyskinesia. *Proc Am Thorac Soc* 8, 430-3.

Zhang, X. M., Ramalho-Santos, M. and McMahon, A. P. (2001). Smoothened mutants reveal redundant roles for Shh and Ihh signaling including regulation of L/R asymmetry by the mouse node. *Cell* 105, 781-92.

Zhou, X., Sasaki, H., Lowe, L., Hogan, B. L. and Kuehn, M. R. (1993). Nodal is a novel TGF-beta-like gene expressed in the mouse node during gastrulation. *Nature* 361, 543-7.